AAiT
ADDIS ABABA INSTITUTE OF TECHNOLOGY
አዲስ አበባ ቴክኖሎጂ ኢንስቲትዩት
ADDIS ABABA UNIVERSITY
አዲስ አበባ ዩኒቨርሲቲ

SCHOOL OF GRADUATE STUDIES
SCHOOL OF CIVIL AND ENVIRONMENTAL ENGINEERING
MASTERS OF SCIENCE IN CIVIL ENGINEERING

THESIS

ON

OVERTOPPING OF DAM BY LANDSLIDE WAVE ACTION A CASE STUDY OF SEGO DAM

BY

AMDEMARIAM SHIFERIE MULU

ADVISOR: NETSANET NIGATU (PhD)

FEBRUARY, 2024 G.C
ADDIS ABABA, ETHIOPIA

ADDIS ABABA UNIVERSITY
ADDIS ABABA UNIVERSITY INSTITUTE OF TECHNOLOGY
SCHOOL OF GRADUATE STUDIES
SCHOOL OF CIVIL AND ENVIRONMENTAL ENGINEERING
(SPECIALIZATION: DAM ENGINEERING)

Overtopping of Dam by Landslide Wave Action a Case Study of Sego Dam

By

Amdemariam Shiferie Mulu

"*A thesis submitted to the School of Civil and Environmental Engineering in partial fulfillment of the Degree of Masters of Science in Civil Engineering (Specialized in Dam Engineering)*"

February, 2024 G.C
Addis Ababa, Ethiopia

APPROVAL SHEET

ADDIS ABABA UNIVERSITY

ADDIS ABABA UNIVERSITY INSTITUTE OF TECHNOLOGY

SCHOOL OF GRADUATE STUDIES

SCHOOL OF CIVIL AND ENVIRONMENTAL ENGINEERING

(SPECIALIZATION: DAM ENGINEERING)

This is to certify that the thesis prepared by Amdemariam Shiferie Mulu, entitled: **" Overtopping of Dam by Landslide Wave Action a Case Study of Sego Dam"** and submitted in fulfillment of the requirements for the Degree of Master of Science complies with the regulations of the Addis Ababa University and meets the accepted standards with respect to the originality and quality.

By:

AMDEMARIAM SHIFERIE

APPROVED BY OF EXAMINERS BOARD:			
	NAME	SIGNATURE	DATE
ADVISOR	NETSANET NIGATU (PhD)		
INTERNAL EXAMINER	ASIE KEMAL (PhD)		
EXTERNAL EXAMINER	TEZERA FREW (PhD)		
CHAIR MAN	ASIE KEMAL (PhD)		

DECLARATION

I, Amdemariam Shiferie, hereby certify that the information contained in this paper was acquired and provided in compliance with laws and ethical standards. I have conducted my research with honesty, integrity, and transparency, striving to adhere to the highest standards of academic and professional ethics.

I further declare that, under these rules of conduct, I have accurately referenced and cited any data, ideas, and results that are not original to this work. I have meticulously acknowledged the contributions of other researchers and authors by providing appropriate citations throughout this thesis. I have taken care to avoid any form of plagiarism, ensuring that all sources are properly attributed.

By my signature below, I confirm that the work included in this thesis is entirely original to me. I have diligently conducted my research, crafted my arguments, and presented my findings based on my own efforts and intellect. Any assistance received from colleagues, advisors, or other individuals has been acknowledged and duly credited.

I further confirm that all information sources used in the preparation of this thesis have been correctly cited, referring to the original works and authors in a consistent and accurate manner. I have utilized a recognized citation style and followed its guidelines to ensure the proper documentation of my sources.

I understand the importance of academic integrity and take full responsibility for the accuracy and integrity of this research work. In the event that any discrepancies or issues are discovered, I am committed to addressing them promptly and transparently.

By signing below, I affirm that this certification is true and accurate to the best of my knowledge.

Signature: _____

Date: _____

Acknowledgement

It is a pleasure to convey my gratitude to those who helped me in making this thesis.

First, I would like to thank God for being the source of my strength, Joy and success. My gratitude also goes to Dr. Netsanet Nigatu,and Dr Asse kemal for keeping me on track to finish my study. I am also sincerely grateful for staff members of Ethiopian Construction Design and Supervision Works Corporation, especially w/o Frehiwot Amha and Ato Yilikal B.for giving me helpful information to finish this thesis. My parents deserve special mention for their support and prayers. My father Shiferie Mulu and my mother Zewditu Mamay deserve special mention for showing me the joy of intellectual pursuit ever since I was a child.

Finally, I would like to express my special gratitude to my friends from the class of Dam Engineering (2014E.C.), Alemayehu M., Mesfin K., Esubalew M., Hafsoa G., and Tegegn F., for having friendly and best academic relations throughout the past two crucial years.

Dedication

I dedicate this thesis work to my older brother 'Dawit Shiferie'

Abbreviations

CSA	Central Statistical Agency
DEM	Digital Elevation Model
ECDSWC	Ethiopian Construction Design and Supervision Works Corporation
EMA	Ethiopian Mapping Agency
ENE-WSW	East-northeast- West-southwest
Eqs	Equation
GIS	Geographical Information System
IDF	Inflow Design Flood
ILWIS	Integrated Land and Water Information System
Masl	Mean above Sea Level
MER	Main Ethiopian Rift
NE-SW	Northeast - Southwest
NW- SE	Northwest – Southeast
SMCE	Spatial Multi Criteria Evaluation
SMER	Southern Segment of Ethiopian Rift valley
SNNPRS	South Nation and Nationalities People Regional State
SRTM	Shuttle Radar Topography Mission
UTM	Universal Transverse Mercator
WNW-ESE	West-northwest-East-southeast

Table Contents

List of Figures

List of Tables

List of Tables in Appendices

Abstract

Since dam failure occurrences have resulted in numerous recorded human casualties and severe economic crises throughout history, it is without a doubt necessary to prepare safety plans and hazard management strategies. It is crucial to set up risk management, emergency action plans, or evacuation planning systems to safeguard people and property during abrupt dam failure phenomena brought on by landslide impulse wave causes. In the context of a case study, this thesis examined the landslide impulse wave in a dam under a number of pre-established scenarios. The case topic was the sego dam, which is situated in Ethiopia's Gamo zone SNNPRS. Landslide zonation map of the area around the reservoir rim has been prepared using ILWIS tool. Considering existing historical landslide spot, susceptibility map and geological structures three main landslide point has been identified for impulse wave analysis. Different maps such as historical inventory map, land use and land cover, soil, slope, aspect, lithological maps, distance from road and distance from rivers have been prepared using ArcGIS. Using the actual topographic map of the area, the geometry of the dam and from prominent literatures design inputs, the wave generation and propagation, wave run-up and overtopping has been estimated by excel spreadsheet templates.

Three main landslide impact zones have been chosen after taking into account the landslide susceptibility map and discovered geological faults. In terms of overtopping volume and depth ,the impact of the event is minimal whenever the slide position is far from the dam (landslide three), and the worst-case scenario occurs when the landslide impact point is close to the dam (landslides one and two).In landslide one with bulk slide volume of 24,000m^3 and drop height of 50m, the wave height ,period, amplitude, length and wave run-up height found to be 6.94m,18.04s,5.55m ,332.14m and 7.34m respectively and overtopping volume per unit length dam crest and across the dam axis length found to be 50.61m^3/m, 13,564.3 m^3 respectively. In land slide number two, which had a bulk slide volume of 27,000 m^3 and a drop height of 35 m, the overtopping volume per unit length dam crest and across the whole axis was determined to be 1.8 m^3/m, 482.4 m^3 respectively, and the wave height, period, amplitude, length, and run-up height were all estimated to be 5.75 m, 18.53 s, 4.6 m, and 4.49 m, respectively. Finally, the wave height, period, amplitude, period, and wave run-up height for landslide three, which situated at the end of the reservoir and has a bulk slide volume of 115,200 m^3 and a drop height of 25 m, were found to be 0.1 m, 6.93 s, 0.07 m, 155.5 m, and 0.11 m, respectively. In conclusion, because the dam's freeboard is 4 meters in the analysis, overtopping of the flood by landslides one and two has observed in the computation.

Key words: ArcGIS, ILWIS, Freeboard, Land slide, Impulse Wave, Wave generation &propagation, overtopping, Wave Height, Wave Run-up, Impact slide velocity and impact product parameter.

1. INTRODUCTION

1.1. General background

Dams are vital to this nation's growth because they provide flood protection, drinking water, agriculture, electricity, transportation, and tourism benefits. Dams have many valuable purposes, but they also pose threats to both property and life since they could end up failing and result in disastrous flooding. Owners and controllers of dams conduct routine examinations and inspections to identify potential causes of failure and implement preventative measures to lower the associated risks. Since no strategy for averting failure can ever be assured and loadings exceeding specified limits can never be totally avoided, projecting potential failures and developing preparations for them is another essential part of risk reduction. Programs for public education, the creation of alert systems and protocols, and the creation of efficient evacuation protocols are a few examples of these strategies. Dam owners can also utilize analysis of the effects of flooding and dam collapse to rank the risks posed by the various dams in their inventory. This prioritization approach makes it easier to employ human and financial resources efficiently in order to improve public safety and lessen the risk of dam failure.

Property damage is almost always a given when dams fail, but the number of fatalities depends on the size of the population at danger, the size of the region flooded, and the amount of warning time. It is apparent that when there is insufficient or no warning, the average number of fatalities per dam failure is higher (Zagonjolli, 2007).

Generally, the main causes of dam failure are flood overtopping due to wave action and insufficient spillway capacity, foundation issues, and piping and seepage. Wave can generate in dam reservoir due to landslide. Due to a landslide, the dam reservoir may experience waves. Characterizing and lowering risks associated with potential dam failures, especially in earthen dams, requires assessment and analysis of landslide potential areas around dam and reservoir (J.E. Costa, 1985).

The most typical causes of landslide-generated impulse waves are rock falls, landslides, coastal instability, glacier avalanche events, or glacier melting in water bodies, bays, reservoirs, or seas. (Heller ,2007).

1.2. Statement of the problem

The spillway's proper releasing capabilities and the dam's overall hydraulic design alone cannot ensure the safety of the structure; even with all the required safeguards in place, severe scenarios such as dam overtopping should be anticipated.

Many lives have been lost, homes have been destroyed, and other infrastructures have been damaged as a result of the failure of hundreds of the thousands of dams that have been built around the world.

Dam development has increased significantly in Ethiopia, and several more are planned, designed, and under construction at various stages. One of its objectives is to promote the growth of agriculture, hydroelectricity, supply of water, or a combination of these. The dam's construction has had a substantial impact on the ecosystem downstream, leading to the development of new towns and residential areas for workers on factories and farms as well as a sizable area covered in irrigated crops. These financial investments, along with all of the current and new residents, are really vulnerable to flooding and run the risk of suffering harm or even dying.

Landslides have the power to obliterate vast tracts of forest, species' habitats, and the rich soils on slopes. They damage or destroy built infrastructure, crops, ecosystems, and deaths and cause financial losses and social unrest. They can also lead to other hazards. Significant consequences of a landslide include the loss of life, destruction of infrastructure, damage to the land, and depletion of natural resources. Debris from landslides can also hinder streams, increasing the risk of flooding.

One of Ethiopia's major natural obstacles to growth is the risk of landslides, which limits urbanization, infrastructure development, and basically all activities carried out on slopes and at their bases (Abebe et al., 2010). More than 200 homes were demolished, more than 500 km of highways were disrupted, and around 300 people dead as a result of landslides in Ethiopia from 1993 to 1998 alone (Ayalew, 1999). Ethiopia's hilly and mountainous terrains are distinguished by a variety of topographical, geological, and hydrological variables, as well as soil and land use factors. The town of Dessie, the Wudmen area in Weldiya, the Gilgel Gibe River, the Uba Dema settlement in Sawla, Gamo gofa, the lower Wabe Shebelle River Valley, the Wendo Genet hill, the Blue Nile canyon, and parts of Tigray have all seen intense landslides (Abebe et al., 2010).

Unfortunately, the Sego dam and irrigation project experience a landslide in the project region, which could result in a dam overtopping and wave generation in the dam reservoir in addition to an unexpected stream flood. There are two towns close to the river that have established immediately downstream of Sego Dam, and the project's intended command area is also in the downstream.

Although there are many reasons why dams fail, overtopping brought on by unanticipated and practical occurrences is the most frequent cause. In the case of Sego Dam, ground sliding is anticipated all around the reservoir rim, which could increase the capacity of the reservoir and lead to overtopping over the dam crest. Given this, it is vital for the dam owner to understand the impulse wave of a land slide when the Sego dam is operating.

1.3. Research questions

The research questions that will be answered at the end of this thesis are:

1. Which part of the reservoir rim contains the land slide hazard spot area?
2. What are the primary initiating factors for a land slide in the Sego dam reservoir?
3. What are the main parameters to be considered when calculating impulse wave run-up depth in dam reservoir?

1.4. Objective of the Study

1.4.1. General Objective

The general objective of this study is to identify landslides potential area near to the dam and reservoir in response to various natural and anthropogenic factors and to examine overtopping of Sego dam by impulse wave actions.

1.4.2. Specific Objective

- To find the potential land slide area in the dam and reservoir and to produce a land slide zonation map.
- To examine the impulse wave generation and propagation under possible bulk slide volume at the reservoir's maximum water level.
- To estimate the wave run-up, the overtopping depth and volume, and provide appropriate freeboard taking in to account the risk.

1.5. Scope of the study

The analysis won't look at seepage failure (piping), only hydraulic failure (overtopping) caused by impulse wave action. The recommended freeboard solely takes into account the wave height caused by impulse wave action caused by landslides not wind wave. Only landslides over the reservoir water level are included in the study. The water level used for the analysis is restricted to the highest reservoir level rather than the normal reservoir level because the worst-case scenario of a landslide occurs during the rainy season.

1.6. Significance of the Study

Identifying the land slide spot area and investigate the geological behavior of land in the reservoir rim and predict flood wave depth over the dam reservoir is crucial to calculate and estimate the adequate freeboard of the dam and safety of the dam generally. To impart to other dams situated in landslide areas a valuable lesson about how landslides impact project safety and to raise awareness and comprehension for additional research in the subject domain.

2. LITERATURE REVIEW

2.1. Background

A landslide-caused failure of a dam is one of the world's most deadly natural disasters. Due to the effects of climate change and overpopulation, the negative impact produced by landslide dam failure has substantially increased in recent years (Vita et al. 1998; Hong et al. 2005; Tsai 2008).

Impulse waves frequently develop from landslides, rockfalls, shore instabilities, avalanches, or glacier calving in open oceans, bays, lakes, and reservoirs. They are categorized as gravity waves and, in severe circumstances, can cause dams to topple, which would have disastrous effects. Given their steep valley flanks, potential for enormous slide volumes with high impact velocities, and abundance of reservoirs, Alpine regions are at a high risk of such catastrophes (Heller 2007).

2.2. Causes of land slide

Landslide dam presents as a mass movement caused by a mountainous slope that blocks a river naturally (J.E. Costa, R.L. Shuster, 1988). The most frequent landslide dam trigging factors include intense rainfall, quick snowmelt, volcanic eruptions, and earthquakes (G.F. Wieczorek, 1996). Various processes, such as overtopping, rapid collapse, or progressive failure, might cause a landslide dam to fail (T. Takahashi, 1991).

Overtopping, however, is the most typical failure mode. (J.E. Costa, 1985). The impact of climate change and overpopulation has caused landslide dam catastrophe damages have been enlarged meaningfully over the past few decades. A devastating flood could occur downstream if the landslide dam breaks, releasing a massive amount of water and sediment at once. Therefore, in order to provide appropriate safety measures and thereby limit losses, the outflow hydrograph and its associated maximum discharge must be precisely projected. In the majority of earlier research, it was expected that landslide dams would fail due to either whole channel breadth or half channel breadth (R. Awal, N. Nakagawa, K. Kawaike, Y. Baba, H. Zhang,2008, Z. Cao, Z. Yue, G. Pender,2011, and Y.Satofuka, T. Mori, T. Mizuyama, K. Ogawa, K. Yoshino.2011). These presumptions aren't entirely accurate, though. The experiments carried out by X.K. Do, R.K. Regmi, and K.S. Jung (2015) and the field observations made by G.G.D. Zhou, P. Cui, H.Y. Chen, X.H. Zhu, J.B. Tang, and Q.C. (2013) showed that the landslide dam

shapes have a continuous decrease of height in lateral direction instead of a constant height with a notch.

Numerous potential reasons for mass movements were put out by Schuster and Wieczorek (2002). They recorded 46 examples of slides that followed fast changes in the water level of reservoirs, such as during first impounding, in addition to conventional events like earthquake and heavy rain.

Several external causes have the potential to cause landslides. According to various studies (Vita et al. 1998; Hong et al. 2005; Tsai 2008), the most significant meteorological component that might activate or accelerate movement of the sliding mass is seasonal and heavy rainfall. The deformation of slopes near reservoirs or lakes can be influenced by elements other than precipitation.

The researcher assumed that the prior triggering cause of the landslide in this study is reactivation of observed landslide by earthquake event.

2.3. Overtopping of dam

Impulse waves from landslides propagate up the upstream dam slope and up the reservoir banks in dam reservoirs. Large enough waves might potentially breach the dam and cause hazardous inundation in the lower region. Therefore, for reservoirs located in landslide-prone areas, it is imperative to provide a means of estimating the possible magnitude of an event that could be produced by landslides along the reservoir margins. This analysis uses a three-dimensional (3D) physical model test to investigate the overtopping process over the dam crest and the waves caused by landslides. As is often the case in natural settings, the way the landslide affects the reservoir in the model setup is perpendicular.

The overtopping volume and the controlling factors, namely the slide volume, slide release height, slide impact velocity, still-water depth, and upstream dam face slope, are related empirically in a dimensionless manner based on the experimental results. Predictive relations for the overtopping volume are presented in situations related to the specific model setup. Additional comparisons are drawn between the measured overtopping volumes and a two-dimensional (2D) example that has been documented in the literature. The fluctuation in time and space, which causes an unequal spreading of the volume of water overtopping the dam crest, is a significant aspect of the overtopping process for the 3D scenario. This observation is made feasible by the 3D model setup and is useful for foundation-related issues, such as erosion

and scouring, as well as for considerations linked to dam safety. (Netsanet N., Leif L., and Asie K. 2019, Fjóla G. Sigtryggsdóttir)

Mountainous areas or highlands are common locations for dam sites that are appropriate for impounding reservoirs, commonly in confined valleys or canyons. Generally speaking, landslides, especially rockslides, are prone to occur on mountain slopes. There are well-known instances of landslides impacting reservoirs, which in turn caused impulse waves to overtop the dam and have disastrous downstream effects. This include the Vajont dam accident from 1963, which resulted in around 2000 fatalities (Steven, NW; Simon, D, 1963).

Three steps make up the overall process that describes such events (Heller, V.; Hager, W.H.; Minor, H.-E, 2009): which are slide impact with wave creation, wave propagation with wave transformation, run-up of the impulse wave and dam overtopping. However, if the wave run-up height at the time of the landslide is lower than the freeboard f, the elevation difference between the dam crest and the reservoir's still-water level, the dam is not overtopped.

However, the surrounding rugged slopes of a dam reservoir pose a risk to the stability of the dam. Therefore, a method of calculating the risk associated with landslide waves overtopping a dam is crucial. The reservoir settings, including the geology and terrain, are significant in this consideration. A reservoir in a slender mountain valley may be disposed to landslides over its entire length since the reservoir's length is commonly greater than its width. In other words, these mountain slopes, which are roughly perpendicular to the reservoir's longitudinal axis, could be the source of a catastrophic landslide.

For a variety of geometries, the Coastal Engineering Manual (USACE 2002) provides instructions on how to compute setup (rise in water surface from wind/water abrasion) and run-up as well as how to get an "equivalent" or "average" overtopping discharge per unit width. The average overtopping discharge estimation is greatly influenced by the distance between the still water level and the top of the embankment. It is possible to predict the possibility of erosion and failure using anticipated average overtopping discharges and the current permissible guidelines.

The overtopping discharge may not always be able to adequately explain erosion caused by wave overtopping, according to later investigations. When both waves have the similar projected overtopping discharge, greater, less frequent waves actually cause erosion more than smaller, more frequent waves (Van der Meer, 2010).

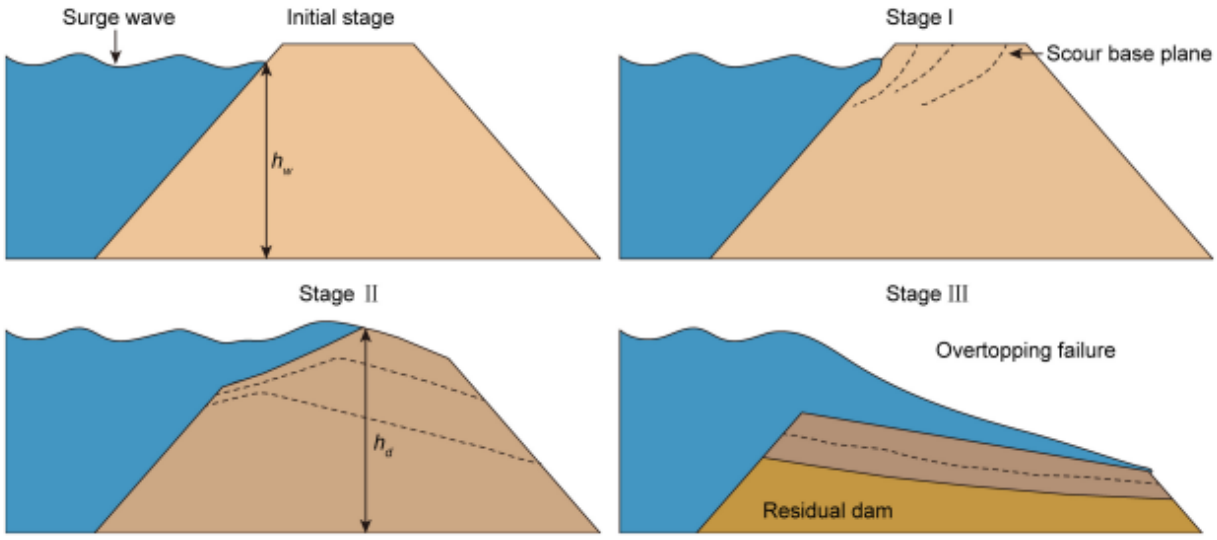

Figure 2. 1 Scouring failure process of a landslide dam by a surge wave. hw and hd are the effective water level and effective dam height, respectively (Hongchao Zheng, Zhenming Shi, Danyi Shen, Ming Peng, Kevin J. Hanley, Chenyi Ma and Limin Zhang (2021).

2.4. Methods for predicting landslide generated impulse waves

For the evaluation of impulse waves caused by landslides, a calculation method based on universally applicable equations is devised. Initially, the existing approaches concerning impulse waves generated by landslides are showcased to assist in assessing the benefits and drawbacks of this technique. There are basically the five techniques listed below:

(i) Generally pertinent equations developed from model tests

(ii) Prototype-specific model tests

(iii) Numerical simulations

(iv) Empirical equations derived from field data

(v) Analytical investigations

The first three techniques, (i) to (iii), have practical application for evaluating impulse waves caused by landslides and their impacts. Occasionally, hybrid modeling—which combines model testing and numerical analysis—might be preferable. This may be done, for instance, when the hydraulic model's criteria for insignificant scale effects permit only the examination of wave generation; the wave propagation will then be computed numerically, or if a portion of

the reservoir is studied using a hydraulic model, the findings are then used to calibrate a numerical model. Obviously, this procedure takes more time and costs more money.

2.5. Impulsive wave generated by landslide

Impulse waves are often caused by landslides, rockfalls, coastline instability, snow avalanches and or iceberg breakup in water bodies, bays, lakes, or reservoirs. They are especially important in the Alpine environment due to the numerous reservoirs, enormous potential slide masses and impact velocities, and steep valley slopes.

The characteristics of the waves produced by landslides must be estimated while building dams and water reservoirs. Any type of geophysical mass flow in dam reservoirs, including rock falls, avalanches of debris, landslides, and debris flows, can cause devastating, impulsive waves that could cause major damage to the dam, banks of the reservoir, surrounding hydraulic systems, and farmland or residential communities. (Semenza 2000).

Additionally, a large sliding mass reduces the dam reservoirs' effective capacity and starts following economic losses. As an illustration, in 1963, one of the most destructive impulsive waves caused by rockslides ever observed occurred in the Vaiont reservoir; the wave exceeded the arch dam by over 100 meters. Nearly 3,000 people died and the community of Longarone, which was downstream from the dam, was completely devastated (Panizzo et al. 2005). Determining the properties of landslide-generated waves in dam reservoirs is crucial.

When simulating landslide-generated waves in dam reservoirs, four separate stages can be identified: the creation, the propagation, the overtopping, and the run-up stages. The landslide-generated waves have been the subject of numerous experimental and numerical research. Most experimental studies primarily aim to define the practical parameters and features of landslide-generated subaerial (Ataie-Ashtian and Nik-khah 2008; Carvalho and Carmo 2007; Risio et al. 2009; Shigihara et al. 2006; Zweifel et al. 2006) and submarine (Enet and Grilli 2005; Grilli and Watts 2005; Liu et al. 2005; Najafi-Jilani and Ataie-Ashtiani 2007) waves.

2.6. Water Wave Theory

2.6.1. Introduction

In contrast to capillary waves, impulse waves produced by landslides fall under the category of gravity waves since they are primarily affected by gravity.

Figure 2-2 displays the pertinent wave characteristics on a defined sine wave with a sine curve-like profile in the (x, z) plane. The sine wave is also referred to as a linear wave if it is small (H/h <0.03) and flat (H/L <0.006). The definition of the original water depth is the still water depth h. The wave height H is calculated by comparing the wave's lowest point, or trough, to its greatest point, or crest.

The distance between the undisturbed sea surface and the wave crest is known as the wave amplitude. a = H/2 for the sine wave depicted in Figure 2-2. For impulse waves, which are typically non-linear and deviate from the ideal sine wave, this is no longer true (Figure 2-2). The wave length L also reaches from wave node to wave node, from crest to crest, or from trough to trough. The amount of time it takes for the crests, nodes, or troughs of two subsequent waves to cross a fixed point is known as the wave period, or T. The sine wave's period can be determined using the formula T = L/c, where c represents the wave's celerity. The square of the celerity for a linear sine wave can be calculated using

$c\text{^}2 = \frac{gL}{2\pi}\tanh\left(\frac{2\pi h}{L}\right)$ ..... Equation (2.1)

Where,

c [m/s] = Wave celerity (Figure 2-2)

g [m/s^2] = Gravitational acceleration; g = 9.81 m/s^2

h [m] = Still water depth

L [m] = Wave length (Figure 2-2)

π [-] = Circular constant; π = 3.14

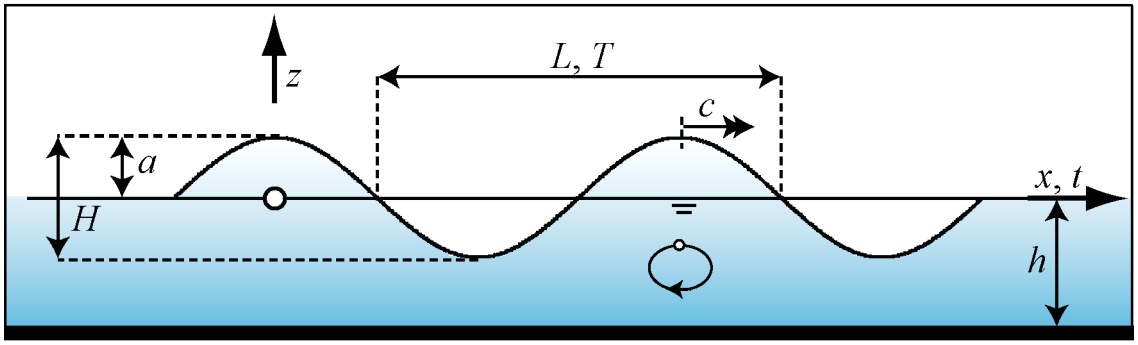

Figure 2. 2 Principal wave parameters presented on an idealized sine wave (in addition, the wave is said to be linear if H/h < 0.03 and H/L < 0.006) (Heller et al., 2009).

The phrases listed below can be used to distinguish between different kinds of water waves:

a) Oscillatory or translatory waves

b) Shallow, intermediate or deep-water waves

c) Periodic or non-periodic waves

d) Linear or non-linear waves

a) Oscillatory or translatory waves

Water particles do not travel in waves in the same way as the water's surface or the wave's celerity. Figure 2-2, which depicts a water particle's orbital motion for an oscillatory wave, can be used to see this. The water particle moves elliptically and, for the period under consideration, stays in the same place, although the water surface appears to progress at wave celerity. Therefore, oscillatory waves only carry energy, which causes the water molecules nearby to move. They do not carry fluid mass. The opposite is true for Translatory waves, when both fluid mass and energy are transported as water particles travel horizontally in the direction of wave propagation (Figure 2-6).

b) Shallow, intermediate or deep-water waves

Waves are classified as shallow, intermediate, or deep in the sea based on their ratio of wave length to still water depth (L/h). For each of these three wave types, the water particle flow for an oscillatory wave is depicted in Figure 2-3. Figure 2-3(a) shows a shallow-water wave with L/h > 20, where the water particles follow elliptical orbits. As the water depth increases, these orbits become flatter and smaller until finally they move parallel to the reservoir bed at a deep depth. The bed restricts the elements' ability to move vertically, which, for instance, changes

the wave height, H.

A tsunami is often a shallow-water wave that results from tectonic plate movement. Equation 2.1 can be used to fix the wave celerity as $c = (gh)^{1/2}$ since the ratio L/h for small, sinusoidal shallow water waves is significant. Heller et al (2009).
Figure 2-3(c) illustrates the opposite situation, a deep-water wave proportional to L/h <2. In this instance, the water molecule orbits are rounded and get smaller as the water depth rises until there is no longer any movement visible on the bed. In other words, neither the lake bed nor the sea bed has an impact on deep-water waves.

Deep-water waves are those caused by wind on open water. Because the ratio L/h is small, applying Eq. (2.1) for a small sinusoidal wave yields a wave celerity of $c = [gL/(2\pi)]^{1/2}$. The zone of intermediate-water waves, where 2< L/h <20, lies between deep and shallow water waves (Figure 2-3b). The lake or sea bottom has an influence on these waves to some extent, and Eq. (2.1) can be used to determine their linear wave celerity. Heller et al (2009).

c) Periodic or non-periodic waves

As seen, for instance, in Figure 2-2, a collection of many waves come together to produce a periodic wave. One wave makes up a non-periodic wave (Figure 2–6) (Heller et al., 2009).

d) Linear and non-linear waves

The definition of waves in mathematics serves as the basis for the concept of non-linearity. According to Dean and Dalrymple ,1991 (Figure 2-2), linear waves have the shape of a sine curve and must have a relative height of H/h <0.03 and a wave steepness of H/L< 0.006. As a result, higher powers are disregarded in the mathematical analysis of the variables H/h and H/L, which only considers them linearly. Additionally, the requirement that sinusoidal waves have a wave height of H = 2a is no longer true. The wave profile departs from this ideal sinusoidal profile more as the degree of non-linearity increases, i.e., the ratios H/h and/or H/L rise. The mathematical representation of the wave profile is typically more difficult and time-consuming the more nonlinearity there is. (Heller et al., 2009).

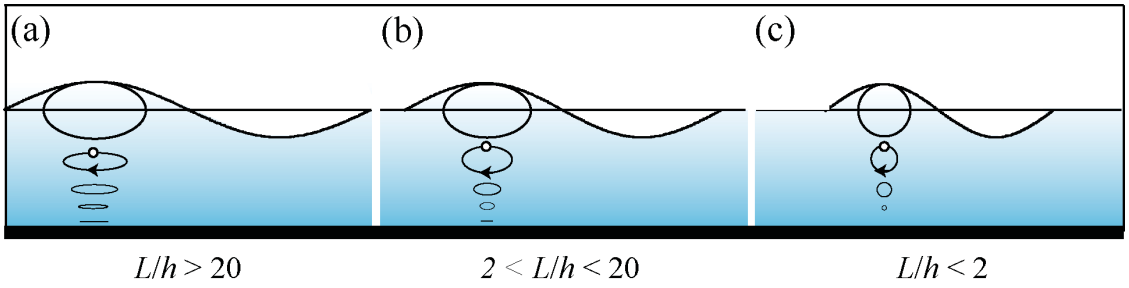

Figure 2. 3 Water particle movement of an oscillatory wave in (a) shallow (L/h > 20), (b) intermediate (2 < L/h < 20) and (c) deep-water (L/h < 2) (Heller et al., 2009).

All of the aforementioned characteristics are present in combination in water waves in their natural state. Since the impulse waves produced by landslides are non-periodic and typically significantly non-linear, mathematical analysis of them is challenging. Furthermore, the amount of fluid mass transported by these waves can range from very little to very much, and they have a translatory nature than an oscillatory one. Although intermediate-water waves frequently result, shallow or deep-water waves can also form depending on the slide's features (Heller et al., 2009).

2.6.2. Theoretical wave types

Water waves deviate more or less from the idyllic sinusoidal profile depicted in Figure 2-2, which can be represented by the linear wave theory for small dimensions (H/h < 0.03 and H/L< 0.006) (Dean and Dalrymple 1991). Here, a few special non-linear water waves that have received a fair amount of theoretical and experimental research are covered. All impulse waves produced by landslides can be classified into one of the four wave categories that are given here. Stokes wave, cnoidal wave, solitary wave, and bore are the four types of waves. (Heller et al., 2009).

a) Stokes wave

A Stokes wave, depicted in Figure 2-4, is a deep- to intermediate-water wave that can be used, for instance, to model wind-generated waves. The Stokes wave is longer and flatter than the sinusoidal wave in Figure 2-2, and it is steeper than that wave. Due to the wave particles' lack of closed orbital motion, very slight fluid mass is being transported. (Heller et al., 2009).

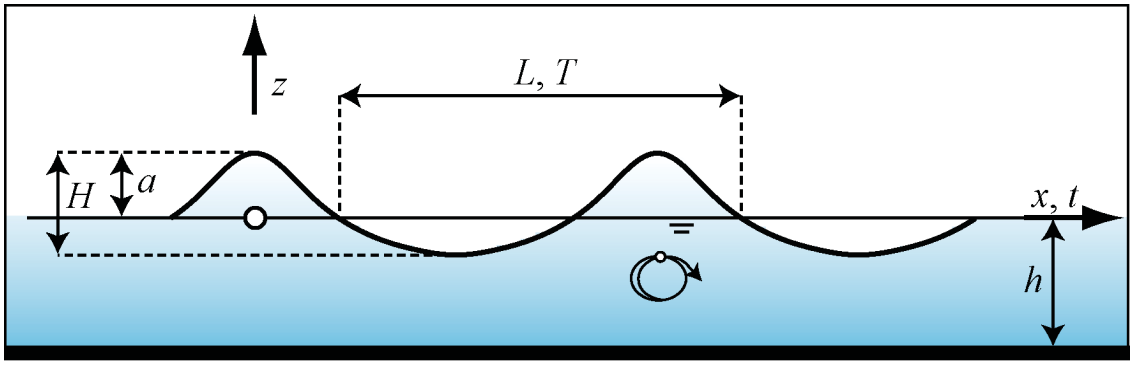

Figure 2. 4 Stokes wave profile displaying the key wave characteristics; little fluid mass transfer (Heller et al., 2009).

b) Cnoidal wave

A periodic wave in shallow or intermediate water is depicted in Figure 2-5 as a cnoidal wave. With the help of this hypothesis, shallow-water wind-generated waves, for instance, can be explained. The cnoidal wave is mostly oscillatory, but it also displays open water particle orbits, which results in the movement of fluid mass. Both the linear wave (also known as a sinusoidal wave) and the solitary wave are considered as restrictive examples in the equation for cnoidal waves. (Heller et al., 2009).

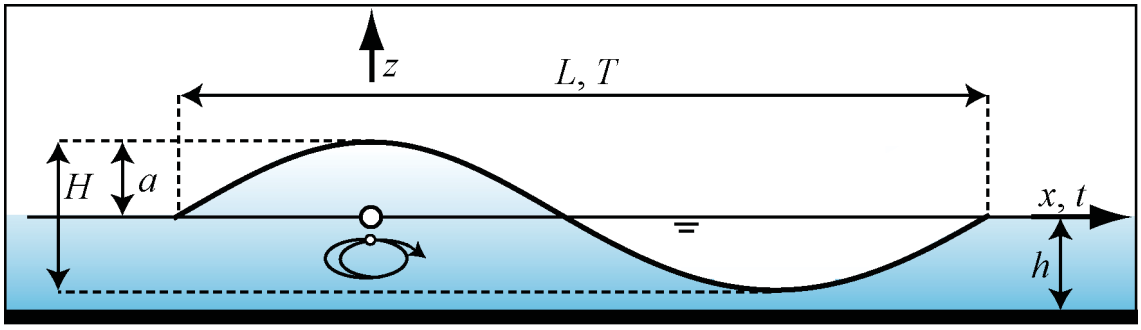

Figure 2. 5 The most significant wave characteristics are displayed in a sinusoidal wave profile, with a small fluid mass transfer. (Heller et al., 2009).

c) Solitary wave

Figure 2-6 displays a solitary wave. The solitary wave theory is frequently employed to explain typical tsunamis, which are brought on by the shifting of tectonic plates. The non-linear water wave that has been studied the utmost through numerical simulations and in lab tests is this one. It simply has a wave peak; there is no trough. As a result, a = H is the equation for wave amplitude. Additionally, the wave length L =∞ and the wave is categorized as a

shallow-water wave (L/h > 20). (Heller et al., 2009).

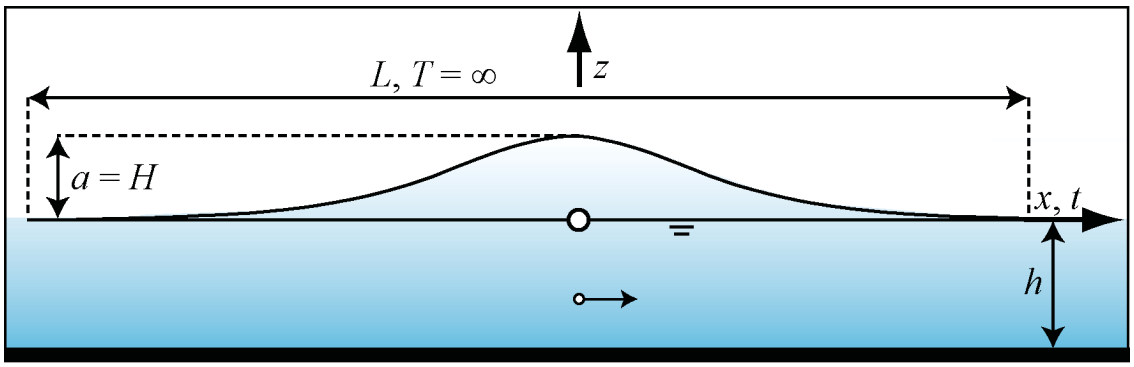

Figure 2. 6 Solitary wave profile displaying the key wave characteristics; significant fluid mass transfer (Heller et al., 2009).

Because water particles move horizontally, there is significant fluid mass movement. The height of this kind of wave in a rectangular channel on a horizontal bottom should theoretically not decrease, and the wave should be able to travel an infinite distance without changing shape. However, this is still less than what happens with other wave types. In actuality, turbulence, which is primarily formed on the bottom of an ocean or lake, results in some lowering of wave height. As the wave period T→ ∞, the solitary wave theory is constructed from the cnoidal wave theory (Heller et al., 2009). Solitary waves' wave celerity is determined by

$$c = [g(h + a)]^{1/2}. \qquad (2.1)$$

a [m]	=	Wave amplitude (Figure 2-3)
c [m/s]	=	Wave celerity
g [m/s^2]	=	Gravitational acceleration; g = 9.81 m/s^2
h [m]	=	Still water depth

A solitary wave over a horizontal bed break and continues as a bore if the wave amplitude a beyond 0.78h. However, a realistic description of this process is impossible analytically.

d) Bore

A bore is depicted in Figure 2-7 and is produced, for instance, when a wave breaks close to the beach and air is attuned at the crest or when the top of the crest folds over. A bore is a shallow-water wave with horizontal particle motion that carries substantial amounts of

fluid. Its steep front and softly sloping back define its profile (Heller et al., 2009).

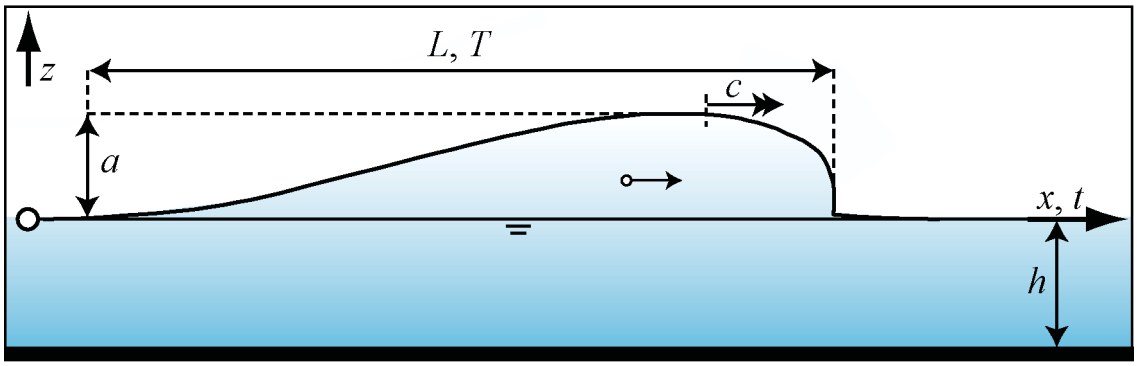

Figure 2. 7 Wave profile of a bore with the key important wave characteristics; large fluid mass carriage (Heller et al., 2009).

2.7. Computation procedure and first step

2.7.1. Introduction

The general equations are used in the 1st step. As illustrated in Figure 2-10, experiments conducted in a rectangular wave basin (3D) and those based on a prismatic wave channel (2D) differ in terms of wave generation. Both approaches are legitimate in practice and address the extremes of constrained transverse and totally unrestricted radial impulse wave propagation above a horizontal sea or reservoir bottom (Figure 2-9). The 2D equations were developed by Heller (2007a), based on Zweifel (2006) and Fritz (2002), and will be translated for 3D situations using a technique indirectly limited in Huber and Hager (1997).

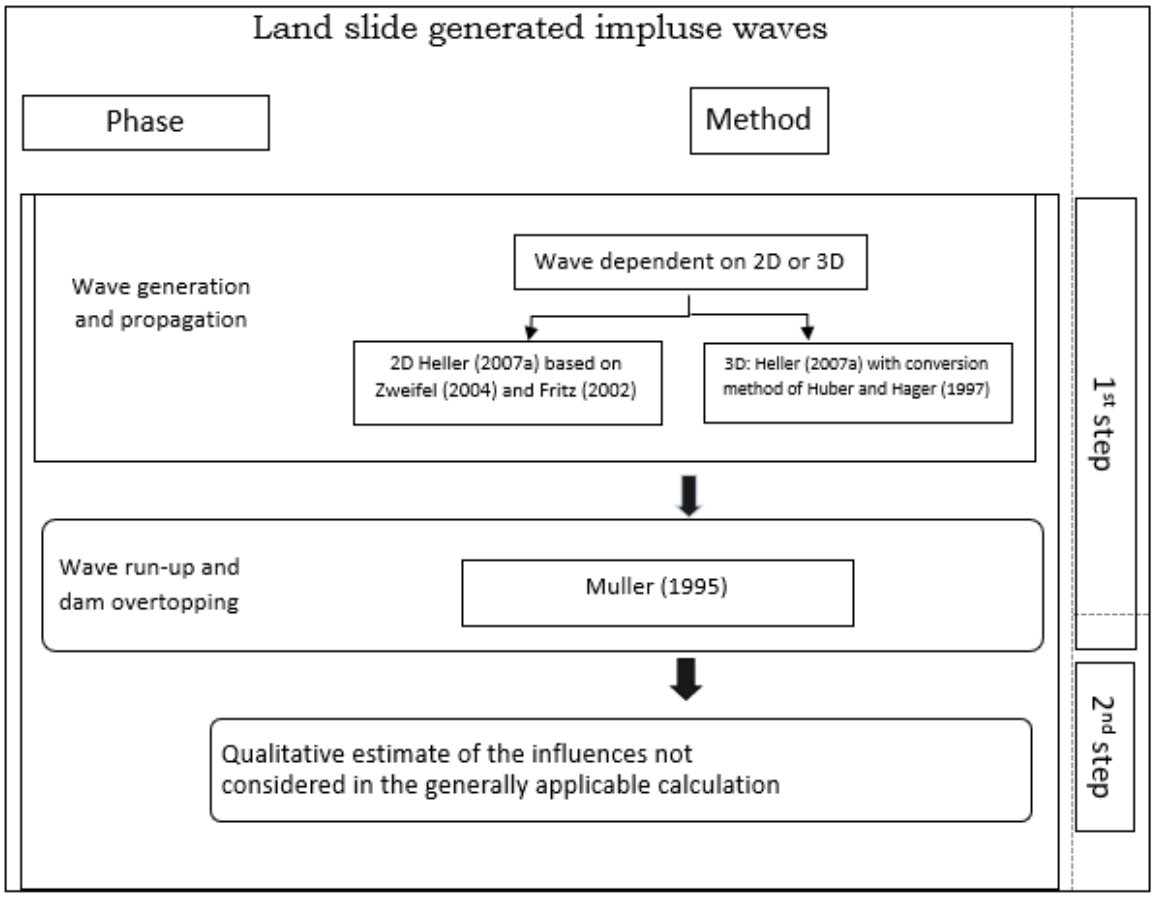

Figure 2. 8 Calculation process for impulse waves caused by landslides, including wave phases, calculation techniques, and section references (Heller et al., 2009).

The separate calculation equations are given after a brief overview, description, and clarification of the relevant governing parameters. Equations for channel-form reservoir geometry (2D) and equations for basin-form geometry (3D) are distinguished from those that are applicable in both 2D and 3D. This distinction includes the extremes of entirely free radial (3D) and restricted transverse (2D) wave propagation in reservoirs (Figure 2-9). The wave parameters for the general reservoir shape are determined by interpolating between these two extreme scenarios or by combining them. (Heller et al., 2009).

2.7.2. Wave generation and propagation

2.7.2.1. Introduction

The approach is predicated on formulas that are generally valid. The wave generation equations were created by experiments in the lab, either (a) in a rectangular wave basin (3D) or (b) in a prismatic wave channel (2D). Figure 2-10 depicts the two extreme examples (a) and (b), which can be defined up as follows (Heller et al., 2009).

- Extreme case (a): The slide mass strikes a long reservoir lengthwise, with a slide width that is equal to or greater than the reservoir width. The impulse waves can't spread laterally because they are constrained as they travel over the reservoir (Figure 2-9a).

- Extreme case (b): The slide mass enters the reservoir at whatever point it can, and the slide width is smaller than the reservoir. Because of the reservoir's geometry, the impulse wave can leave the slide impact zone fully freely and travel in all directions (Figure 2-9b).

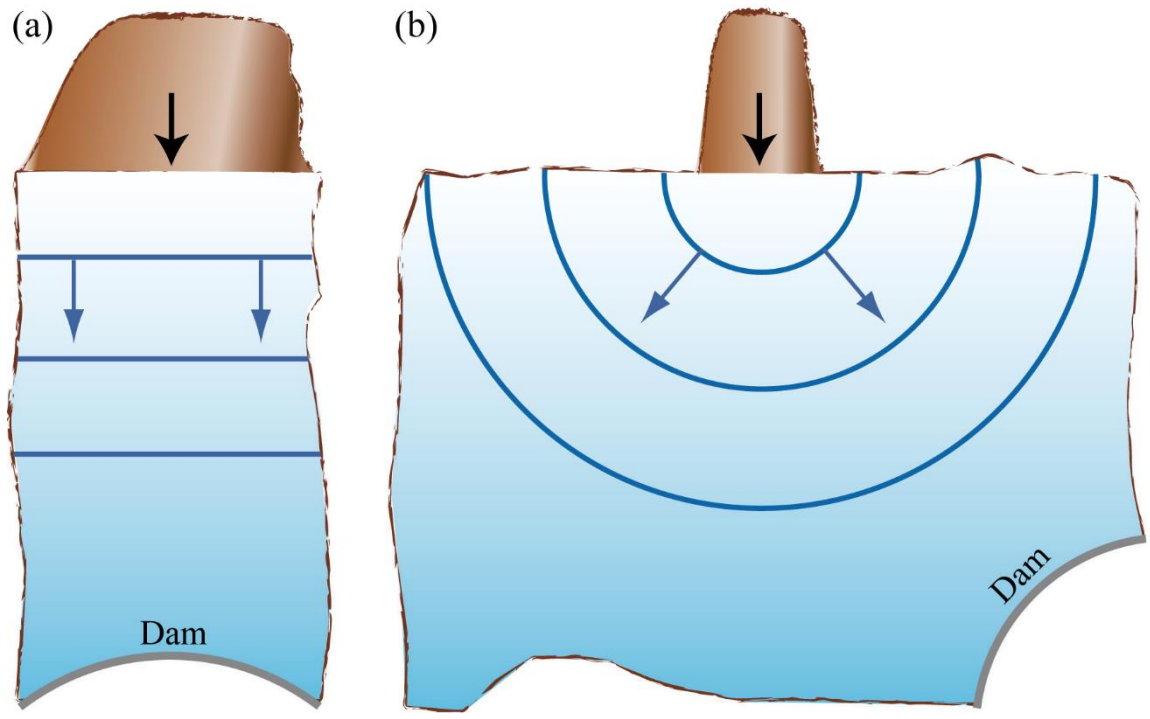

Figure 2. 9 Reservoir geometries for two idealized cases that are directly characterized by broadly applicable equations: (a) the extreme case (a) in which transverse wave propagation is confined and longitudinal impacting slide is present, and (b) the extreme case (b) in which transverse wave propagation is completely free and the slide impacts across the reservoir (Heller et al., 2009).

The calculation of the wave production for extreme instances (a) and (b) uses the same controlling parameters. In reality, for 2D and 3D examples close to the slide impact zone, the wave parameters only differ marginally (Huber 1980). The wave height falls more quickly than in case (a) because in extreme instance (b), impulse waves (and consequently their energy) spread over a larger area. As a result, the attenuation terms for the two situations are different.

To generalize the results to prototypes, the model testing needs to be geometrically similar to the prototypes. Model effects, such as the relative wave heights not correlating between model and prototype, may be caused by deviations in the geometry. Geometric shapes that are perfect for 2D and 3D model tests are shown in Figure 2.9. in the wave parameters that were computed for these two extreme examples (Heller et al., 2009).

2.7.2.2.Governing parameters

Figure 2-10 shows sketches highlighting key factors for the formation of impulse waves in (a) channel-form (2D) and (b) basin-form (3D) reservoirs. The estimations of the maximum

wave height H_M and the maximum wave amplitude a_M in both 2D and 3D cases depend on the following characteristics. (Heller et al., 2009).

- Slide impact velocity V_S
- Bulk slide volume $\forall_S$
- Slide thickness *s*
- Slide width or reservoir width *b*
- Bulk slide density ρ_S
- Bulk slide porosity *n*
- Slide impact angle α
- Still water depth *h*

Despite the fact that these have a insignificant effect on wave generation. Other regulating elements are the slide length ls and the slide front angle φ.

The junction of the still water level and the slide slope (Figure 2–10) serves as the basis of the coordinate system (x, z). The regulating factors of the slide are not related to the slide's initial position but rather to where it impacts the ground. The first six of the seven slide parameters listed above can change between the slide's starting position and its point of impact. The bulk slide porosity n is made up of the bulk slide volume $\forall_S$ and the bulk slide density ρ_S. Neither this nor the slide mass $m_S = \forall_S \cdot \rho_S$ are presented as independent parameters in the calculating process.

The formulae for converting between grain and bulk slide parameters are provided in Table 2-1. The bulk slide volume $\forall_S$ and the bulk slide density ρ_S, which take the bulk slide porosity n into account, must be distinguished from the slide grain volume $\forall_g$ and grain density ρ_g. (Heller et al., 2009).

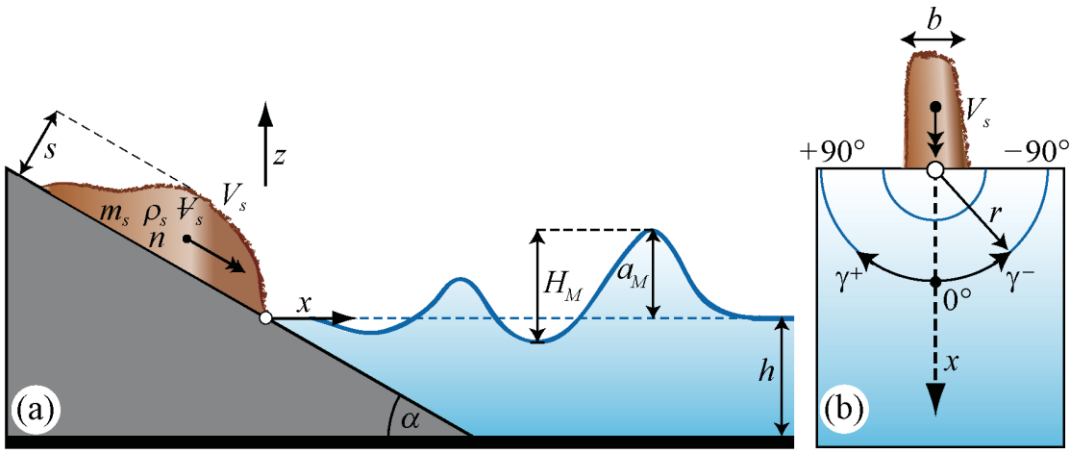

Figure 2. 10 Illustrations outlining the key wave parameters in (a) 2D and (b) 3D as well as the governing parameters for the formation of impulse waves (Heller et al., 2009).

Table 2. 1 Using the bulk slide porosity, grain to bulk slide characteristics can be converted and vice versa. (Heller et al., 2009).

	Granulate properties	Slide properties
Density	$\rho_g = \rho_s / (1-n)$	$\rho_s = (1-n)\rho_g$
Volume	$\forall_g = (1-n)\forall_s$	$\forall_s = \forall_{g/(1-n)}$

The maximum thickness of the slide at the time of impact, measured perpendicular to the slide slope, is known as the slide thickness (s). The average width at impact should be chosen to be slide width b. It is appropriate to consider b to be the reservoir width if the slide width is bigger than the reservoir width. The angle from the straight or the hill slope angle at the impact position is called the slide impact angle α (Figure 2-11a). This indicates the slide's impulse transmission angle on the water body. The average depth in the slide impact zone, along the slide axis (γ = 0°; Figure 2-11), is determined by taking the still water depth, h. The energy equation, which takes into account the resistance between the slide and the underlying slope of constant inclination, can be used to express the slide impact velocity Vs, which is that of the center of gravity of the slide mass during impact (Körner 1976).

$$V_s = \sqrt{2g \triangle Z_{sc}(1 - tan\delta cot\alpha)} \quad (2.2)$$

$g\left[m/s^2\right]$	=	Gravitational acceleration; g =9.81m/s^2
$V_s[m/s]$	=	Slide impact velocity (Figure 2-12)
α[°]	=	Slide impact angle (Figure 2-12)
δ[°]	=	Dynamic bed friction angle (Figure 2-12)
$\triangle Z_{sc}[m]$	=	Drop height of the center of gravity of the slide (Figure 2-12)

Figure 2-11(a) depicts the parameters in Eq. (2.2) for a slope with constant inclination. The vertical distance between the center of gravity of the slide mass in its initial location and where it will strike is known as the drop height of the center of gravity of the slide (ΔZ_{SC}). The friction at the point where the sliding mass and underlying slope come into contact is characterized by the dynamic bed resistance angle δ. As friction increases, the value of δ, which generally varies between 15° and 35°, also rises. A value of δ ≈ 20° can be taken regardless of whether or not the slide mass is composed of rock, ice, or snow (Hutter 2008). The average slope angle is the number for the slide impact angle α. The slide velocity at the point of slope change V_{SNK} may be derived from Eq. (2.2) by introducing values for the pertinent parameters Δz_{SCN}, δ_N and α_N. The gradient of the slope may vary at any point, as illustrated in Figure 2-11(b). With the value of V_{SNK} derived from Eq. (2.2), it is possible to calculate the increase in slide velocity to the slide impact velocity using Eq. (2.3) (Heller et al., 2009).

$$V_s = \sqrt{{V_{sNK}}^2 + 2g \triangle Z_{sc}(1 - tan\delta cot\alpha)} \quad (2.3)$$

$g\left[m/s^2\right]$	=	Gravitational acceleration; g =9.81m/s^2
$V_s[m/s]$	=	Slide impact velocity (Figure 2-12)
$V_{sNK}[m/s]$	=	Slide velocity at point of slope change (Figure 2-12b)
α[°]	=	Slide impact angle (Figure 2-12)
δ[°]	=	Dynamic bed friction angle (Figure 2-12)
$\triangle Z_{sc}[m]$	=	Drop height of the center of gravity of the slide (Figure 2-12)

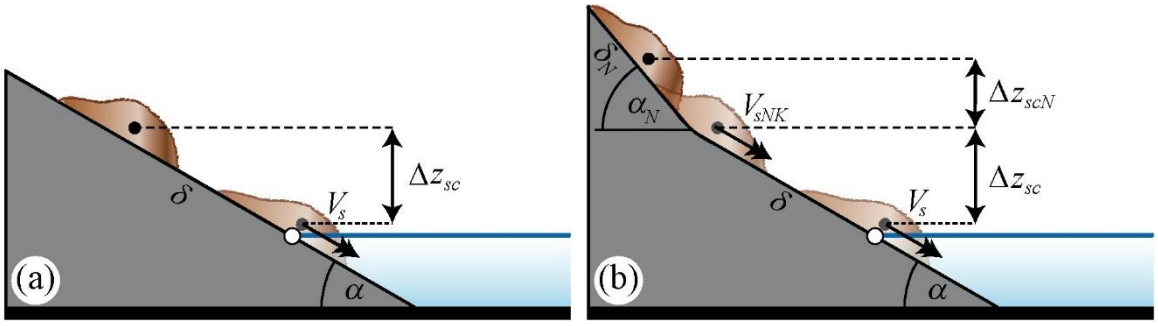

Figure 2. 11 Illustrations outlining the parameters for calculating the slide impact velocity Vs for (a) Slope of constant slide impact angle α and (b) for slopes with a slope change (Heller et al., 2009).

The following parameters (Figure 2-10) describe changes in an impulse wave formed and spreading in reservoirs with level, channel-form, or basin-form geometry.:

- Distance *x* (2D)
- Radial distance *r* (3D)
- Wave propagation angle γ (3D)

The impulse wave in a channel-form reservoir (2D; Figure 2.10a) solely varies in relation to the distance (x). Both the radial distance *r* and the wave propagation angle γ are important factors in a basin-form reservoir (3D; Figure 2-10b) (Heller et al., 2009).

2.7.2.3.Computation procedure

a) Values independent from 2D or 3D

The solitary wave celerity equation can be used to calculate the celerity c of an impulsive wave caused by landslides. The following equations apply to both extreme cases of idealistic reservoir shapes (a) and (b) (Heller et al., 2009).

$$c = [g(h + a)]^{1/2} \qquad (2.4)$$

$a[m]$	=	Wave amplitude (Figure 2-12)
$c[m/s]$	=	Wave celerity
$g[m/s^2]$	=	Gravitational acceleration; g =9.81m/s^2
$h[m]$	=	Still water depth

Locally or between two places, the value of c can be found. In the latter scenario, Eq. (2.4) is used to comprise the mean values of a and h between the two points. The wave height H

indirectly used to get the value of a. Applying Eqs. (2.7), (2.11), or (2.14) will accomplish this. For a given height of the wave H, the wave amplitude a of the impulse waves caused by subaerial landslides is:

$$a = (4 / 5)H \qquad (2.5)$$

$\alpha[m]$ = Wave amplitude (Figure 2-13)

$H[m]$ = Wave height (Figure 2-13)

In both 2D and 3D computations, the impulse product parameter P of Heller (2007) and Heller and Hager (2009) plays a significant part and is stated as

$$P = FS^{1/2}M^{1/4}\{\cos[(6/7)\alpha]\}^{1/2} \quad \text{for } 0.17 \leq P \leq 8.13 \qquad \ldots\ldots (2.6)$$

$b[m]$ = Slide width (Figure 2-11b)

$F[-]$ = Slide Froude number; $F=V_s/(gh)^{1/2}$

$g[m/s^2]$ = Gravitational acceleration; g =9.81m/s^2

$h[m]$ = Still water depth (in the slide impact zone)

$M[-]$ = Relative slide mass; $M = \rho_s \forall_s/(\rho_w bh^2)$

$s[m]$ = Slide thickness (Figure 2-11a)

$S[-]$ = Relative slide thickness (Figure 2-11a)

$V_s[m/s]$ = Slide impact velocity from Eq. (2.2) or Eq. (2.3) (Figure 2-11a)

$\forall_s[m^3]$ = Bulk slide volume (Figure 2-11a)

$\alpha[°]$ = Slide impact angle (Figure 2-11a)

$\rho_s[kg/m^3]$ = Bulk slide density (Figure 2-11a)

$\rho_w[kg/m^3]$ = Water density

Table 2. 2 Limitation for the computation of the impulse wave formation (Heller et al., 2009).

Term	Range	Meaning
Slide Froude number	$0.86 \leq F \leq 6.83$	$F = V_S/(gh)^{1/2}$
Relative slide thickness	$0.09 \leq S \leq 1.64$	$S = s/h$
Relative slide mass	$0.11 \leq M \leq 10.02$	$M = \rho_s \forall_s/(\rho_w bh^2)$
Relative slide density	$0.59 \leq D \leq 1.72$	$D = \rho_s/\rho_w$
Relative granulate density	$0.96 \leq \rho_g/\rho_w \leq 2.75$	ρ_g/ρ_w
Relative slide volume	$0.05 \leq V \leq 5.94$	$V = \forall_s/(bh^2)$
Bulk slide porosity	$30.7\% \leq n \leq 43.3\%$	n
Slide impact angle	$30° \leq \alpha \leq 90°$	α
Relative slide width	$0.74 \leq B \leq 3.33$	$B = b/h$
Relative radial distance	$5 \leq r/h \leq 30$	r/h

Wave propagation angle	$-90° \leq \gamma \leq 90°$	γ
Relative streamwise distance	$2.7 \leq X \leq 59.2$	$X = x/h$
Impulse product parameter	$0.17 \leq \mathrm{P} \leq 8.13$	$P = FS^{1/2}M^{1/4}\{cos[(6/7)\alpha]\}^{1/2}$

b) Extreme case (a) (2D)

The formulas given here are based on Heller (2007), as seen in Figure 2-8. They are employed in the computation of impulse waves that travel constrained longitudinally in a reservoir and follow the impact of a slide mass in a longitudinal path (Figure 2-9a; extreme example (a)). In terms of how impulse waves affect dams, height of the wave H and wave amplitude *a* are of utmost significance. Furthermore, consideration is given to the wave length L and wave period T, which, in accordance with the linear wave concept, are linked to the wave speed c as L = Tc. In the slide impact zone, a wall of water frequently forms the maximum wave height H_M rather than a coherent wave.

$$H_M = (5/9)\mathbf{P}^{4/5}h \qquad (2.7)$$

$h[m]$ = Still water depth (in the slide impact zone)
$H_M[m]$ = Maximum wave height (Figure 2-10a)
$\mathbf{P}[-]$ = Impulse product parameter from Eq. (2.6)

The maximum wave height's separation from the slide impact position x_M is calculated using

$$X_M = (11/2)\mathbf{P}^{1/2}h \qquad (2.8)$$

$h[m]$ = Still water depth (in the slide impact zone
$\mathbf{P}[-]$ = Impulse product parameter from Eq. (2.6)
$X_M[m]$ = The maximum wave amplitude's streamwise distance from the impact place (Figure 2-10a)

The maximum height of wave H_M 's maximum wave period T_M can be computed as

$$T_M = 9\mathbf{P}^{1/2}(h/g)^{1/2} \qquad (2.9)$$

$g[m/s^2]$ = Gravitational acceleration; g =9.81m/s^2
$h[m]$ = Still water depth (in the slide impact zone)
$H_M[m]$ = Maximum height of wave (Figure 2-10a)
$\boldsymbol{P}[-]$ = Impulse product parameter from Eq. (2.6)

$T_M[s]$ = Wave period from H_M

The wave length L_M of H_M shall be calculated using T_M from Eq. (2.9), L = T c, and the linear relationship between the two.

$$L_M = T_M c \qquad (2.10)$$

$c[m/s]$ = Solitary wave celerity from Eq. (2.4)
$H_M[m]$ = Maximum wave height (Figure 2-10a)
$L_M[m]$ = Length of wave H_M
$T_M[s]$ = Period of wave H_M

Not just the maximum wave height H_M in the slide impact zone, but also height of the wave at the dam or reservoir coast is needed for the evaluation of wave run-up. The streamwise coordinate x must also be taken into account (Figure 2-10a). If the wave height H required is placed farther from the slide impact site than where the maximum height of the wave H_M happens ($x/h = X > X_M = x_M/h$), Consequently height of wave H can be calculated as

$$H(x) = (3/4)\left(\mathbf{P}X^{-1/3}\right)^{4/5} h \qquad for\ X > X_M \qquad (2.11)$$

$h[m]$ = Still water depth (in the slide impact zone)
$H[m]$ = Wave height (Figure 2-12)
$\mathbf{P}[-]$ = Impulse product parameter from Eq. (2.6)
$x[m]$ = Streamwise coordinate in the direction of the longitudinal channel (Figure 2-10a)
$x_M[m]$ = The maximum wave amplitude's streamwise distance from the impact place
$X[-]$ = Relative streamwise distance; $X = x/h$
$X_M[-]$ = Relative streamwise distance between the hit location and the maximum wave amplitude $X_M = x_M/h$

Only apply equation (2.11) when $X_M < X$. The wave period T(x) is calculated as follows:

$$T(x) = 9\mathbf{P}^{1/4}X^{5/16}(h/g)^{1/2} \qquad for\ X > X_M \qquad (2.12)$$

$g[m/s^2]$ = Gravitational acceleration; g =9.81m/s^2
$h[m]$ = Still water depth (in the slide impact zone)
$\mathbf{P}[-]$ = Impulse product parameter from Eq. (2.6)

$T[s]$ = Wave period (Figure 2-12)
$x[m]$ = Streamwise coordinate in the direction of the longitudinal channel (Figure 2-10a)
$x_M[m]$ = The maximum wave amplitude's streamwise distance from the impact place
$X[-]$ = Relative streamwise distance; $X = x/h$
$X_M[-]$ = Relative streamwise distance between the hit location and the maximum wave amplitude $X_M = x_M/h$

According to the linear wave theory, the wave length L(x) can be calculated from

$$L(x) = T(x)c(x) \qquad (2.13)$$

$c[m/s]$ = Solitary wave celerity from Eq. (2.4)
$L[m]$ = Wave length (Figure 2.12)
$T[s]$ = Wave period from Eq. ((Figure 2.12)
$x[m]$ = Streamwise coordinate in the direction of the longitudinal channel (Figure 2.10a)

c) Extreme case (b) (3D)

Based on Heller (2007) and Huber and Hager's (1997) conversion technique, the equations for the 3D situation are shown in Figure 2.8. The extreme scenario (b) in Section 2.7.2 and Figure 2.9 b show how they can be utilized to analyze impulse waves that are traveling radially and fully freely in a reservoir. In the sliding impact zone, there is little alteration in the magnitude of the impulse waves between the 2D and 3D models (Huber, 1980). As a result, Eqs. (2.7), (2.9), and (2.10) can also be used to estimate the maximum values of height of the wave H_M in the slide impact zone as well as the associated period T_M and wave length L_M, respectively. For r/h > X_M, height of the wave H (r, γ) at any specific place in the reservoir can be calculated as

$$H(r,\gamma) = (3/2)P^{4/5}cos^2\left(\frac{2\gamma}{3}\right)(r/h)^{-2/3}h \qquad for \qquad r/h > X_M \qquad (2.14)$$

$h[m]$ = Still water depth (in the slide impact zone)
$H[m]$ = Wave height (Figure 2-12)
$P[-]$ = Impulse product parameter from Eq. (2.6)
$r[m]$ = Radial distance from the impact location in the wave basin (Figure 2-10b)
$x_M[m]$ = Streamwise distance of the maximum wave amplitude from the impact place
$X_M[-]$ = Relative streamwise distance of the maximum wave amplitude from the impact place $X_M = x_M/h$
$\gamma[°]$ = Wave propagation angle (Figure 2-10b)

From Eq. (2.14), height of the wave H (r, γ) and wave period T (r, γ) may be calculated as.

$$T(r,\gamma) = 15\left(\frac{H}{h}\right)^{1/4}(h/g)^{1/2} \qquad for\ r/h > X_M \qquad (2.15)$$

$g[m/s^2]$	=	Gravitational acceleration; g =9.81m/s^2
$h[m]$	=	Still water depth (in the slide impact zone)
$H[m]$	=	Wave height (Figure 2-12)
$P[-]$	=	Impulse product parameter from Eq. (2.6)
$r[m]$	=	Radial distance from the impact position in the wave basin (Figure 2-10b)
$x_M[m]$	=	Streamwise distance of the maximum wave amplitude from the impact position
$X_M[-]$	=	Relative streamwise distance of the maximum wave amplitude from the impact position $X_M = x_M/h$
$\gamma[°]$	=	Wave propagation angle (Figure 2-10b)

Finally, using the linear wave concept once more, length of the wave L (r, γ) is computed by

$$L(r,\gamma) = T(r,\gamma)c(r,\gamma) \qquad (2.16)$$

$c[m/s]$	=	Solitary wave celerity from Eq. (2.4)
$L[m]$	=	Wave length (Figure 2-12)
$r[m]$	=	Radial distance from the impact location in the wave basin (Figure 2-10b)
$T[s]$	=	Wave period from Eq. ((Figure 2-12)
$\gamma[°]$	=	Wave propagation angle (Figure 2-10b)

2.8. Wave run-up and dam overtopping

2.8.1. Introduction

The equations for wave run-up and dam overtopping, in contrast to wave formation, are only based on 2D investigations. In general, it is not possible to account for 3D variables like as the curvature of the dam or asymmetric wave impact angles. After the first calculation is finished, they must be calculated in the second phase using the generally applicable formula (Heller et al., 2009).

2.8.2. Governing parameters

A drawing outlining the impacts of impulse waves on dams is depicted in Figure 2-12 along with the appropriate parameters. The following variables can affect the run-up height R and the overtopping volume ~~V~~ per unit length dam crest (Heller et al., 2009).

a) Wave height, H (2D)

b) Wave amplitude, a (2D)

c) Wave length, L (2D)

d) Wave period, T (2D)

e) Still water depth, h (2D)

f) Run-up angle equal to dam face slope, β (2D)

g) Freeboard, f (2D)

h) Crest width b_K (2D)

The incoming impulse wave is characterized by the first four variables H, a, L, and T. They express of the cross-section before the dam, where the dam has not yet had an impact on them (Figure 2-12). The level directly upstream of the dam should be considered the still water depth at h. The run-up angle β is computed from the horizontal (Figure 2-12). The freeboard *f* and the dam crest width, b_K are significant for the overtopping volume ~~V~~ per dam crest unit length as seen in Figure 2-12.

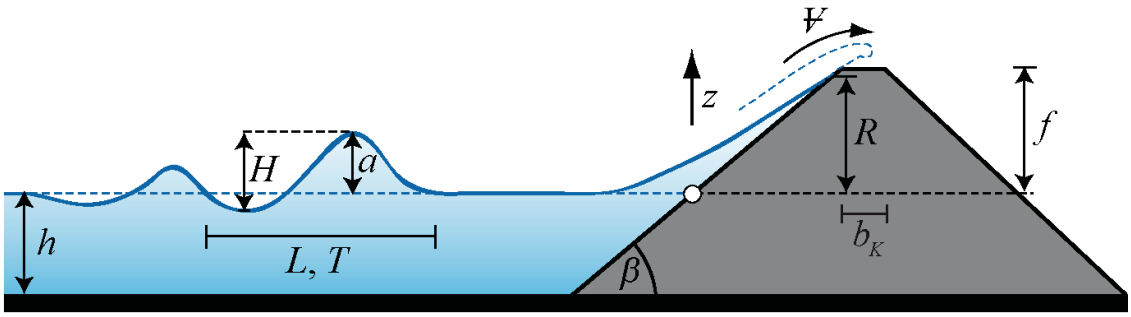

Figure 2. 12 Diagram outlining the conditions for the dam overtopping and wave run-up (Heller et al., 2009).

2.8.3. Wave run-up and overtopping

The following formulas are obtained from Müller (1995) (Figure 2–8). the run-up height R may calculate by using

$$R = 1.25\left(\frac{H}{h}\right)^{5/4}\left(\frac{H}{L}\right)^{-3/20}\left(\frac{90°}{\beta}\right)^{1/5} h \qquad (2.17)$$

$h[m]$ = Still water depth (in front of the dam)
$H[m]$ = Wave height (in front of the dam) (Figure 2-12)
$L[m]$ = Wave length (in front of the dam) (Figure 2-12)
$R[m]$ = Run-up height (Figure 2-12)
$\beta[°]$ = Run-up angle equal to dam face slope (Figure 2-12)

Table 2. 3 Limitation for the computation of the wave run –up (Heller et al., 2009).

Term	Range
Relative wave height	$0.011 \leq H/h \leq 0.521$
Wave steepness	$0.001 \leq H/L \leq 0.013$
Relative angle	$1.0 \leq 90°/\beta \leq 4.9$

An intermediary step is necessary to calculate the overtopping volume per unit length of the dam crest ~~V~~. The first step is to determine the overtopping volume $\sim\!\!V_0$ per dam crest unit length for f = 0.

$$\forall_0 = 1.45k\left(\frac{H}{h}\right)^{4/3}\left(\frac{T}{\sqrt{h/g}}\right)^{4/9}h^2 \qquad (2.18)$$

f[m]	=	Freeboard (figure 2-12)
g[m/s^2]	=	Gravitational acceleration; g =9.81m/s^2
h[m]	=	Still water depth (in front of the dam)
H[m]	=	Wave height (in front of the dam) (Figure 2-12)
T[s]	=	Wave period from Eq. ((Figure 2-12)
$\forall_0$[m^3/m]	=	Overtopping volume per unit length dam crest for f =0
k[−]	=	Overfall coefficient for overtopping; $k = k_q k_b k_w{}^{3/2}$
k_b[−]	=	Overfall coefficient for crest width
k_q[−]	=	Overfall coefficient for steady case
k_w[−]	=	Overfall coefficient for the increased flow energy compared with the steady case

Similar to the Poleni formula, the overfall coefficient in Eq. (2.18) was defined as $\kappa = \kappa_q \kappa_b \kappa_w{}^{3/2}$ (see, for example, Hager 1995). Here, κ_q is the overfall coefficient for the steady case, κ_b accounts for the dam's crest width's influence, and κ_w accounts for the larger wave energy than in the steady case, leading to a faster flow rate over the dam. Values of the three are:

(a) κ_q = 0.41 (β = 90°), κ_q = 0.47 (β = 45°) and κ_q = 0.51 (β = 18.4°), which allows for the interpolation of intermediate values

(a) κ_b is get from Figure 2-13(a) as a function of the relative maximum over- topping depth $a_{Max,T}/b_K$ and

(b) κ_w = 1.3 for the entire range 18.4° ≤ β ≤ 90°.

Figure 2-13(b) shows the greatest depth at which overtopping occurs over the dam (aMax, T). Since this is significantly larger than the wave amplitude an in front of the dam, Müller (1995) found that it is roughly similar to the wave height H in front of the dam. See Figure 2-12).

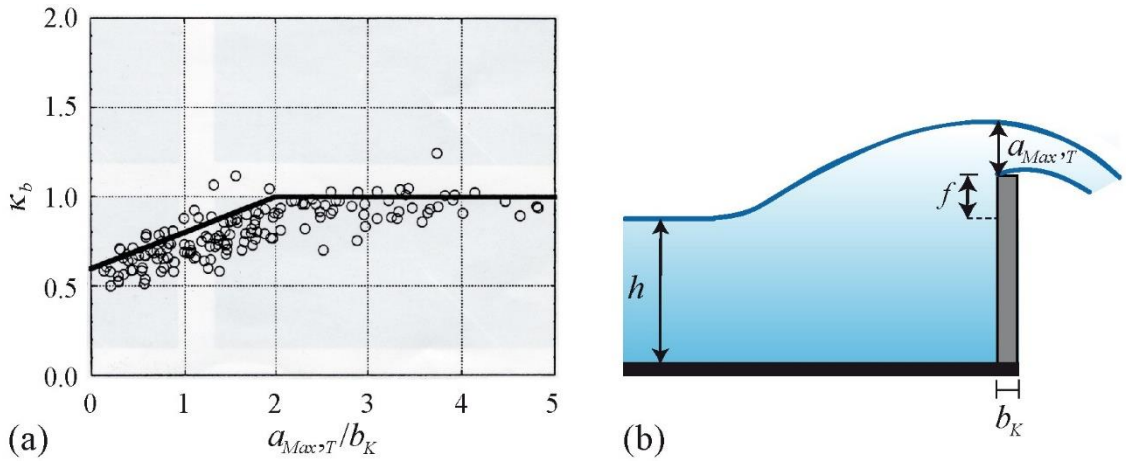

Figure 2. 13 (a) The crest width b_K's overfall coefficient, κ b, as a function of the maximum overtopping depth $a_{Max,T}$ / b_K over a dam (Müller 1995). and (b) a matching definition diagram (Heller et al., 2009).

According to Eq. (2.18), the overtopping volume $\forall_0$ per unit length dam crest for $f = 0$ will be reduced in the prototype since the freeboard is often more than zero. If $f > 0$, the equation for the dam crest's overtopping volume per unit length is derived as.

$$\forall = \left(1 - \frac{f}{R}\right)^{11/5} \forall_0 \qquad (2.19)$$

f[m]	=	Freeboard (figure 2-12)
R[m]	=	Run-up height (Figure 2-12)
$\forall[m^3/m]$	=	Overtopping volume per dam crest unit length (Figure 2-12)
$\forall_0[m^3/m]$	=	Overtopping volume per dam crest unit length for f =0

Table 2. 4 Restrictions on the overtopping computation (Heller et al., 2009).

Term	**Range**	**Term**	**Range**
Relative wave height	$0.019 \leq H/h \leq 0.488$	Relative wave celerity	$0.83 \leq c^2/(gh) \leq 1.40$
Non-linearity	$0.59 \leq \alpha/H \leq 0.95$	Relative wave length	$60. \leq L/h \leq 24.0$
Wave steepness	$0.001 \leq H/L \leq 0.023$	Relative angle	$1.0 \leq 90°/\beta \leq 4.9$
Relative period	$9.0 \leq T(g\ /\ h)^{1/2} \leq 21.0$		

The discharge per unit length of the dam crest is also significant in addition to $\forall$. According to Müller (1995), only the average discharge q_{0m} per dam crest unit length for $f = 0$ can be

estimated, and for this, Müller (1995) found that the duration of overtopping t0 for f = 0, as a function of the wave period with larger difference of −12% is

$$t_0 = 4\left(T\sqrt{g/h}\right)^{4/9}(h/g)^{1/2} \qquad (2.20)$$

$g[m/s^2]$ = Gravitational acceleration; g =9.81m/s^2
$h[m]$ = Still water depth (in front of the dam)
$t_0[s]$ = Duration of overtopping for f=0
$T[s]$ = Wave period from Eq. ((Figure 2-13)

For f=0, the average discharge q_{0m} per dam crest unit length is calculated from

$$q_{0m} = \forall_0/t_0 \qquad (2.21)$$

$q_{0m}[m^2/s]$ = Average discharge per unit length dam crest for f=0
$t_0[s]$ = Duration of overtopping for f=0
$\forall_0[m^3/m]$ = Overtopping volume per unit length dam crest for f =0

for f = 0, The maximum discharge $q0M$ per unit length dam crest is q0M ≈ 2·q0m

Table 2. 5 Restrictions for the computation of the duration of overtopping t_0 (Heller et al., 2009).

Term	**Range**
Relative period	$14 \leq T(g/h)^{1/2} \leq 22$
Relative duration of overtopping	$10.5 \leq t_0(g/h)^{1/2} \leq 13.5$

For f > 0, there is no empirical equation available for the discharge. As $\forall$ less than $\forall_0$, the values of q_{0m} and q_{0M} are higher for f = 0 and serve as upper limiting values for the unknown values with f > 0.

In addition to Heller et al. (2009), Kobel et al. (2017) also provide a one-step solution for forecasting the overtopping volume caused by solitary waves on inflexible dams while taking into account two approaches. The upstream dam slope is not taken into account in the first formula (Eq. (2.22), but it is in the second formula (Eq. (2.23).

$$\frac{V}{bh^2} = 1.42\left[\varepsilon\left(\frac{h}{w}\right)^{2.5}\left(\frac{a_w}{b_k}\right)^{0.105}\right]^{0.8} = 1.42{W_1}^{0.8}; \qquad (2.22)$$

with limitations; $0.35 < {W_1}^{0.8} < 0.95,\ 0.07 < b_k/w\ < 0.53$.

$$\frac{V}{bh^2} = 1.35\left[\varepsilon\left(\frac{h}{w}\right)^{(2/\varepsilon)\left(\beta/90^\circ\right)^{0.25}}\left(\frac{a_w}{b_k}\right)^{0.105}\right]^{0.7} = 1.35{W_2}^{0.7}; \qquad (2.23)$$

with limitations; $0.15 < {W_2}^{0.7} < 0.95$, $0.07 < b_k/w < 0.53$.

$$\varepsilon = \frac{a}{h} \text{ and } a_w = h + a - w$$

where,

a	Amplitude
h	Still water depth
β	Run-up angle at dam
ε	Relative wave amplitude
w	Dam height
h/w	Relative still-water depth
a_w	Effective wave amplitude
b_k	Dam crest width
a_w/b_k	Relative maximum wave height
β/90	Relative angle
b	slide width
V	Overtopping volume
W	Wave overtopping volume parameter

Additionally, Kobel et al. (2017) provided two equations to calculate the maximum overtopping depth over the dam crest caused by waves formed by landslides. The adjusted d_o/w versus the relative wave amplitude ε, the relative still water depth h/w, and the dam front face angle β follows the empirical fit with R^2= 0.95 and R^2 = 0.99 respectively as:

$$\frac{d_o}{w} = 1.34\left[\varepsilon\left(\frac{h}{w}\right)^{1.7}\left(\frac{\beta}{90^\circ}\right)^{0.25}\right] = 1.34E_1; 0.40 < E_1 < 0.70 \qquad (2.24)$$

and

$$\frac{d_o}{w} = 1.32\left[\varepsilon\left(\frac{h}{w}\right)^{4\left[(\beta/90^\circ)^{-0.21}-\varepsilon\right]}\left(\frac{\beta}{90^\circ}\right)^{0.16}\right] = 1.34E_2; 0.10 < E_2 < 0.75 \ldots\ldots \quad (2.25)$$

Where,

d_0	Overtopping height
d_0/w	Relative overtopping depth
E_1	Overtopping volume parameter while taking the relative wave amplitude into account
R^2	Coefficient of determination

2.9. 2nd step and safety allowance

2.9.1. Introduction

In comparison to those determined in the first step, the influences discussed below may result in substantial variations to the wave characteristics and subsequently the run-up heights. According to Tables 2-2, 2-3, 2-4, and 2-5, the effects of going beyond the threshold for the determining of impulse waves must also be taken into account in this second step. Large variations from the values generated in the first step due to violating the relevant constraints are often not anticipated, but they do raise the extent of ambiguity (Heller et al., 2009).
If the slide volume is big in comparison to the reservoir capacity, a displacement mechanism will also be present in addition to the impulse transmission. The approach in Figure 2-8 does not account for the subsequent increase in reservoir level, but one can approximate it by dividing the slide volume by the reservoir's surface area. (Heller et al., 2009).
The equations are based on a horizontal bed and either a rectangular, 3D wave basin or a 2D prismatic channel. The impact which a reservoir geometry changing from one or the other of these ideal forms has on the wave parameters. Although the equations are based on granular slide movement, mass movement can also involve a solid entity. (Heller et al., 2009).

2.9.2. Effects of the reservoir shape

In accordance with Figure 2-9, this Section examines the impacts of reservoir shape that deviate from the two extreme instances of (a) limited transversal and (b) totally free, radial propagation of the generated waves. They are shown here so that, in the second step, according to Figure 2-8, their effect on wave height and, consequently, on run-up height, may be qualitatively analyzed. Impulse wave propagation is significantly impacted by the reservoir's geometry (Camfield, 1980). A deep-water wave ($L/h < 2$) initially transforms into an intermediate-water wave ($2 < L/h < 20$), then becomes a shallow-water wave (L/h > 20), i.e., is impacted by the bottom, as the still water depth h lowers. Since the friction losses of the bed can be overlooked in comparison to shoaling, the contact with the bed typically causes an rise in wave height. Shoaling and refraction both have an impact on waves in shallow water. Any wave will be vulnerable to diffraction, constriction, and reflection regardless of whether it is classified as a shallow, intermediate, or deep-water wave (Coastal Engineering Manual USCE 2006). These outcomes can be summarized as follows:

.

a) Refraction (Figure 2-14a): A wave in shallow water reverses direction so that it primarily crashes onto the shore.

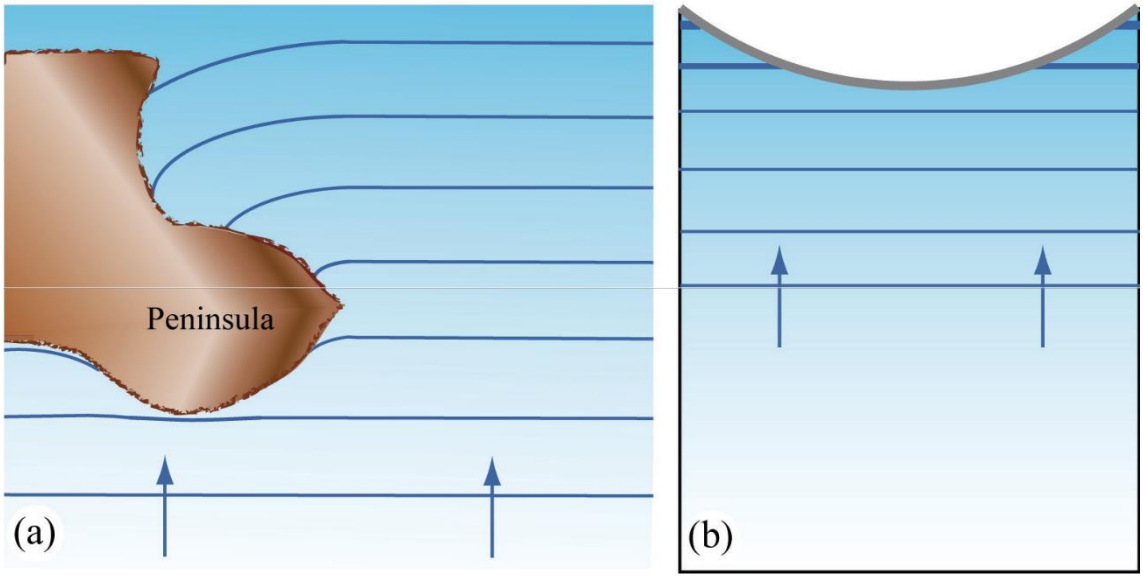

Figure 2. 14 (a) Principles of refraction near a shore and diffraction around a peninsula and (b) wave height increase resulting from constrictions near the flanks of an arch dam (Heller et al., 2009).

b) Shoaling (Figure 2-15b): A rise in wave height in shallow water occurs at the same time as a decrease in wave length. According to Dean and Dalrymple (1991), the shoaling-related increase in wave height can be calculated as

$$\frac{H_2}{H_1} = \left(\frac{h_1}{h_2}\right)^{1/4} \left(\frac{b_1}{b_2}\right)^{1/2} \qquad \ldots\ldots\ldots (2.26)$$

$b_1[m]$ = Reservoir width at cross-section 1 of Figure 2-15(b)
$b_2[m]$ = Reservoir width at cross-section 2 of Figure 2-15(b)
$h_1[m]$ = Still water depth at cross-section 1 of Figure 2-15(b)
$h_2[m]$ = Still water depth at cross-section 2 of Figure 2-15(b)
$H_1[m]$ = Wave height at cross-section 1 of Figure 2-15(b)
$H_2[m]$ = Wave height at cross-section 2 of Figure 2-15(b)

c) Diffraction (Figure 2-14a): A wave moves through an obstruction and releases some of its energy lateral to the wave shadow.

d) Constriction (Figure 2-14b): Due to the concentration of wave energy, a wave in a restricted area of a reservoir will heighten. This might happen, for instance, against a dam's flank. Eq. (4.1) can be used to estimate shallow-water waves once more, and for deep-water waves, it can be simplified to $H_2/H_1 = (b_1/b_2)^{1/2}$ because $h2 \approx h1$.

e) Reflection (Figure 2-15a): A wave is reflected when it reaches the coast and returns with less height. The amount of wave energy lost during run-up determines the height of the reflected wave. Since wave overtopping cannot occur against vertical-faced dams, there is essentially little energy dissipation during run-up, resulting in 100% reflection. The height and amplitude of the reflected wave are actually similar as the arriving wave $a \approx aR$ (Figure 2-15a). If neither of the waves has broken, non-linear superposition occurs where an approaching wave meets a reflected wave.

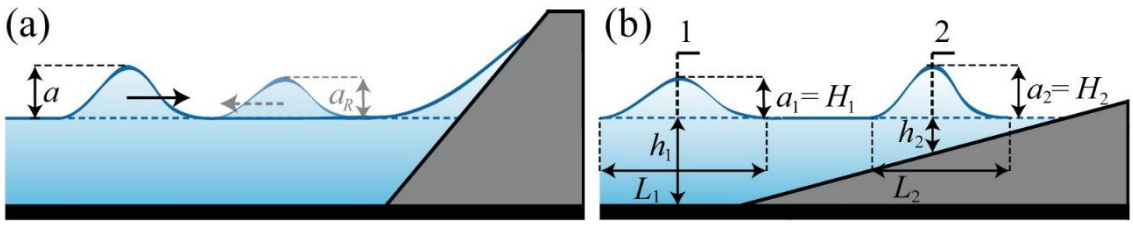

Figure 2. 15 Principle sketches from (a) reflection of a solitary wave by the face of a dam with a > aR and (b) Shoaling of a solitary wave close to the shore with a1 < a2 and L1 > L2 (Heller et al., 2009).

2.9.3. Mass Movement Types

The aforementioned formulas assume that the slide is made of granular material. However, there are many other kinds of mass movement in the natural world. When a mass is moving as a solid body, the wave height H is roughly equal to that of granular material for high impact speeds, but significantly higher for low impact velocities. Water can enter the pore volume when a granular slide impacts at a low velocity, however all the water is displaced by a solid body with porosity $n \approx 0$. Moreover, the shape of a granular slide may change during impact (Zweifel 2004).

Classification aids in determining whether a mass travels as a solid body or a granular slide.

The mass movement types and associated procedures for rock, debris, or soil are covered in the section, according to Cruden and Varnes (1996). This knowledge aids in understanding glacier calving, snow and ice avalanches, and other related phenomena. Nemcok et al. (1972), for example, develop a different classification.

Generally speaking, a mass movement can be described by two nouns: the material in question and the movement type, such as a landslide or rockfall. Five types of mass movements were recognized by Cruden and Varnes (1996) (Figure 2-16):

- **Sliding**: The slide mass can be translated on a plane or rotated along a curved concave slide plane (Figure 2-16a). Slides can travel in two different ways: as a solid body or as a granular mass. In the latter situation, the bulk slide volume $\forall_S$ rises proportionally up to the impact zone.
- **Flowing**: the mass acts as a viscous liquid. (Figure 2-16b).
- **Falling**: If the hill slope angle $\alpha > 76°$, a fall may be considered to be primarily free-fall; if this angle is smaller, the mass descends onto the slope where it may break. (Figure 2-16c).
- **Toppling**: The mass rotates about an axis that is below its center of gravity (Figure 2-16d).
- **Spreading**: The bulk breaks up into smaller pieces as it spreads. The most frequent cause of this movement type, which happens when the slope angle is between 0.3° and 5°, is an earthquake. This type of movement is rarely important for the generation of impulse waves, especially in Alpine locations. (Figure 2-16e)

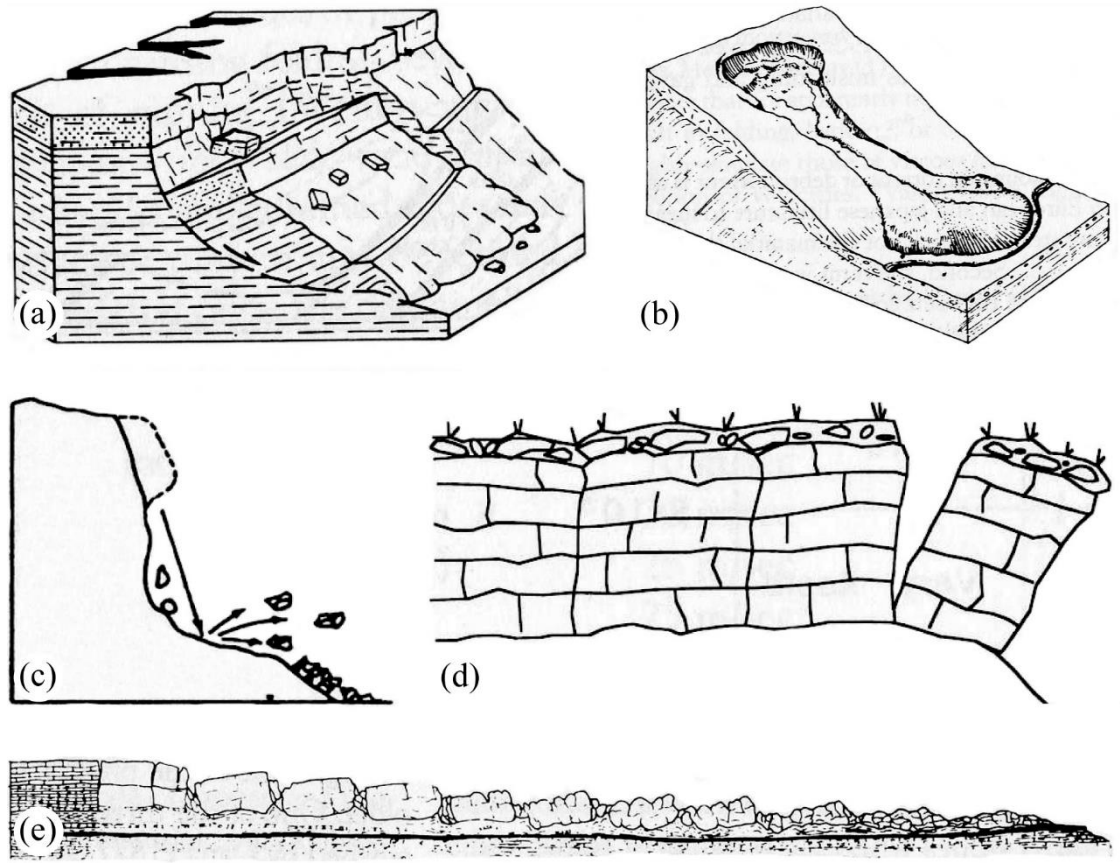

Figure 2. 16 Mass movement types: (a) sliding (b) flowing (c) falling (d) toppling and (e) spreading (Cruden and Varnes 1996).

Zweifel (2004) investigated the distinction between impulse waves produced by solid bodies and granular slides. With a solid body of constant density ρ_S = 1,340 kg/m^3 and a range of still water depths h between 0.15 m and 0.6 m, he conducted 11 tests. As opposed to the 11 tests of Zweifel (2004), the majority of the equations in Subsection 3.2.3 are based on tests carried out using granular slides in the same hydraulic model. He has $0.5 \leq F \leq 2.8$, $0.3 \leq S \leq 1.4$, $0.3 \leq M \leq 4.1$ and $\alpha = 45°$ as his dimensionless parameters.

Zweifel (2004) compared the maximum wave amplitudes aMb caused by solid substances with matching values from empirical equations for the maximum wave amplitudes aM (Figure 2-10) caused by a granular slide. Figure 2-17 displays this comparison. Plotting the highest wave amplitude relative percentage difference (aMb /h − aM /h)/ (aMb /h) against the slide Froude number F on the abscissa. The maximum wave height H_M from Eq. (2.7) can be multiplied by the coefficient (4/5) to get a_M. Figure 2-17 shows a description of the differences between the maximum wave amplitudes produced by a solid body and granular slide with a coefficient of determination R^2 = 0.97 and a deviation of less than ±10%.

$$\frac{\alpha_{Mb}\,|h-\alpha_M|h}{\alpha_{Mb}/h} = 1 - 0.26\text{F} \qquad \text{for } 0.5 \leq \text{F} \leq 3.0 \qquad (2.27)$$

$\alpha_M[m]$	=	Maximum wave amplitude (due to granular slide)
$\alpha_{Mb}[m]$	=	Maximum wave amplitude as result of a solid body
$\text{F}[-]$	=	Slide Froude number; F=$F = V_s/(gh)^{1/2}$
$g\left[{}^{m}/_{s^2}\right]$	=	Gravitational acceleration; g =9.81m/s^2
$h[m]$	=	Still water depth (in the slide impact zone)
$V_s[{}^{m}/_{s}]$	=	Slide impact velocity

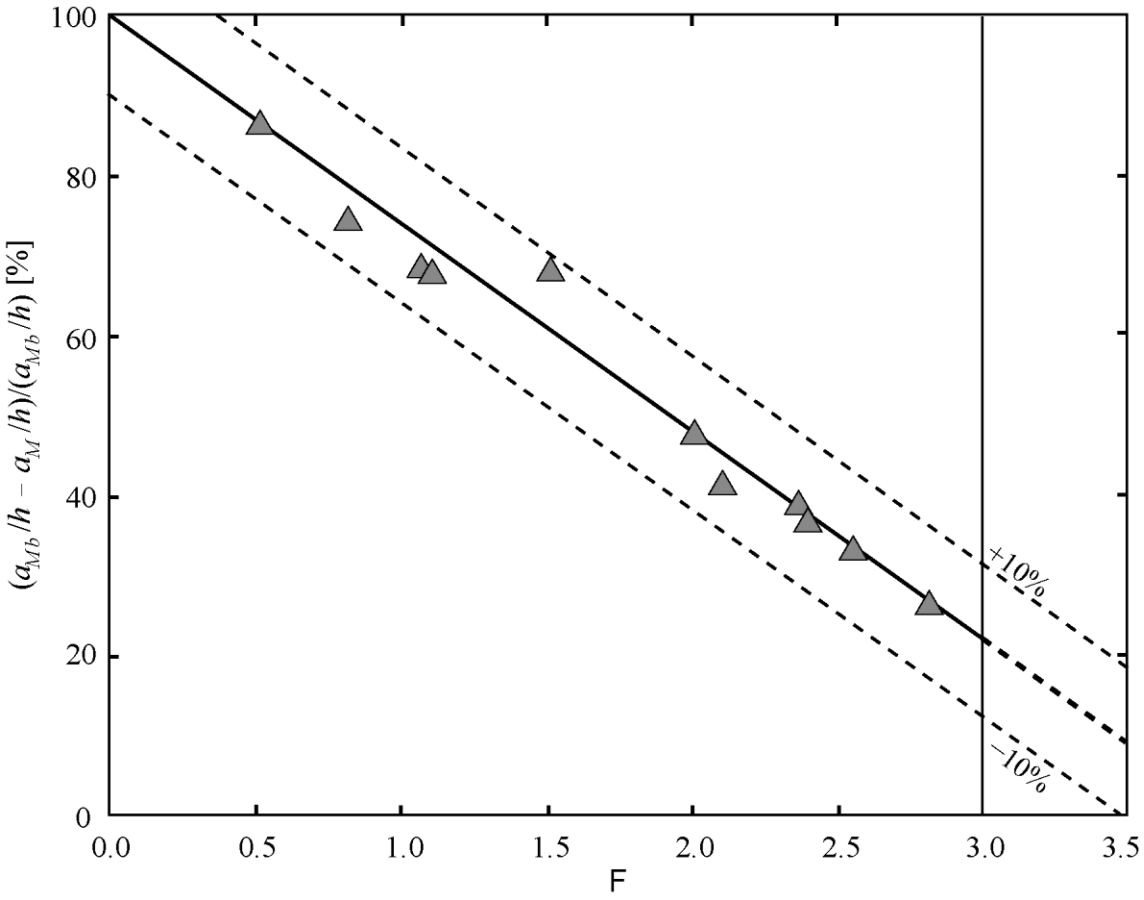

Figure 2. 17. Comparison between the maximum wave amplitude generated by a solid body and a granular slide (after Zweifel 2004).

Zweifel (2004) found that the maximum wave amplitude aMb for solid bodies is up to seven times bigger than for granular slides, but the difference is negligible for F > 3.0. This is due to the fact that water cannot enter the pore volume of the slide at high Froude numbers and slide impact velocities Vs. Zweifel's (2004) comparison only takes into account the highest wave amplitude, or a_M, within a fairly small range. More inclusive researches on this effect have not been conducted.

2.10. Consequences of overtopping of dam

In hilly terrain, landslides frequently happen during or after periods of heavy rainfall, causing fatalities as well as harm to the built environment and/or the natural environment (Fuchu et al., 2002). Landslides are naturally triggered by earthquakes, torrential rain, and volcanic eruptions (Kessarkar et al. 2011). On the other side, anthropogenic triggering mechanisms include human activities like deforestation and slope disturbance (slope cutting). The frequent changes in the reservoir's water level, caused by variations in pore water pressure, will make the slope adjacent to the reservoir susceptible to landslides in projects with high dam reservoirs.

One of the most important geological phenomena is a land slide, which results in fatalities as well as significant damage to civil engineering facilities like houses, bridges, roads, dams, and hydropower plants (Fuchu et al., 2002).

2.11. History of land slide in the world

The stability of reservoir slopes, which could pose risks to reservoirs and dams, has drawn more attention in several parts of the world. Jones et al. (1961) analyzed 500 landslides that were connected to the building of the Grand Coulee Dam in Washington State (USA) in the early 1960s. According to the findings of these investigations, 49% of the landslides happened when the reservoir was filling up and 30% happened when it was drawing down. For a Japanese case study, Nakamura (1990) determined that around 60% of reservoir landslides were sparked by a sudden drop in water level and another 40% by a rise in water level.

According to Schuster (1979), landslides brought on by changes in reservoir water levels involve a variety of geologic elements and movements. These studies collectively provide compelling evidence of how reservoirs affect the stability of adjacent slopes.

Our understanding of the impact of reservoirs on the stability of nearby slopes can be improved by studying the Vajont landslide of October 9, 1963 (Kilburn and Petley 2003). The Vajont landslide has been back-analyzed in depth by Paronuzzi et al. (2013) to investigate the impact of reservoir activities (filling and drawdown) on the stability of the slope of Monte Toc. The pace of filling and

drawdown, which had a significant impact on the slope stability, was identified by the authors as the primary destabilizing factor in the landslide.

In mountainous regions, large landslides or debris flows resulting from storms or earthquakes frequently obstruct rivers and create landslide dams. When the landslide dam fails, the region upstream is buried underwater and the area downstream is inundated. In the northern region of Nagano Prefecture in central Japan, as many as 22 landslide dams have developed in recorded history; and all except three have subsequently collapsed. These dams were formed upstream of the Shinano River and the Hime River. This region, which is situated at the western end of the "Fossa Magna" major tectonic line, has a geotectonic background that is likely to be the origin of the abundance of landslide dams. The authors of this study looked at three significant historical landslide dams and outburst disasters in the north Fossa Magna region (Kimio. I, Toshio. M, and Takahisa. M 2012).

In 1974, the 105m high, 297m long rockfill dam on the Aliakmon River was built in Polyphyton, north-central Greece, 80 kilometers southwest of Thessaloniki. Downstream, two additional smaller dams and reservoirs have been built. A 360MW hydroelectric power plant is housed in the 2 km^2 Polyphyton Reservoir, which also has a capacity for around $2x10^9$ m^3 of water. The "Alexis" landslide, which is located next to the dam's spillway (Riemer et al., 1996), and the "Beta" landslide, which is located about 1 km upstream, are two significant landslides that are slow creeping (average velocity 10-15 cm/year, but with peaks of the order of 1 cm/day; Riemer et al., 1996). Compared to the rock mass that caused the Vaiont (North Italy) disaster in 1963, both landslides affect substantially smaller rock masses (Petley, 2000). The Polyphyton Reservoir landslides, however, are still active and close to the Polyphyton Dam's rockfill. Due to this, these landslides have been thoroughly investigated using geodetic methods for roughly 20 years. This geodetic monitoring system's objective was to spot accelerations in the landslide's movement and signal the need for immediate action.

The risk of landslides is one of the most important environmental barriers to Ethiopia's development, acting as a barrier to urbanization, infrastructure development, and, more broadly, to all operations carried out on or at the base of slopes (Abebe et al., 2010). More than 200 homes were demolished, more than 500 km of roads were disrupted, and around 300 people lost their lives

as a result of landslides in Ethiopia from 1993 to 1998 alone (Ayalew, 1999). Variable topographical, geological, hydrological, and lands-use characteristics define Ethiopia's hilly and mountainous terrains. There have been imposing landslide events in the northern Omo River basin, the lower Wabe shebelle river valley, the Wendo Genet slope, the Blue Nile gorge, the town of Dessie, the Wudmen area in Weldiya, the Gilgel Gibe River, the Uba Dema village in Sawla, and portions of Tigray (Abebe et al., 2010).

The effects of slides on a reservoir and dam have not been well researched, despite the fact that the majority of Ethiopia's dams are built on reservoirs with steep slopes. Nevertheless, there are instances of slides entering reservoirs in Ethiopia. One such is the Gilgel Gibe catchment, where silt from landslides that entered the reservoir was recorded as coming from the Gilgel Gibe I hydroelectric power station (Broothaerts et al., 2012).

Due to its steep reservoir barrier, constrained reservoir geometry, potential for massive slide masses, and high impact velocities, the Tekeze arch dam is determined to be vulnerable to landslide-triggered impulse waves (Aman et al., 2019). As a result, a large slide happened in April 2008 close to the Tekeze dam site. to avoid the creeping slides from collapsing into the reservoir, a retaining wall has been built along the reservoir gorges (Hailemariam Gugsa and Schneider, 2010).

2.12. Landslide Models

2.12.1. Overlay analysis (Arc GIS)

In GIS, overlay analysis is the process of combining numerous layers of datasets reflecting various topics in order to analyze or determine the relationships between each layer. By combining various attribute and geometry of datasets or entities, overlay analysis represents the composite map. Overlay is the comparison of variables over various coverages. By combining data from two or more input data layers, new spatial data sets are produced in the overlay analysis. Undoubtedly one of the most popular and effective GIS techniques is overlay analysis. It uses common coordinate systems to analyze the many layers and identify what is on the top layer. Overlay operations create new geometries and units of change by combining data from the same entity or from separate entities. (Ahlqvist O. 2009).

Raster dataset overlays combine map algebra or pixel-based calculations. Cell-by-cell combination or operation is the term used for it. It requires less computational power. Raster datasets with overlay typically contain two or more distinct sets of data that come from the same grid. Typically, each unique collection of data consists of specified numerical values. These values are mathematically combined in the raster to provide a fresh set of values for just one output layer. The raster-based overlay is used to build risk surfaces and perform other procedures such as sustainability and value assessments. (Ahlqvist O. 2009).

2.12.2. ILWIS

The Integrated Land and Water Information System is known by the abbreviation ILWIS. It is an image processing-capable Geographic Information System (GIS). The International Institute for Aerospace Survey and Earth Sciences (ITC), located in Enschede, the Netherlands, created ILWIS. ILWIS lets you enter, organize, analyze, and show geospatial data as a GIS and Remote Sensing package. You can derive information about the spatial and temporal patterns and processes on the surface of the earth from the data. (ILWIS,2001).

Nowadays, geographic information systems are essential in a wide range of applications to support decision-making. A few geographical facts have an impact on the majority of judgments. What is that which is there? Where are the best locations? What changes happened, when, where, and how? Here are some illustrations:

- GIS is used in land use planning to assess the effects of various development scenarios in a region.
- GIS is used in geology to identify regions that are vulnerable to natural hazards or to locate the best locations for mining.
- Using GIS functions, areas that might be impacted by pollution are examined.
- On the basis of study of several spatial and temporal patterns, etc., city extensions are planned.

Access to various types of information is necessary in order to be able to make the best decisions. In order to get valuable information from the analysis, the data needs to be updated and maintained. The ILWIS can be a useful tool in this procedure (ILWIS,2001).

In addition to weighting, we may score the sub-factors. There is also a criteria tree that is used to conveniently present the influence factors in a row. We have the option of grouping the influential factors for analysis or performing separate analyses. It is quick, easy, and effective to use data sets for processes.

Consequently, the researcher chooses the ILWIS model to simulate the Sego Landslide Analysis due to its broad capabilities, compatibility with Arc- GIS software packages, and other advantages listed above.

3. MATERIAL AND METHODOLOGY

3.1. Description of the study area and the dam under analysis

3.1.1. Location

The Sego dam, which stretches on both sides of the Arba Minch-Konso asphalt road, is located in the Southern Nations Nationalities and Peoples Regional State (SNNPRS) of Ethiopia in the Arba Minch Zuria Woreda (Gamo and Gofa Zone), approximately 27 kilometers south of Arba Minch town. The study region is defined geographically by latitude 650968 N and longitude 323587 E (Figure 3.1.). The eastern and southern borders of this flood plain region are formed by Lake Chamo, while the northern and western borders are formed by mountains. The area is drained by Sego River, which drains into Lake Chamo. (ECDSWC, 2022).

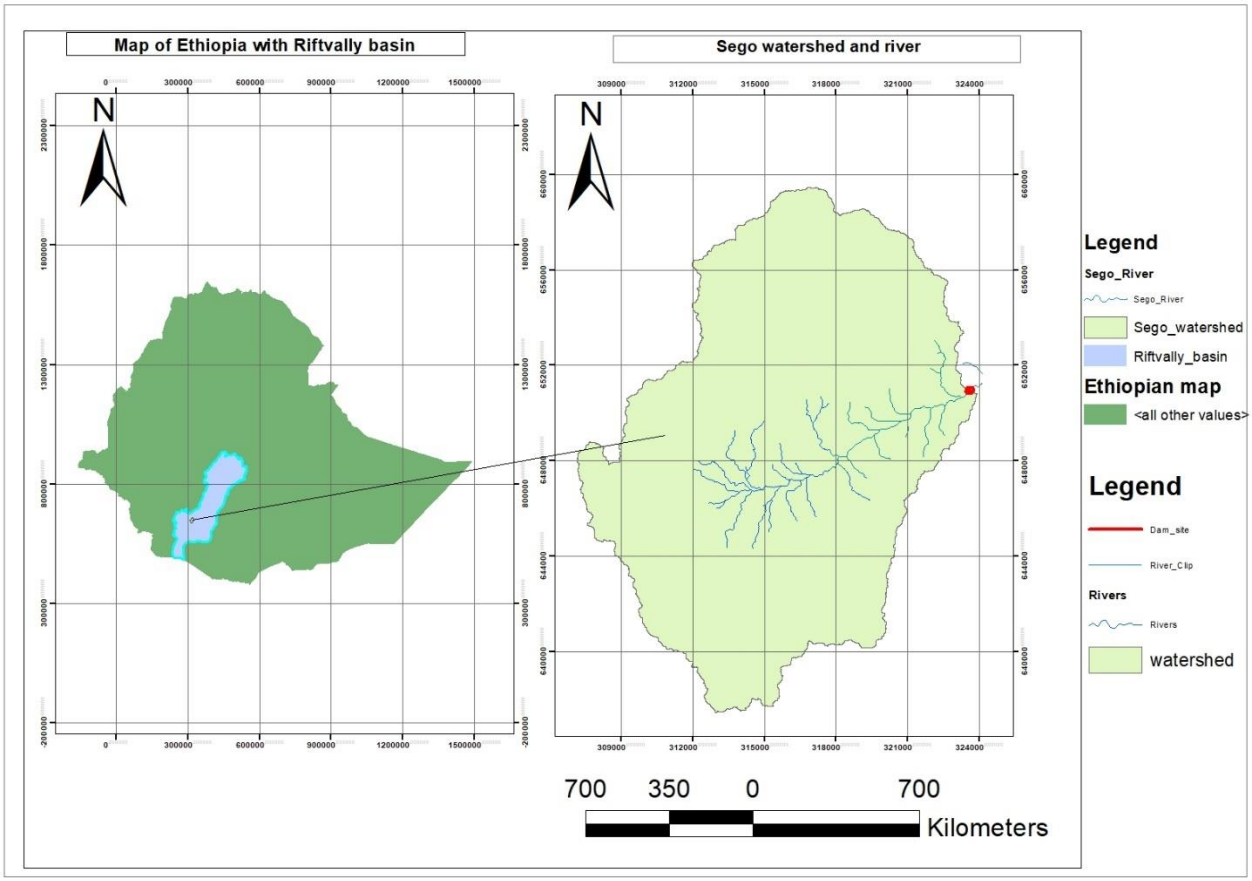

Figure 3. 1 Location map of Sego dam project

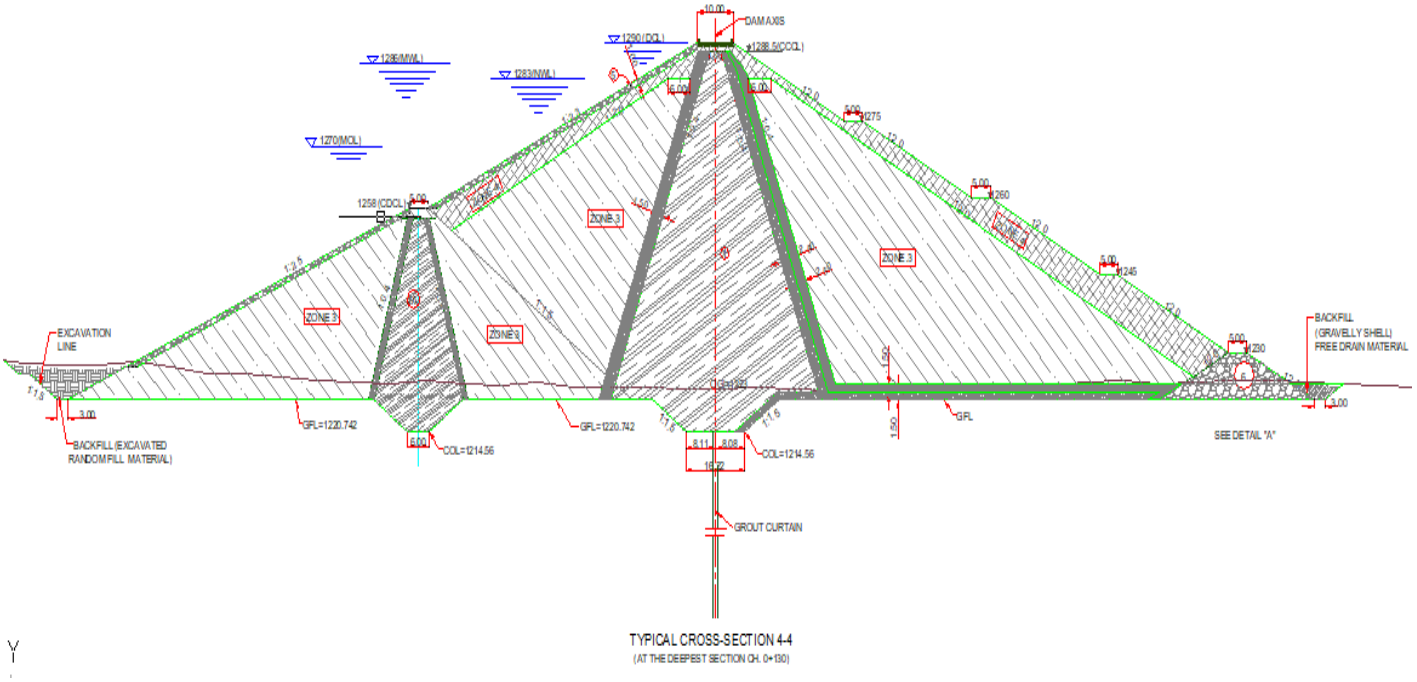

Figure 3. 2 Typical Cross Section of Sego Dam at the river bed (ECDSWC, 2023)

3.1.2. Description of the dam under study

The dam has a central clay core, a crest length of 268 meters, and a crest width of 10 meters. It is a Zoned Earth (shell)-Rock Fill Dam Type. The dam crest level (DCL), full reservoir level (FRL), maximum water level (MWL) is fixed at 1290,1283, and 1286 m.a.s.l respectively. and the river bed level is at 1223 m.a.s.l.; it has a height of 67 m above the riverbed level and 69.26 m above the general excavation foundation level. The dam has slopes of 1V:2.3 H and 1V:1.2 H, respectively, upstream and downstream. The intake gate's invert level is set at 1267 meters above sea level, and the outlet's invert level is set at 1225 meters, which pass under the dam cutoff level in the right abutment.

The reservoir is intended to store a total of 17.95 million cubic meter of water, A free overflow side channel spillway's control section is connected to the discharge channel by transition (bottom expansion from 20 m to 25m width)., required for the safe passage of half PMF flood discharge of 621.4m^3/sec without dam overtopping; and Outlet pipe has 3-meter diameter which intended to release water from the Outlet Tower of the reservoir for irrigation of 4000 ha, for downstream environmental releases, and for reservoir evacuation. (WWDSE, 2010).

3.1.3. Climate characteristics

The basin has both tropical and alpine climates. The bimodal rainfall system, which is brought about by humid airflow from the Indian Ocean, is caused by the inter-tropical convergence zone (ITCZ). In addition to the ITCZ, altitude has an impact on the area's rainfall distribution. (ECDSWC, 2022).

For Chamo and Southern Abaya, the wet rainy seasons are March through May and September through October. The months of July through October are considered the wet and rainy season in Northern and North Abaya (Bilate), while April through May and October are considered the same in the other catchment areas. The high rate of evaporation (approximately 2300 mm annually on average) and the average precipitation of about 600 mm per year further define the climate of the Abaya-Chamo Subbasin. Global climate change has historically had an impact on the region, shifting precipitation peaks to lower levels and having an effect on the Lakes. (ECDSWC, 2022).

The yearly migrations of equatorial low-pressure zones over the nation, which are brought about by the convergence of dry north-easterly winds with moist south-easterly or south-westerly winds, significantly define the general characteristics of the climate, which alternates between rainy and dry seasons.

The Arbaminch weather station records an average temperature of 220C to 240C for the lowland sections each year. The difference in temperature between day and night is approximately 120C (in the highlands at 2.700 meters above sea level). Chencha experiences significantly cooler temperatures, ranging from 120 to 140 degrees Celsius. (ECDSWC, 2022).

3.1.4. Soil

The soil parent materials found in the Rift Valley include basalt ignimbrite, lava, gneiss, volcanic ash and pumice, riverine, and lacustrine alluvium. These soil types are intimately connected to each other. Locally, at lower elevations, on colluvial fans, cracking clays are a hallmark of the Abaya and Chamo basins. Materials that rivers and lakes have recently deposited have built up the fans, deltas, and flood plains surrounding Abaya and Chamo Lakes. As long as there is adequate precipitation, soil fertility, structure, and drainage are generally beneficial for agriculture (EPA, 2006). Based on FAO/UNDP categorization, the primary soil classes found in the area include Vertisols, Nitosols (Alfisols), Lithosols, Andosols, Cambisols, and Fluvisols. The chromic vertisols and eutric nitosol soils that surround Lake Chamo are classified as clay to clay-loam in

terms of texture. With a textural classification of clay to clay, the soil types along the eastern shore of Lakes Abaya and Chamo are vertisols, luvisols, and nitosols. (ECDSWC, 2022).

The major soil type in the Sego Dam watershed is chromic luvisol associated with Luvisol on a flat plain of 0-2% slope; at the altitude range from 1,122-1,278. masl. Soils are moderately deep to very deep soil, moderately well drained, very dark brown to dark brown in color. Soils are silty clay to clay textured with stratified thin coarse textured layers, a moderately developed structure and friable consistency with intensively cultivated land. The soils of Sego River catchment are classified into chromic vertisols (88.7%) and humic andosols (11.3%). All the soil types belong to hydrologic soil group type B. (ECDSWC, 2022).

3.1.5. Sego watershed

The Sego watershed covers a high land and a rugged, undulating to flat lowland terrain draining to Lake Chamo. It is covers an area of 1436 km^2. Settled agriculture is a recent phenomenon here, and is largely rain-fed except for some irrigation on the river.

The slope steepness of the Sego watershed is extremely susceptible to erosion by water that is about 18,329.5ha (84 %) of the watershed area strictly coupled with improper land use practices. Slope steepness has a major correlation with soil erosion by water. It determines direction, speed, soil type, rainfall intensity, detachment and transportation of soil particles. The Sego watershed is mainly characterized with, moderately steep slope, hilly, hilly plains (35.21%), Steep hilly (23.59%), Sloping, rolling plain (15.91%), Gently sloping, undulating plain (12.15%), Very steep and mountainous (9.41%) and Flat or almost flat (3.73%). Moreover, 84.12 % of the watershed has sloping, rolling plain, moderately steep slope, steep hilly and very steep and mountainous. (ECDSWC, 2022).

3.1.6. Sego land use and land cover

The major land use and land cover of Sego watershed is mainly characterized by Shrubs land having an area coverage of about 8018.82ha (36.7%), Annual and Perennial crops 7499.4 ha(34.35%), Forest land 5120.01ha (23.45%), Grass land 1180.53ha (5.4%), and others 15.7ha (0.07%).

The high degree of steepness at the uplands coupled with the absence of vegetation cover and miss management of land use in the areas is believed to have exacerbated to start the expansion and abundance of gullies and mass landslides. When in the time of transact walk the team has been observed the gullies that are affected the cultivated and grazing lands; which are expanding trend of gullies and continual degradation of land and landslides in watershed areas. The severity of soil loss/ fertility, gully formation and mass land slide further affected the survival of cultivated land, shrub land, and riverine vegetation, grazing land and forest lands in the watershed and as well as huge influence on the constructed life span of Sego dam. (ECDSWC, 2022).

3.1.7. Sego River

The Sego River Valley is characterized by broad and rolling plains in the upper course, but it is formed narrow and deeply dissected valley characterized by steep cliffs at middle to lower course. The Sego River valley at Dam Site is formed very steep and narrow gorges, which is formed by felsic to intermediate volcanic flows. (ECDSWC, 2022).

3.1.8. Geomorphology of the dam area

Segen basin (where sego valley is located) is part of the Southern Segment of Ethiopian Rift valley which belongs to the southern highlands, plateaus and associated lowlands and rift valleys of Southern Ethiopia represented by rugged topography as a result of uplift and subsequent development of the Main Ethiopian Rift (MER) (ECDSWC, 2022)

The Sego Dam and Irrigation Project area is formed the Rift Valley Lakes Basin, where the topography prevalent to the project site is the result of recurring and prolonged geo-tectonics and geo-morphological processes; such as faulting/uplift/subsidence, weathering and erosion heavily modified the landform related to the evolution of the SMER. Common landforms of the area are represented by fluvial, volcanic and tectonic geomorphic systems. The fluvial geomorphic systems, which are resulted from both tectonic and surficial processes are composed of meandering river/stream channels, wider flood plains at places and weakly incised gulley and valleys. The tectonic process as seen from interactions of fractures and lineaments resulted in formation of mass wasting (landslides) in the area. The volcanic related landforms are characterized by volcanic flows and plugs. (ECDSWC, 2022)

3.1.9. Geology of reservoir area

The geology of the Reservoir area of Sego Dam and Irrigation Project is underlying by Tertiary volcanic rocks and Quaternary superficial deposits. The Tertiary volcanic rocks are represented by varying proportions of basaltic flows, felsic-intermediate flows and pyroclastics, which are grouped into eight mappable lithological units (Fig. 3.3). From oldest to youngest these are; (i) Basalt (Tv1), (ii) Felsic flows and pyroclastics (Tv2), (iii) Basalt (Tv3), (iv) Felsic-intermediate flows (Tv4), (v) Basalt (Tv5), (vi) Trachyte (Tv6), (vii) Felsic-intermediate flows (Tv7), and (viii) Trachyte flows and plugs (Tv8). (ECDSWC, 2022)

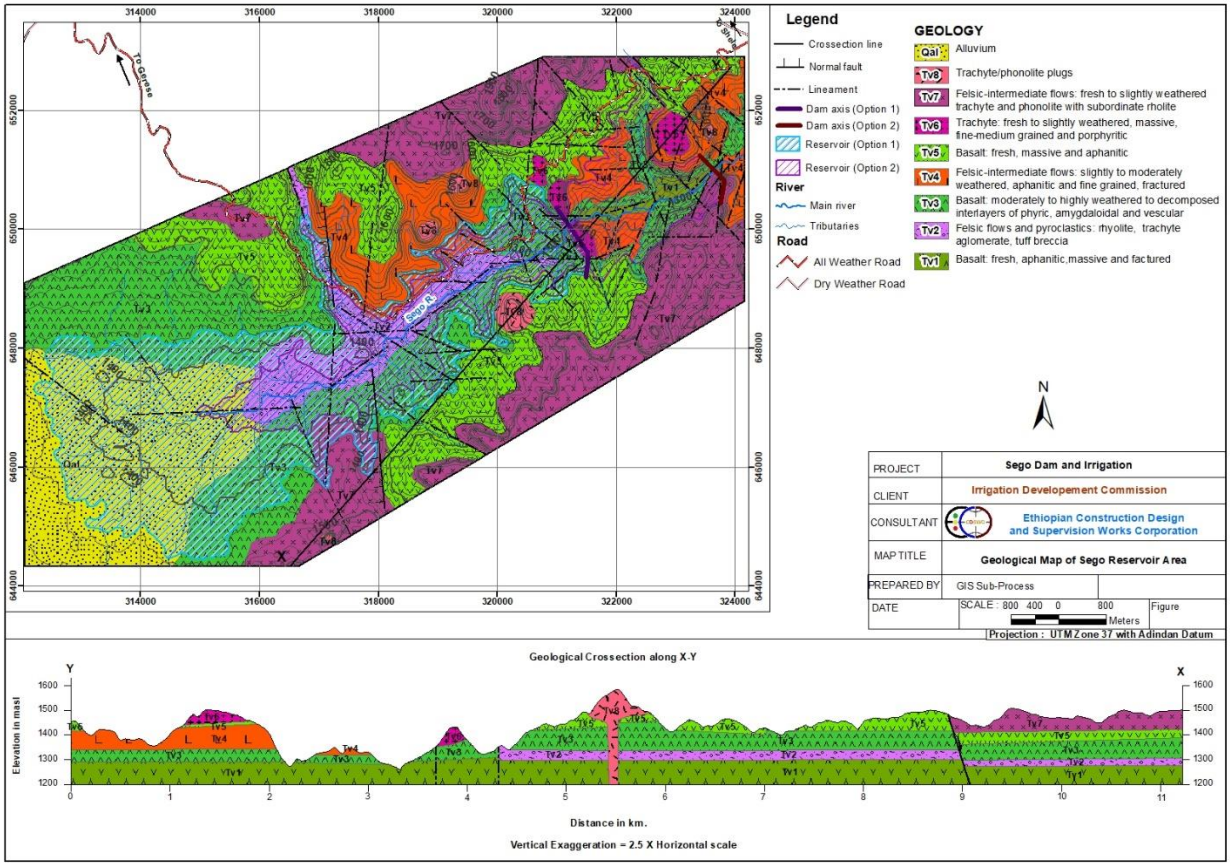

Figure 3. 3 A cross-section and geological map of the Reservoir region (1:10,000). (ECDSWC,2022)

3.1.10. Population settlement

Areba-minch zuria Wereda has 132,377 and about 20 % are living in urban area and whereas 80% are living in the rural area. The population density is 202 persons per square Kilometer. Gamo and Zeyise are the major ethnic groups living in the project area and speak their own language, which

belongs to Omotic language group. There are many inhabitants in the downstream of the dam. (ECDSWC, 2022).

3.1.11. Land Sliding (Mass Movement)

At Sego watershed in most upper part of the watershed or undulating mountain chains of the watershed which are one or more above mentioned possible natural and man-made causes could be observed especially; Ploughing of very steep slopes, due to inappropriate land management widely, deforestation, frequent cultivation on farmland for cereal crops, impoverishment of the vegetation cover, inappropriate road construction and others (ECDSWC, 2022).

Figure 3. 4.Mass land slide observed in sego watershed (ECDSWC,2022)

3.1.12. Site specific seismicity data

Seismicity data for the Sego project site are displayed in Figure 3.5. Red circles denote earthquakes that have occurred in the area within the last 110 years, and the size of the circles corresponds to their magnitude. The locations of the proposed Sego dam site are shown by the lower yellow star. (ECDSWC, 2022).

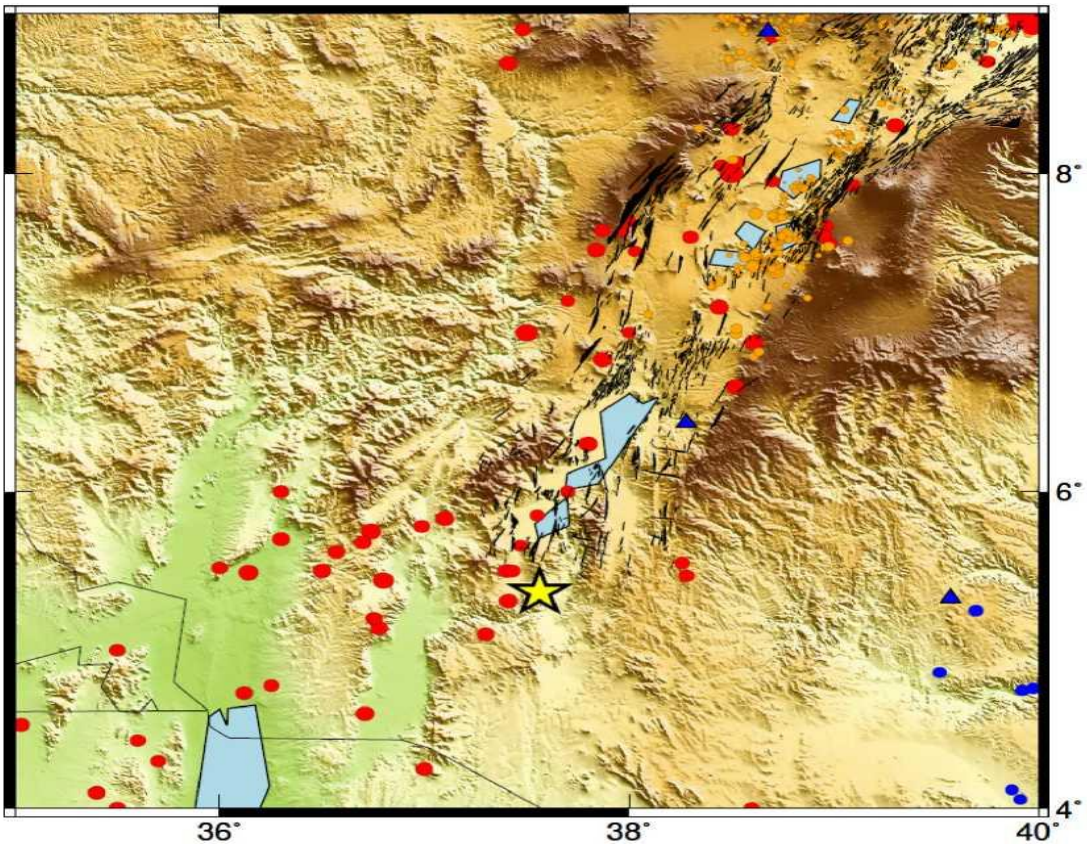

Figure 3. 5 Seismicity data at the Sego project site (ECDSWC,2022)

3.2. Materials used

The materials used for this research are Arc GIS to prepare different map different influencing factor such as land use and land cover, soil, slope, aspect, curvature and others and ILWIS model tools to prepare land susceptibility map of the area by SMCE method, HEC- GeoHMS to delineate the watershed, Global mapper to prepare DEM data as suitable for GIS and to convert shape files to Google Earth format (KML), Google Earth to identify and find historical landslide location. QGIS to convert raster data to ILWIS format data (mpr). Microsoft EXCEL 2010 to prepare template of impulse wave analysis. Finally, AutoCAD 2018 was used to draw and show the landslide with reservoir and the dam both the alignment and sections.

3.3. Data collection

In conducting the research, a field visit was made on the study area to have a good perception on the reservoir area, dam, river morphology and downstream flood plain area. Both primary and secondary data have been collected as listed below.

3.3.1. Primary Data

Physical observation and measurement made on site to visualize the dam site and reservoir rim, to notice the active geological faults and relevant photos taken on site that would be essential for the study. Location of some existing landslide point have taken from the study area for validation of landslide which identified by Google earth tool.

3.3.2. Secondary Data

Different types of data such as geological, geotechnical, and geophysical, important engineering and infrastructure information on the dam and reservoir, and overall study area were collected from Ethiopian Construction Design and Supervision Works Corporation (ECDSWC). These data are Salient features of the dam, Salient features of the reservoir, Reservoir area-elevation-volume curves, Topographical survey map, Topographical map from EMA (Ethiopian Mapping Agency), Regional and local geology of the area, Geophysics investigation of the dam and reservoir and Geotechnical information in the dam abutment and the reservoir.

3.4. Data analysis

Initially the land slide hazard spot area has identified by ILWIS software and land slide zonation map has prepared with the help of GIS tools using different spatial landslide influencing factor input data.

Using the prepared map and geological faults, the primary landslide impact zone has then been determined. The volume of the land slide wage that will submerge and create waves in the reservoir has then been estimated. this has been done while utilizing several governing and dimensionless design parameters. Different numerical models have been used to assess and estimate the wave generation and propagation, wave run-up, and wave overtopping at various extreme scenarios, and the maximum and adequate freeboard of the dam has estimated and suggested. These procedures are showed on the conceptual framework given in Figure 3.6

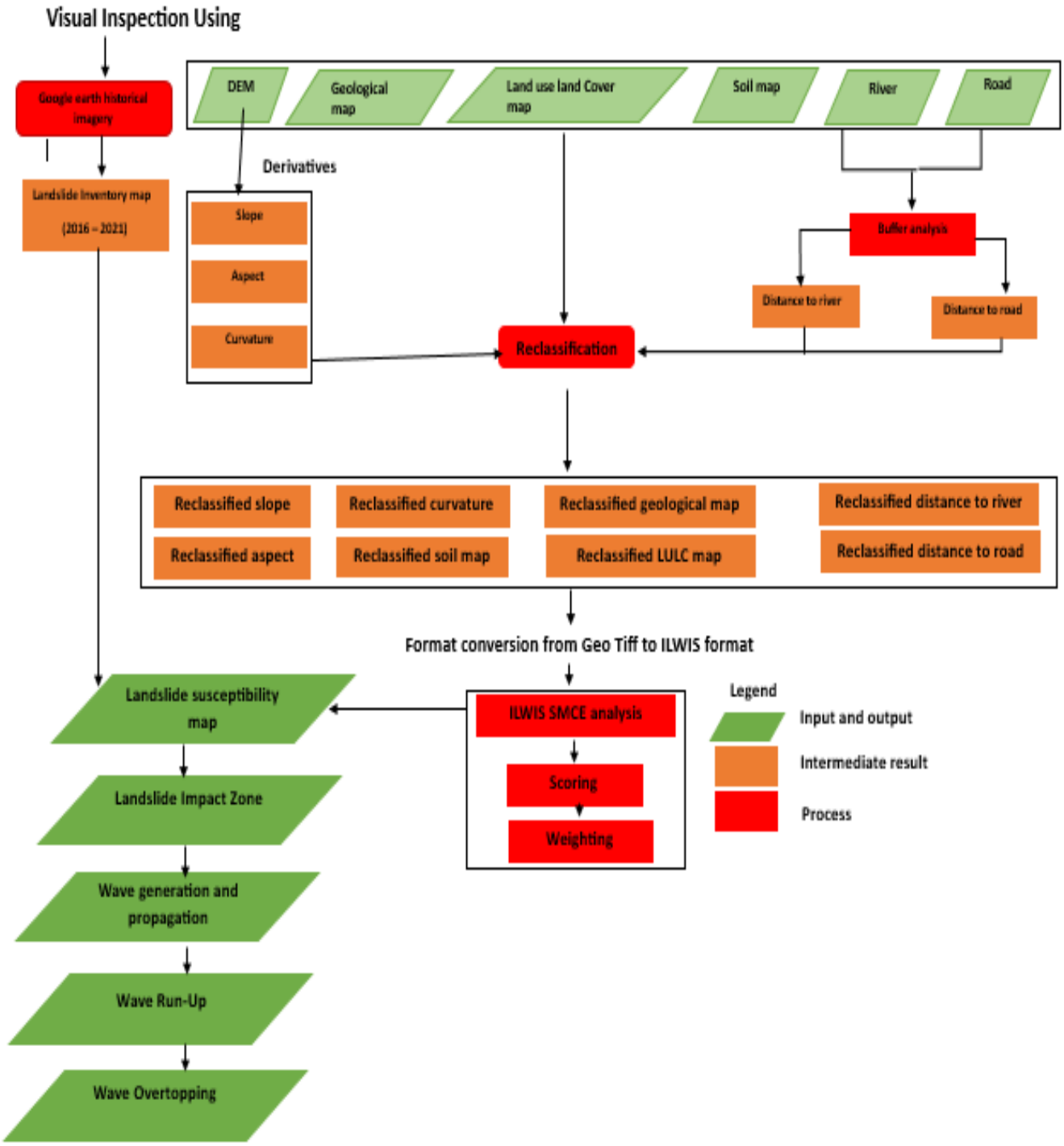

Figure 3. 6. Conceptual Framework of the whole work

3.4.1. Land slide zonation map preparation

3.4.1.1.Data preparation

3.4.1.1.1. Landslide inventory map

Landslide inventory is a dataset that shows the distribution and characteristics of past landslides (Hervás, 2013). To assess landslide susceptibility, hazard and risks landslide inventories are basic (Soeters and van Westen, 1996; Aleotti & Chowdhury, 1999; Ardizzone et al., 2002; Dai, Lee, & Ngai, 2008; van Westen et al., 2008). It gives understanding on different landslide phenomena for example locations, date, type, volume and damages.

To conduct the landslide susceptibility analysis using SMCE the landslide inventory map compiled. The inventory map was produced using visual inspection, the landslides were mapped on georeferenced and ortho-rectified images by using Google Earth historical imagery of the time slider as polygons (Van Westen, 2014). The landslide scars and accumulation area were identified. As much as possible the visible historical landslide areas were mapped. In this study, 138 historical landslide locations were mapped (Figure 3.7). The occurrences were the events that happened a period from 2016 to 2021 see Table 3.1.

Table 3. 1 Number of landslides with the occurrence of year

Year of occurrence	Number of landslides
2016/2	2
2017/12	11
2018/1&12	14
2019/9&12	76
2020/2& 8	12
2021/1	24

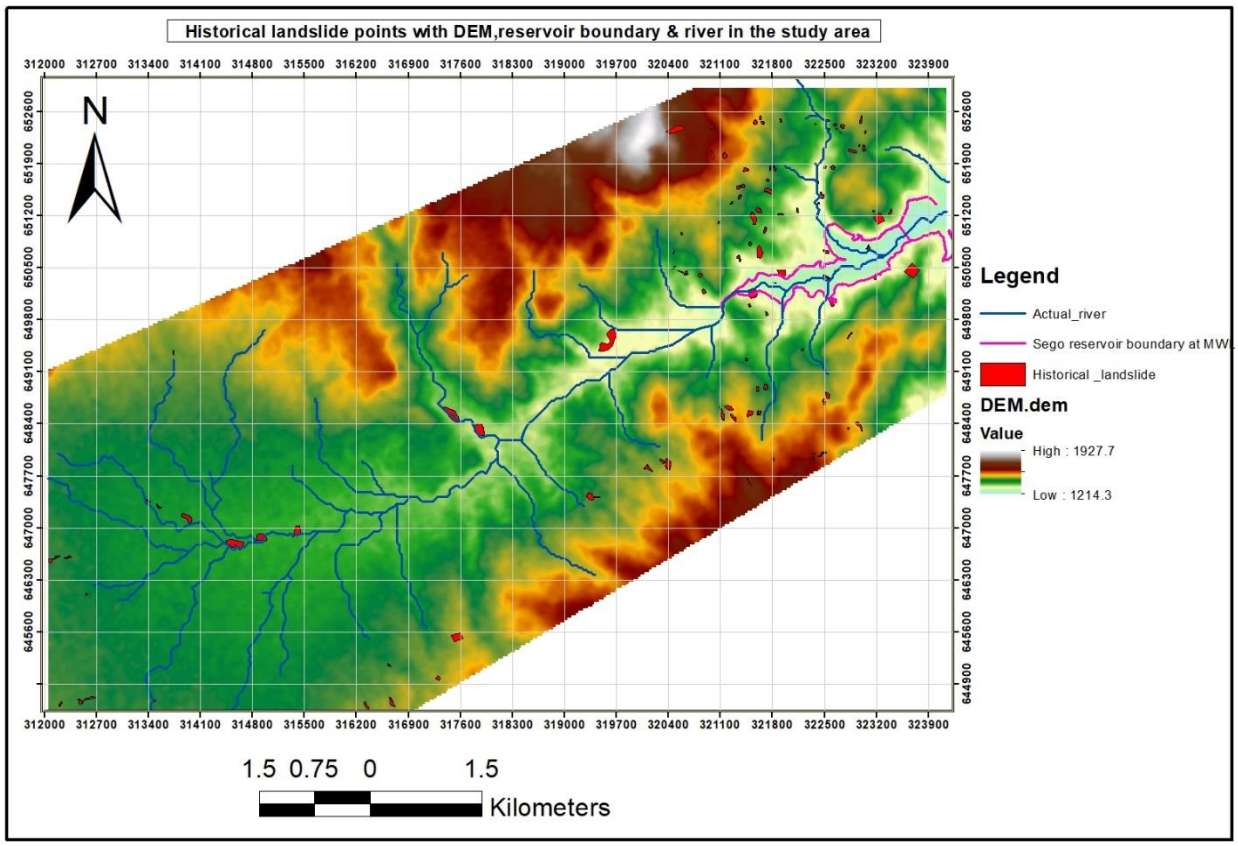

Figure 3. 7 Landslide inventory map with elevation variation

3.4.1.1.2. Influential factors

The reasons why a particular location is slope-prone are known as influencing variables, and they have an impact on the likelihood of landslides. In a GIS-based analysis, one must ensure that the factors chosen for selection are operational (have some affinity with landslides), complete (fairly represented throughout the study area), non-uniform (varies spatially), and measurable (have measurement level), according to Ayalew et al. (2005).

In practice, Soeters and van Westen (1996) noted that the following five dataset sets are frequently utilized to evaluate the vulnerability of landslides:

- Geomorphology, including terrain forms and geomorphological subunits
- Topography or morphology, such as the slope, aspect, and curvature of a digital terrain model
- Geology, or engineering geology, in the case of lithology, sequence material

- Land use and landcover
- Hydrology, including factors like temperature, evaporation, rainfall, and closeness to catchment areas and drainage

Due to a lack of data, not all relevant factors could be included in the study, for instance rainfall and pore water condition; but those that are widely recognized in science were nevertheless included (Table 3.2).

- Aspect, curvature, and slope as topographical grouping elements
- Distance to a road and land usage as indicators of human-induced group
- Soil and geology as a component of soil group
- River distance as a hydrology group component.

Table 3. 2 Available datasets relationship with landslides

Factor map	Relation with landslide
DEMs	Landslide directly related to elevation when the elevation increased the probabilities of landslide will increase.
Planer curvature	The concavity and convexity of curvature have the potential to initiate landslide.
Aspect	The slope face direction has a high impact on the landslide.
Slope	Slopes are more critical information for landslide because landslide occurs between 20 to 45-degree steepness.
Land use	Land-use change has a significant influence on landslides like new roads.
Geology	The area covered by volcanic rocks these rocks are young, weathering condition and the strength of the rock depends on the cooling rate of the rock most types of geology in Sego area are weak and young, so it has potential to support the landslide occurrence
Soil type	Soil types are highly related to landslide because soil has different kinds of properties, e.g., grain size distribution this related directly to the capacity of saturation, porosity and plasticity of soil which can cause proneness to landslides.
Distance to road	The closest distance to the road will lead to slope instability; this factor

	has the potential to initiate landslides.
Distance to river	River caused erosion this will increase the frequency of landslide when the area close to the river.

i. Digital Elevation Model (DEM)

DEM data source is from SRTM with 30m resolution, the data used to generate the derivate maps like slope, aspect and curvature, the minimum and maximum value of the SRTM elevation is 1218.5 and 1937.9m, respectively.

Planer curvature: is the surface's shape. three types are separated by the curvature. According to Pradhan and Lee (2010), a concave surface is represented by a negative curvature value, a flat surface by a curvature value around zero, and a convex surface by a positive curvature value. The earth's concave and convex surfaces have a greater impact on the occurrence of induced landslides. The distribution of the various curvature classes is shown in Table 3.3 and Figure 3.8 below.

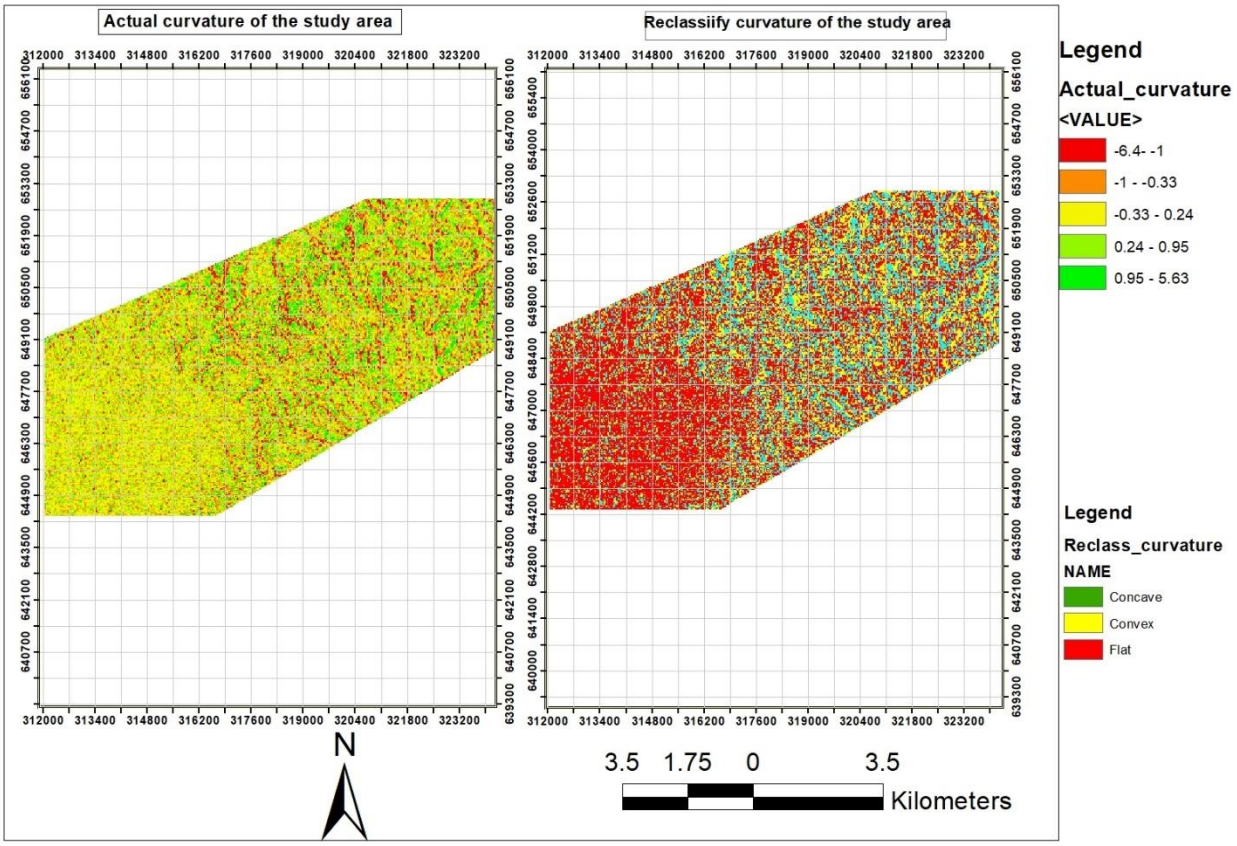

Figure 3. 8 Spatial distribution of curvature and classified curvature

Table 3. 3 Classes of curvature with area

Factor	Class	Class name	Hectares	%
Curvature	1	Concave	3440.09	48.77
	2	Flat	59.29	0.84
	3	Convex	3553.20	50.38

Aspect: is defined as the horizontal direction that a hill slope or mountain faces. Typically, it is stated from 00 to 3600 in a clockwise manner. Because aspect confronts the sun's rays, it can affect the microclimate, or local climate, in a given area. The amount of rainfall on a slope can change based on its aspect if rainfall has a significant directional component due to the influence of a prevailing wind (Wieczorek et al., 1997). This further suggests that aspect also indirectly signals a

precipitation effect from rainfall. As a result, certain faces stabilize more than others. In summary, it can be stated that this feature indirectly affects land sliding because it is connected to other elements like rainfall, weathering, and soil moisture. Regarding the distribution, classes, and related areas of aspect, see Figure 3.9 and Table 3.4.

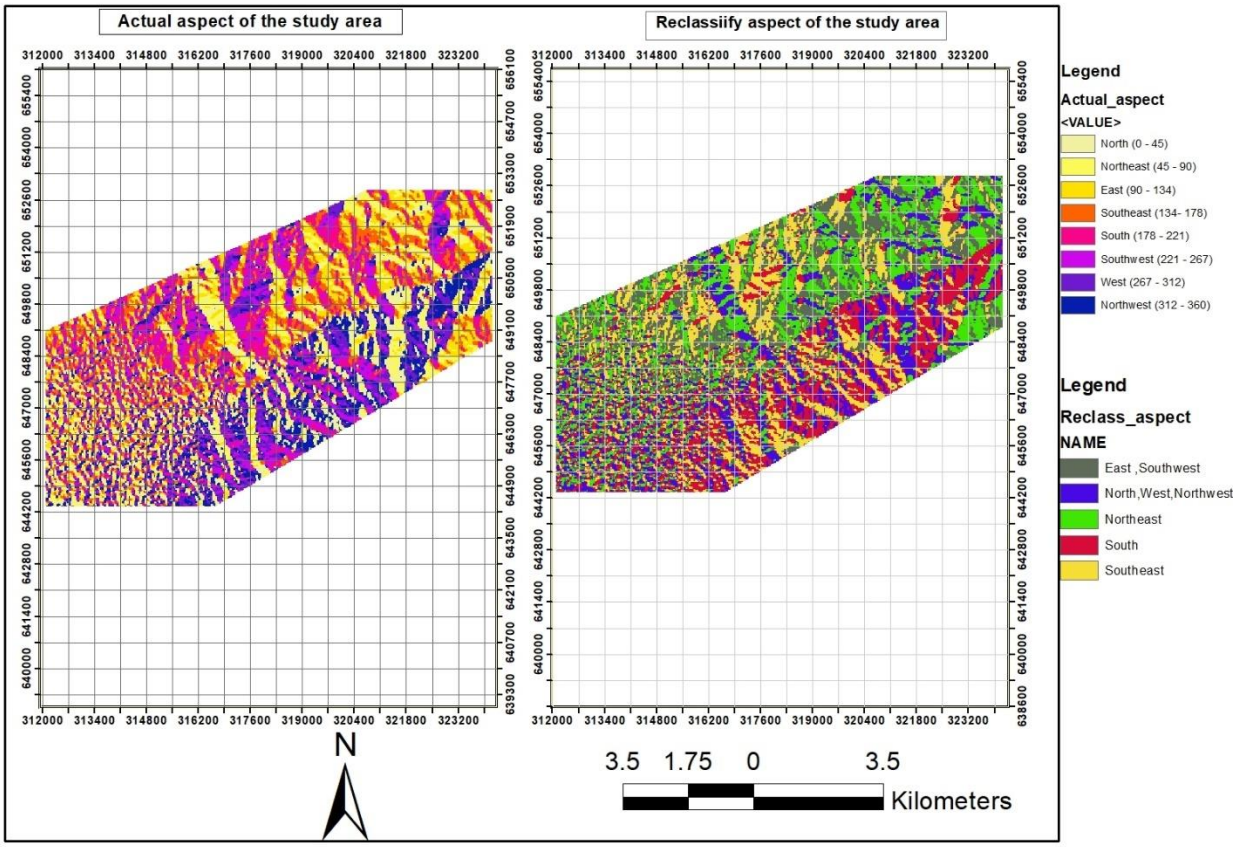

Figure 3. 9 Spatial distribution of aspect and classified aspect

Table 3. 4 Aspect classes and area

Factor	Class	Class name	Hectares	%
Aspect	1	North	877.58	12.44
	2	Northeast	954.27	13.53
	3	East	912.08	12.93
	4	Southeast	958.31	13.59
	5	South	968.97	13.74
	6	Southwest	799.74	11.34
	7	West	748.62	10.62
	8	Northwest	832.99	11.81

Slope: is the angle formed between the horizon and a spot on the surface. It might be stated as the percentage or degree at which 45^0 and 100% are identical. According to Dai et al. (2001), slope or slope gradient is a crucial influencing factor since it is recognized that slope failure, or instability, would ultimately be the primary source of mass movement. The pushing force (shear stress) and resisting force (shear strength) in a given region are managed by the slope. (Wati, 2010) stated that the likelihood of failure increases with slope because shear stress increases with slope. It indicates that steeper slopes are often the location of more frequent landslides (Gómez & Kavzoglu, 2005). The study area (Figure 3.10 and Table 3.5) is nearly completely covered by a steep slope.

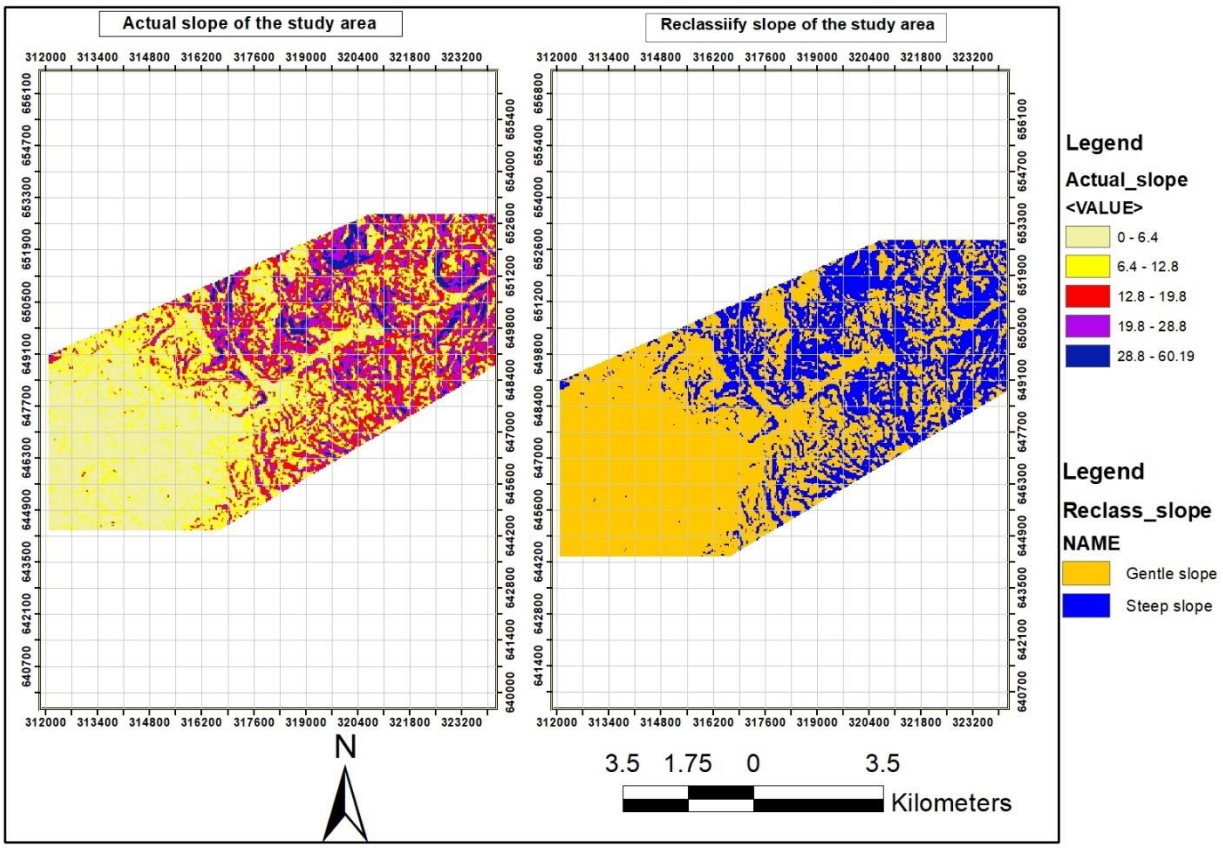

Figure 3. 10 Spatial distribution of slope and classified slope

Table 3. 5 Slope class and area

Factor	Class	Class name	Hectares	%
Slope	$<20^0$	Gentle slope	3597.58	51
	$>30^0$	Very steep	3455	49

ii. Land use

Slope stability may be indirectly impacted by land use. For instance, the hydraulic conductivity effect of vegetation cover affects hydrological processes (Van Westen et al., 2008). Vegetable gardens or sparse vegetation on steep slopes may make more susceptible since their roots are unable to hold the soil together in the event of rain. Soil erosion might so occur with ease. Construction of buildings adjacent to hills including cut and fill operations may increase pressure, leading to instability of the slope. The land use map that is now in place divides land use types into six classifications, the most common of which are crop land and trees. The class with area and spatial distribution can find in Table 3.6 and Figure 3.11 respectively.

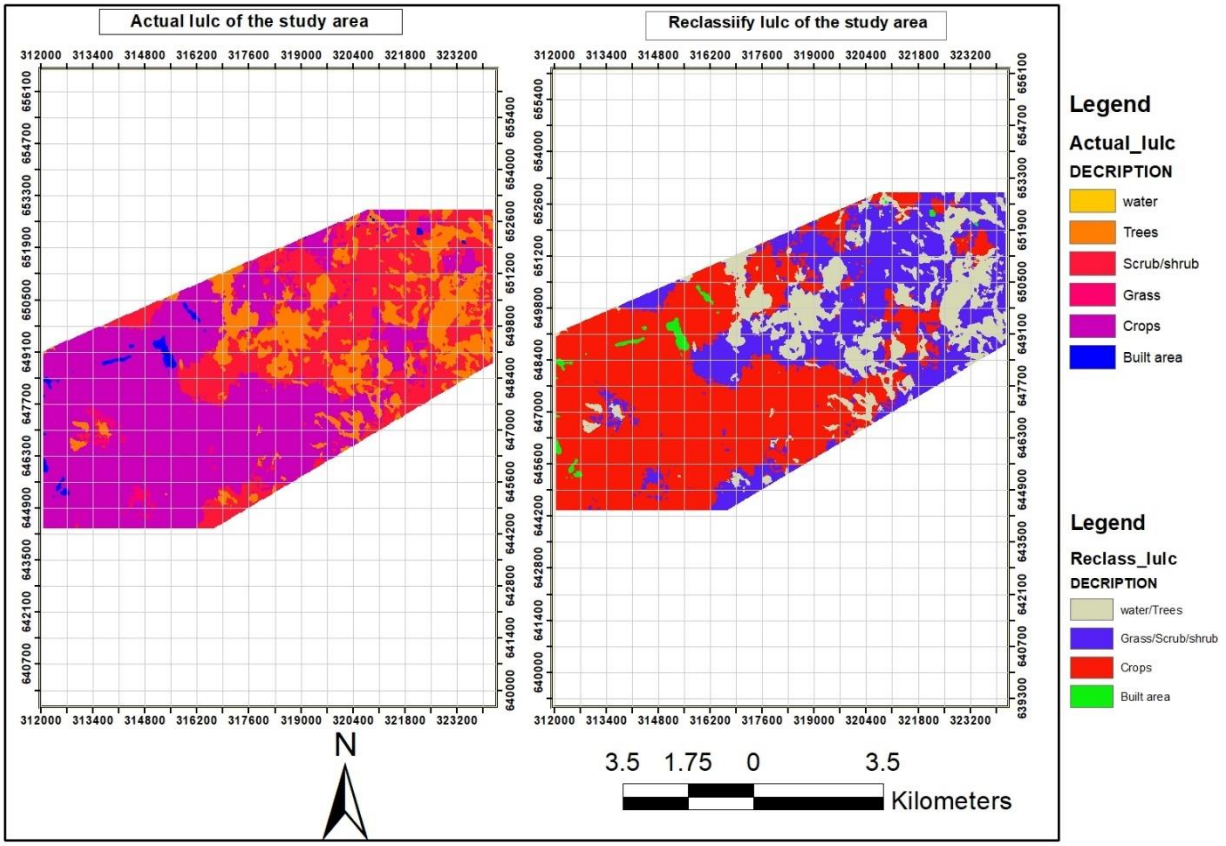

Figure 3. 11 Spatial distribution of land use and classified land use (source, ESRI,2020)

Table 3. 6 Land use class and area

Factor	Class	Class name	Hectares	%
Land use	1	Built area	65.23	0.93
	2	Crop area	3783.16	53.68
	3	Grass	58.31	0.83
	4	Shrub area	1952.34	27.70
	5	Trees	1187.96	16.86
	6	Water body	1.099	0.02

iii. Geology

The geology of Sego area is originated by Tertiary volcanic rocks and Quaternary superficial deposit. It includes 9 lithostratigraphic-units in the area, four of them are dominant, and the parent material is volcanic rock (ECDSWC, 2022). This indicates that the area is geologically active and complex which cause induce of landslides. The lithostratigraphic-unit are; Alluvium deposit (Qal), Basalt (Tv1), Fesic flows and pyroclastics (Tv2), Basalt (Tv3), Felsic-intermediate flows (Tv4), Basalt (Tv5), Trachyte (Tv6), Felsic-intermediate flows (Tv7) and Trachyte flows and plugs (Tv8). The information of the classes with their area and spatial distribution found in Table 3.7 and Figure 3.12 respectively.

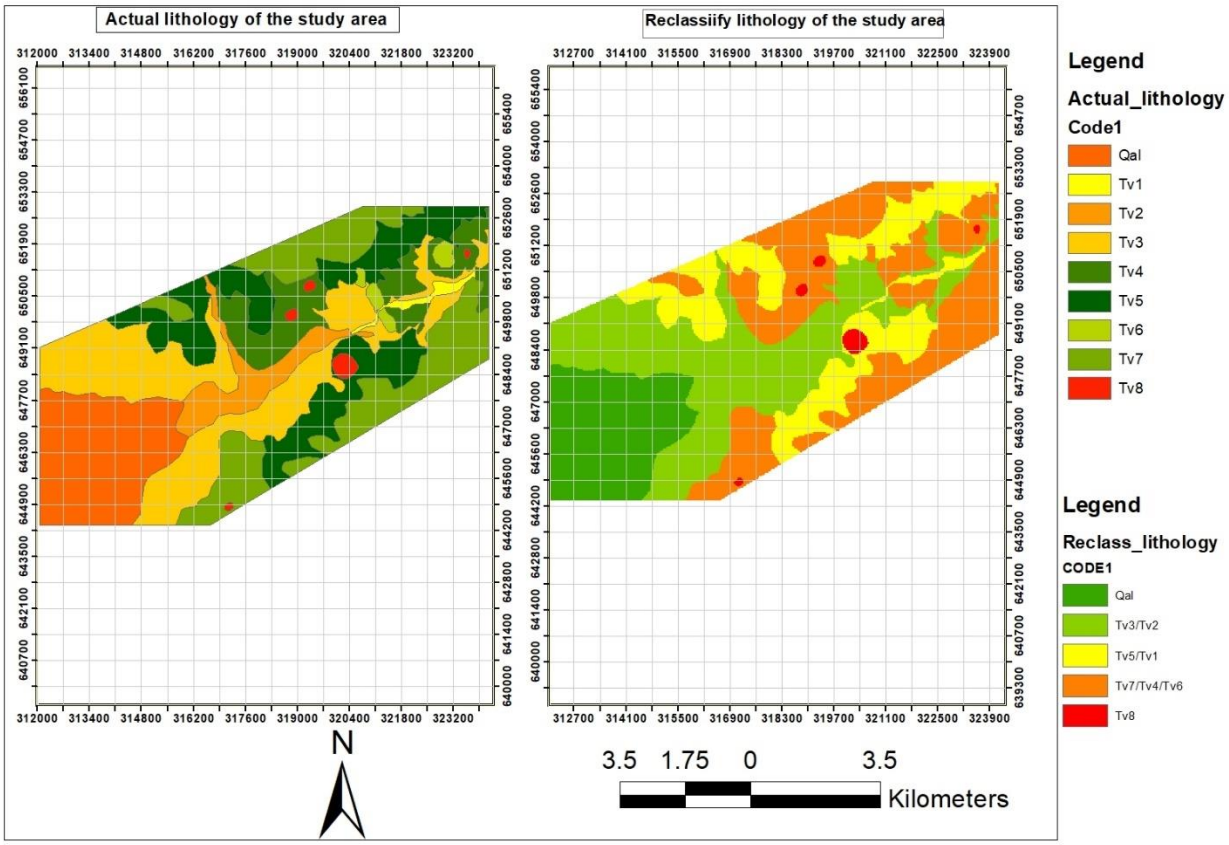

Figure 3. 12 Spatial distribution of geology and classified geology (source,ECDSWC, 2022)

Table 3. 7 Geological classes and area

Factor	Class	Class name	Hectares	%
Geology	1	Qal	1164.47	16.50
	2	Tv1	61.8	0.88
	3	Tv2	410.65	5.82
	4	Tv3	1822.5	25.83
	5	Tv4	718.55	10.18
	6	Tv5	1320.52	18.72
	7	Tv6	83.35	1.18
	8	Tv7	1414.03	20.04
	9	Tv8	60.01	0.85

iv. Soil type

The study area covered by 3 types of soils (i.e., Leptosols, Luvisols, and Vertisols), 76% (see Table 3.8) of the area covered with Luvisols. The Leptosols are shallow depth over the hard rock which includes more than 80% gravel, and boulders. Due to the shallow depth and coarse texture of Leptosols have low water holding which makes highly prone to erosion in sloppy area (Spaargaren, 2007). Luvisols also shallow depth and the physical properties are granular surface that are porous and well aerated. It have high silt content which is makes prone to erosion in sloppy area (Spaargaren, 2007). In addition to this, in depression areas shallow groundwater may occur in Luvisols (ISRIC, n.d.). Vertisols have moderate depth with fine grained, high plastic, low porosity and water transmission capacity. The soil create deep crack when it dry and high proportion of swelling in wet season (Spaargaren, 2007). The spatial distribution of the soil can be seen in Figure 3.13.

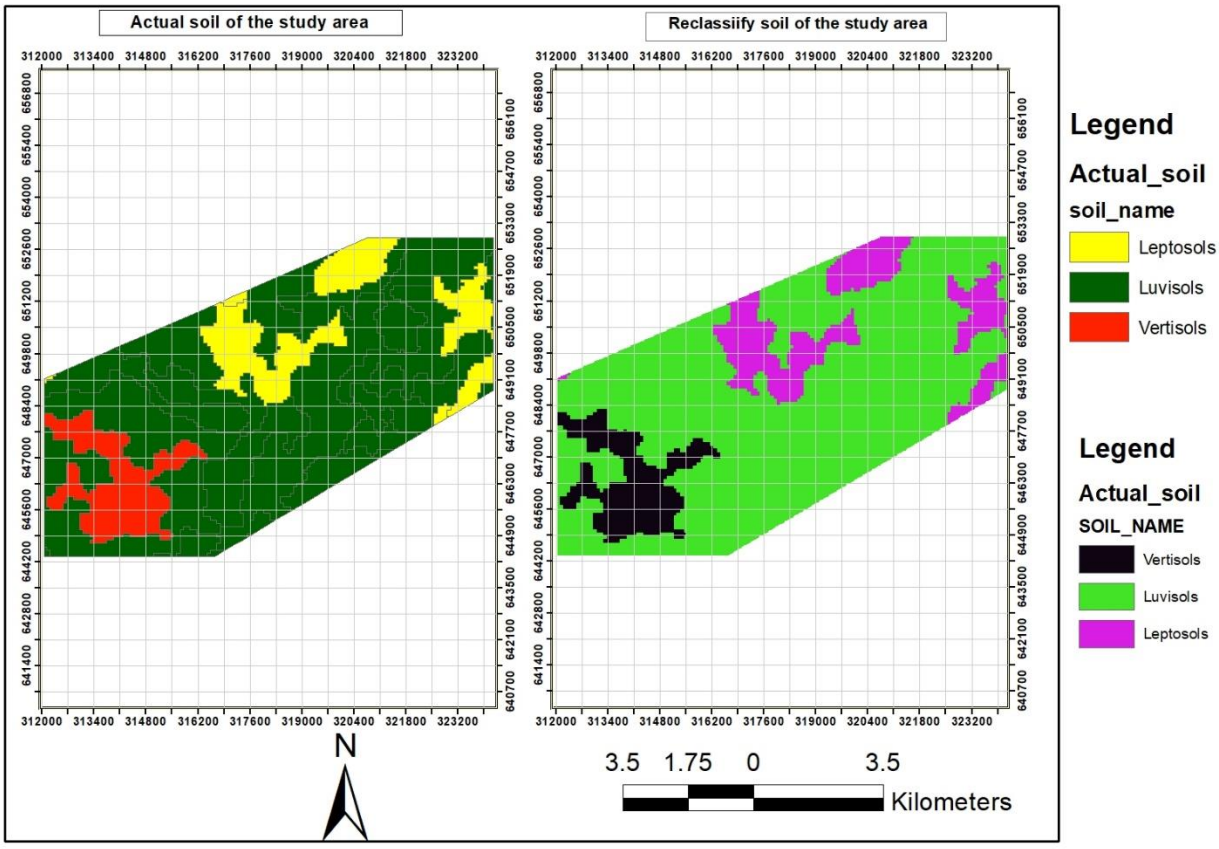

Figure 3. 13 Spatial distribution of soil and classified soil (source, ETHIO SOIL,2016)

Table 3. 8 Soil classes and area

Factor	Class	Class name	Hectares	%
Soil	1	Leptosols	1010.96	14.33
	2	Luvisols	5386.56	76.35
	3	Vertisols	657.92	9.33

v. Distance to road

In areas with hills or mountains, road constructions are locations of instability caused by human activity (Ayalew & Yamagishi, 2005). From a hydrological perspective, road segments can function as a sink, a barrier, or a corridor for water flow, which might impact slope stability. This makes it simple to discover that landslides have happened above or close to highways. The factor map was created using proximity analysis method. The maximum distance observed from the analysis result is 2400 m for the roads. We used the minimum distance of the roads to analyze the relationship with the landslides. The classes with area and the spatial distribution of the buffer found in Table 3.9 and Figure 3.14 respectively.

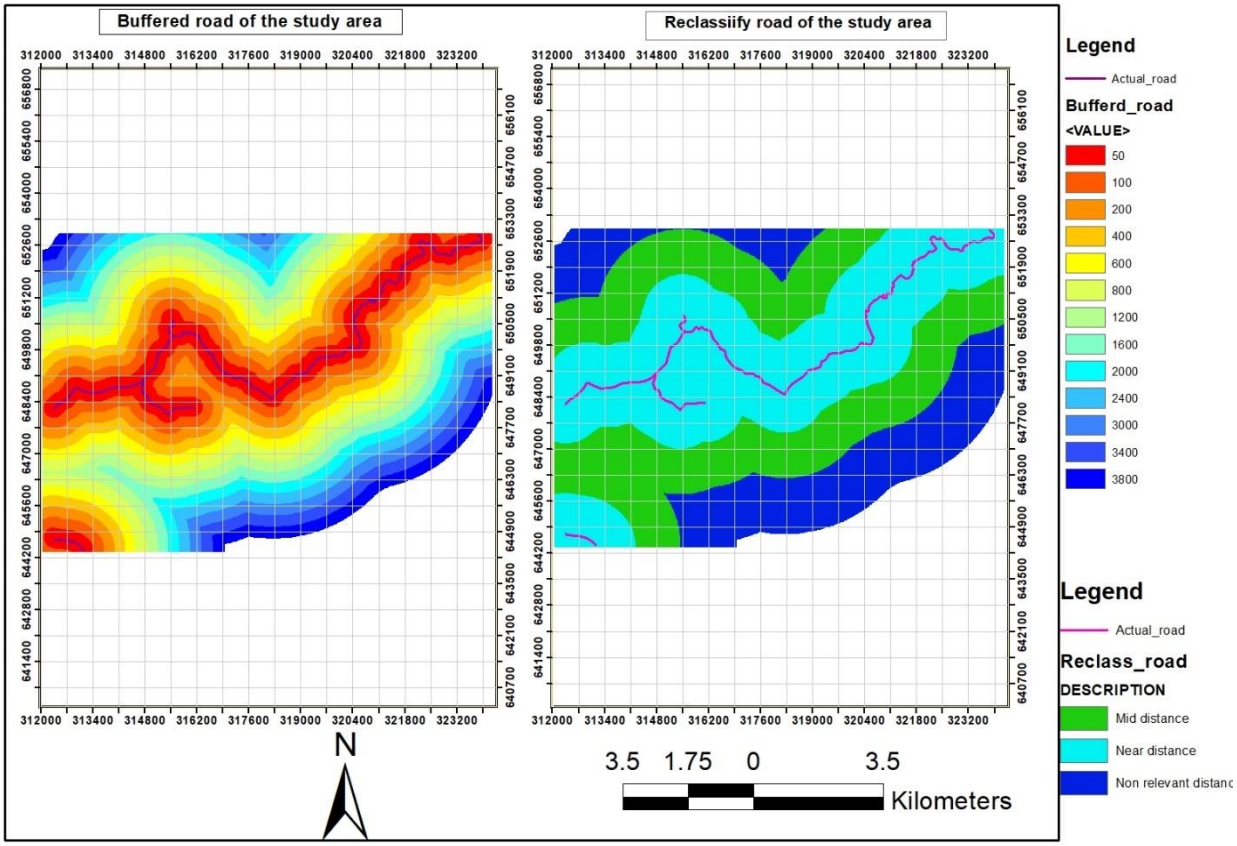

Figure 3. 14 Spatial distribution of distance to road and classified distance to road (source, CSA admin data)

Table 3. 9 Class and area of road buffer

Factor	Class	Class name	Hectares	%
Distance to road	1	50m	211.80	3.01
	2	100m	208.44	2.96
	3	200m	403.91	5.73
	4	400m	754.51	10.71
	5	600m	702.94	9.97
	6	800m	643.92	9.14
	7	1200m	1056.99	15.00
	8	1600m	927.80	13.17
	9	2000m	838.89	11.90
	10	2400m	626.22	8.89
	11	3000m	514.92	7.31
	12	3400m	108.37	1.54
	13	3800m	48.60	0.69

vi. Distance to river

It is very common to see landslide near to rivers. Rivers or streams drainage may induce river bank failure because of slope undercutting and stream erosion. These factor maps were categorized into three classes. Those are near, mid and non-relevant distance from the river. Most of the time, landslides occurred near the river because of erosion. Table 3.10 and Figure 3.15 shows the classes with area and spatial distribution.

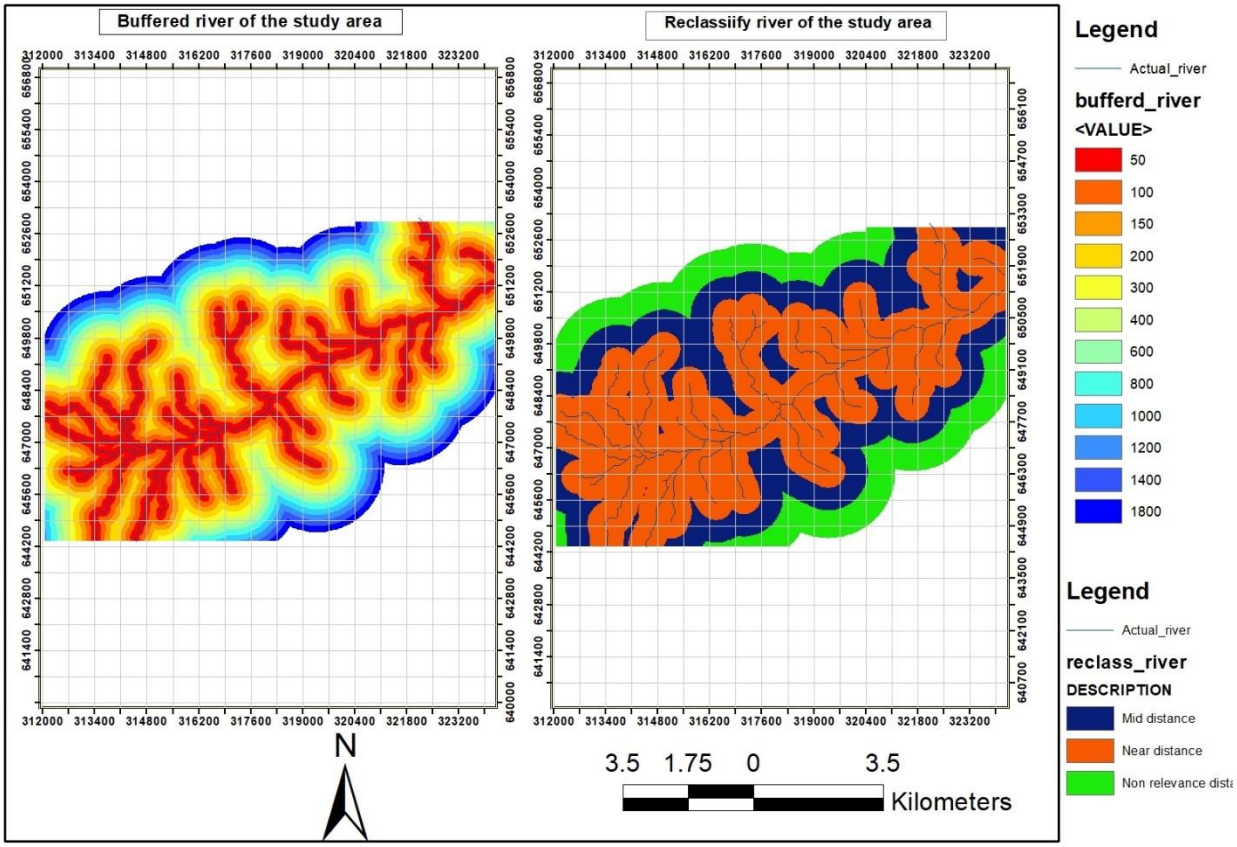

Figure 3. 15 Spatial distribution of distance to river and classified distance to river (source, CSA admin data)

Table 3. 10 River classes and area

Factor	Class	Class name	Hectares	%
Distance from river	1	50m	683.07	9.69
	2	100m	644.44	9.14
	3	150m	598.08	8.49
	4	200m	547.79	7.77
	5	300m	970.73	13.77
	6	400m	824.68	11.70
	7	600m	512.30	7.27
	8	800m	712.39	10.11
	9	1000m	446.65	6.34
	10	1200m	248.37	3.52
	11	1400m	127.14	1.80
	12	1800m	9.58	0.14

vii. Geological structure in the project area

The faults affecting the area are normal faults, which are represented by two sets; Northeast-Southwest, and Northwest -Southeast. Lineaments striking, NW-SE, WNW-ESE, NE-SW, and ENE-WSW are mapped from DEM. Major rivers and streams are developed following these linear features. The topographic configuration of some ridges also coincides with longer and prominent lineaments. Such structures combined with earthquake event are very common cause of landslide formation. These structures were observed in the dam and reservoir (Figure 3.16).

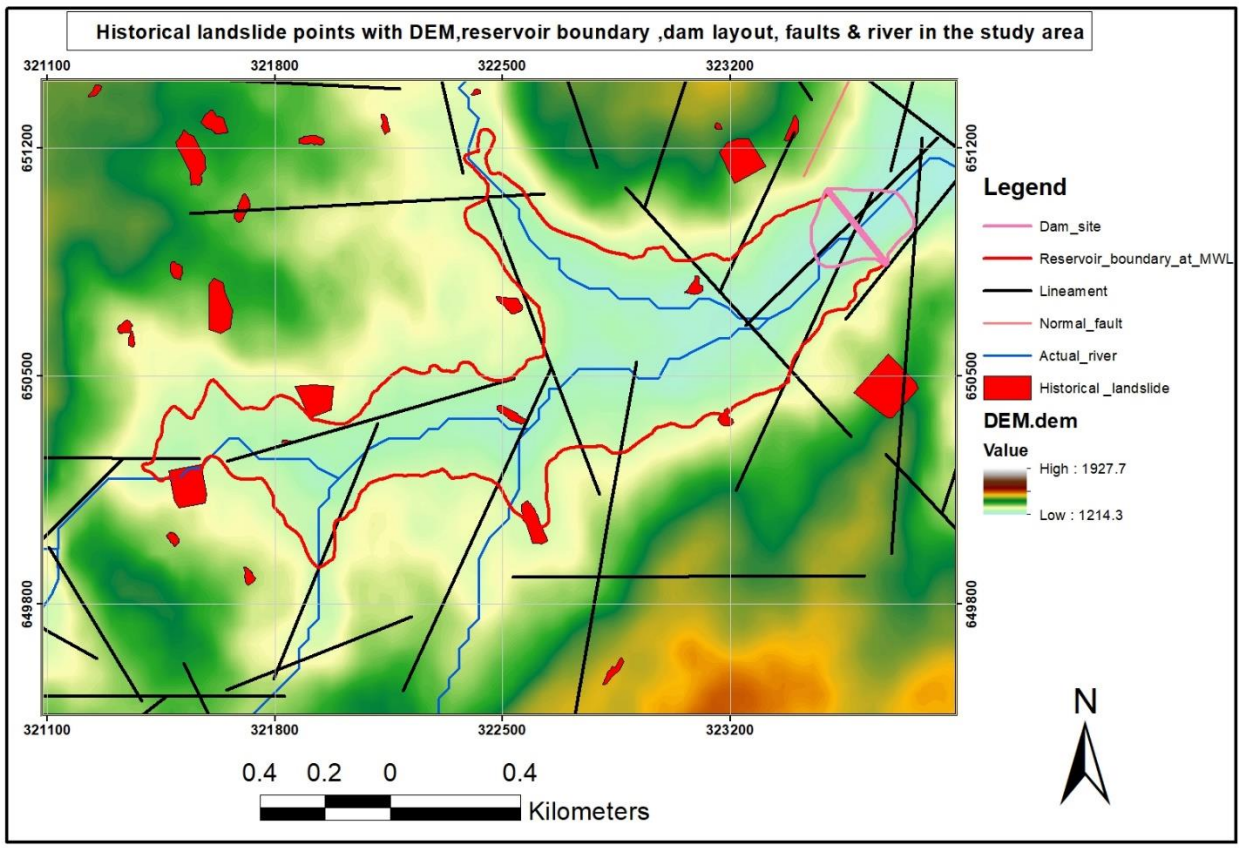

Figure 3. 16.Geological structures in Sego dam and reservoir

3.4.1.2.Method to Produce Landslide Susceptibility Map by ILWIS

In general, the landslide inventory map was produced by using the visual inspection then the landslide induced factors were selected based on the literature review and the relationship with the landslides. After selecting the most relevant influential factors the input data was prepared using Arc GIS. The slope, aspect and curvatures derived from DEM data using 3D analyst tool. Buffer analysis was made to create distance to road and river. All the input data was classified using spatial analyst tool and the format was converted by using QGIS. Finally, the SMCE tree was created in ILWIS, the scoring and weighting the factor maps was done. In addition to this, the final map classified by using natural breaks method. For detail information see Figure 3.6.

3.4.1.2.1. Landslide Inventory Map

The method used to produce landslide inventory map was using visual inspection, the landslides

were mapped using Google Earth historical imagery of the time slider as polygons from 2016 to 2021 (Van Westen, 2014). The landslide scars and accumulation areas were identified. As much as possible the visible historical landslide has been mapped.

3.4.1.2.2. Landslide susceptibility map

Spatial multi-criteria analysis is a knowledge-driven method for decision making for multiple alternatives. The algorithm is based on the hierarchical analytical process developed by (Saaty, 1987). The Spatial Multi-Criteria Analysis (SMCE) provides weights for each factor in each alternative, and they are again grouped by their types. Each group are again weighted to create the final goal. Based on the type of the factor, each class on factor map are standardized with weight based on their impact on the goal. If the classes are not categorized, they are standardized as cost functions or benefit functions or combinations of both based on their positive or negative effect on the final goal. The SMCE algorithm for the landslide susceptibility suggested by (Abella & Van Westen, 2007) is shown in Figure 3.17, which explains the process of obtaining the result (susceptibility in this case) as a Goal.

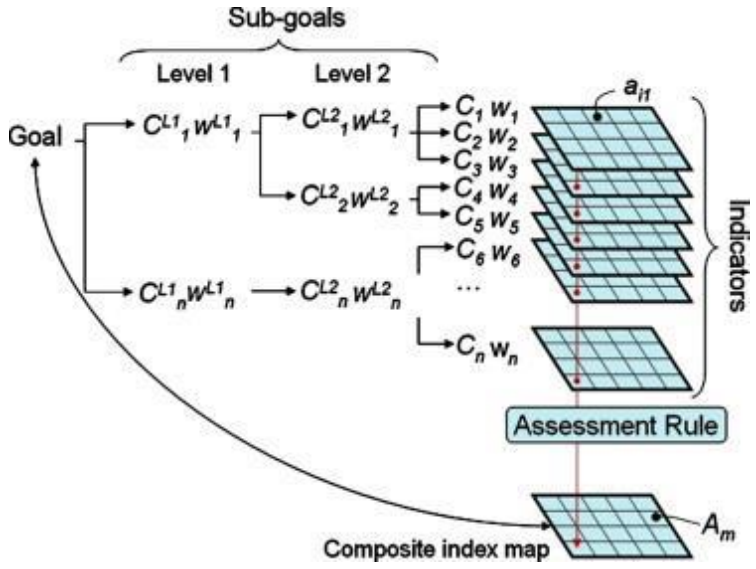

Figure 3. 17 SMCE algorithm for the landslide susceptibility

i. Scoring

After careful understanding of the roles of factor maps in generating the landslide through the overlay analysis. A scoring assessment was assigned to score every class. One class have one score. Although there are many ways to rank each class, for most of the factors, this study uses scoring

system from 0 to 1. Score 0 represents the lowest value and 1 represents the highest value Low values reflect low contribution.

Historical landslide: score assigned based on identified existing land slide get 1 and non-land slide area get score 0.

Slope: Slope's gradient categorization was used to assign a score. The likelihood of a landslide occurring increases with slope height. Thus, the highest-class gradient (>30%) receives the highest score, while the lowest class gradient (<20%) receives the lowest score. in this study's **aspect** was rated according to the equatorial region's general characteristic that the northern or western slopes are often drier than the others. Five scoring classes are then created from eight aspect classes.

There are just three classes for **curves**. Because concave and convex surfaces are thought to have similar influential conditions toward the occurrence of landslides, this study employs two values, 0 and 1, to rank the classes. As a result, the concave and convex sections receive a score of 1, while the flat areas receive a score of 0. Because landslides happen so infrequently in areas with flat and peak surfaces, these terrain forms receive the lowest scores for topographical shape (Caniani et al., 2008). On the other hand, the same research indicates that saddle, convex, and concave hillsides are the places where landslides occur most frequently.

The **geological** factor scores assigned based on the resistance toward slide. The resistance was determined by massiveness, brittleness. In this study, according to the geology of Sego, the alluvium (Qal) gain the high score due to the high amount of silt and clay. Felsic flow and pyroclastic (Tv2) is formed by rhyolite and pyroclastic rocks, the pyroclastic comprised of welded tuff and basalt (Tv3) which is moderately to highly weathered rocks are more exposed to erosion than the trachyte flows and plugs (Tv8). Felsic-intermediate flows (Tv4), Trachyte (Tv6), and Felsic-intermediate flows (Tv7) are considered moderately exposed to erosion which are fresh to slightly weathered rock. Basalt (Tv1), and Basalt (Tv5) rocks are fresh, aphanitic, and massive which gain lower score value.

Regarding **land use**, the lowest score given to water body and trees because the water body area is comparatively flat, and the trees has dense vegetation that could prevent erosion. Shrub and grasses are slightly increased the score value because both of them have a capacity to lower the pressure of erosions. Built and crop areas have the highest score.

For **distance to road and river**, the scores were determined based on the proximity of the distance to road and river without considering the type of roads. The occurrence of landslides increased

when the distance of the features decreased.

Table 3. 11 Scoring of Influencing factors for ILWIS analysis

Influencing factors	Class	Score
Historical landslide	Landslide area	1
	Non landslide area	0
Curvature	Concave	1
	Flat	0
	Convex	1
Aspect	North (N), West (W), Northwest (NW)	0
	Northeast (NE)	0.4
	East (E), Southwest (SW)	0.6
	Southeast (SE)	0.8
	South (S)	1
Slope	$<20^0$ (gently slope)	0
	$>30^0$ (very steep slope)	1
Geology	Tv1, Tv5	0.2
	Tv4, Tv6, & Tv7	0.45
	Tv8	0.55
	Tv2, Tv3	0.8
	Qal	1
Land use	Water body, trees	0.15
	Shrub area, grass	0.4
	Crop area	0.8
	Built area	1
Soil	Vertisols	0.2
	Luvisols	0.8
	Leptosols	1
Distance to road	>1200m (no effect)	0
	400, 600, 800, & 1200m (mid distance)	0.5
	50, 100, & 200m (near)	1
Distance to river	>500m (no effect)	0.2
	200, 300,400 & 500m (mid distance)	0.55
	50, 100, 150m (near river)	1

ii. Weighting process using ILWIS SMCE

SMCE is a module in ILWIS software that facilitates users in doing multi criteria evaluation in a spatial way. All datasets in advance were converted into ILWIS raster format and surely have the same georeferences (coordinates, borders, and number of pixels). The first step to apply SMCE

was creating a criteria tree. The criteria tree consists of root (main goal or final map) and leafs (criteria or influencing factors map). The factors cannot be straight off usable in weighting process unless had been standardized. The standardization has aims in order to make the factors comparable. Afterwards, to assign weight the software provides three tools: direct, pair-wise and rank ordering comparison. This study used pairwise comparison method. Pair-wise method calculates the magnitude (importance) based on an appraisal to every unique pair of two factors qualitatively (Figure 3.18). In this study totally 28 comparison was made and the software has consistency value which helps to check the quality of the method. If the consistency value shows greater than 0.1 the comparison considered as inconsistence. In addition to this, the factor maps standardize by using the maximum standardization which means by dividing the factors by the maximum value. After that the factor maps grouped based on their properties and weighted them based on their impact on the landslide creation and their quality of data. Each group was weighted based on their relevance, quality, effect, and properties. After completion of the weighting and standardization, the landslide susceptibility index was computed using AHP algorithm.

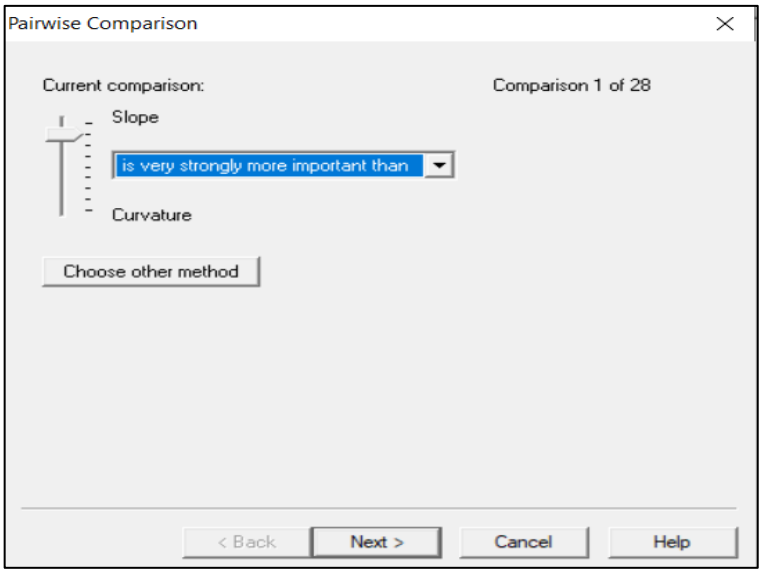

Figure 3. 18 Pairwise comparison of SMCE

After computing the SMCE the landslide susceptibility index was classified into five classes (i.e., very low, low, medium, high and very high) using ARCGIS classification which is natural break method.

3.4.2. Computation of impulse wave generation, propagation, run-up and overtopping

Three main landslide impact zones have been chosen after taking into account the landslide susceptibility map and discovered geological faults. The first and the second landslide point are situated near to the left and right side of the dam abutment, 310m,480m far from the dam respectively. And the third landslide zonation point is located at the end of the reservoir on right side of the reservoir 2,250 meter from the dam.

Following are step-by-step discussions of the computations for impulse wave generation and propagation at the three sites.

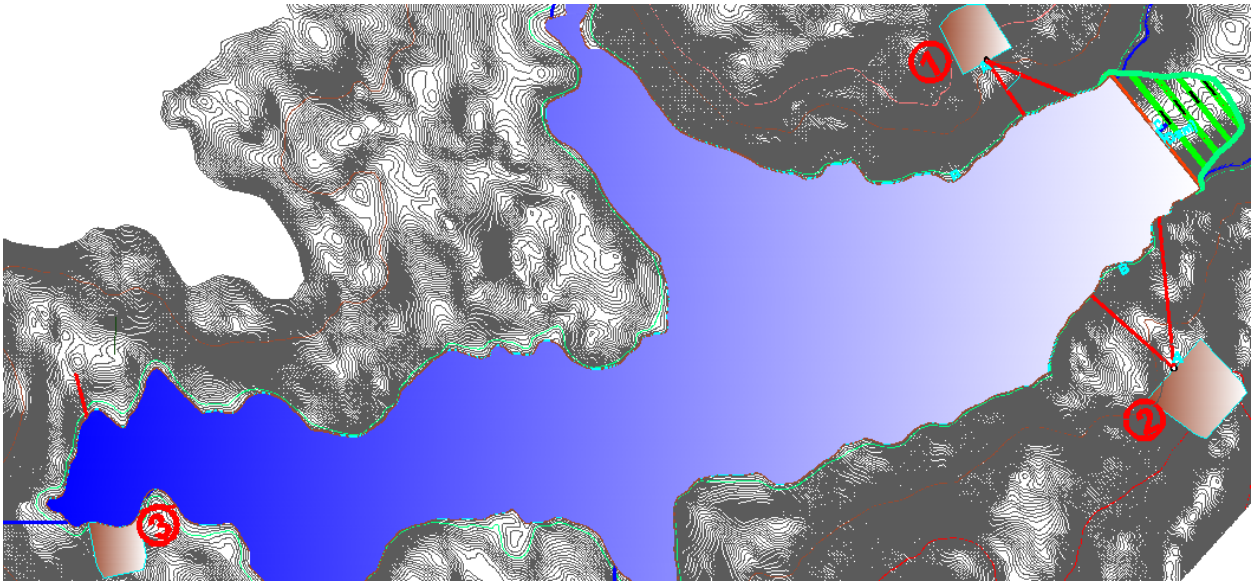

Figure 3. 19 The three main identified landslide point with sego dam and reservoir

3.4.2.1. Landslide One.

This is located at latitude 323257m and longitude 651099.8m on the left side of the reservoir, close to the dam. The historical satellite image and the created landslide zonation map proved that there is an active landslide and high to very high susceptible class at this specific location (Figure 4.3). In addition, a geological structure runs through the point from North West to South East. (Figure 3.16).

3.4.2.1.1. Governing Parameters

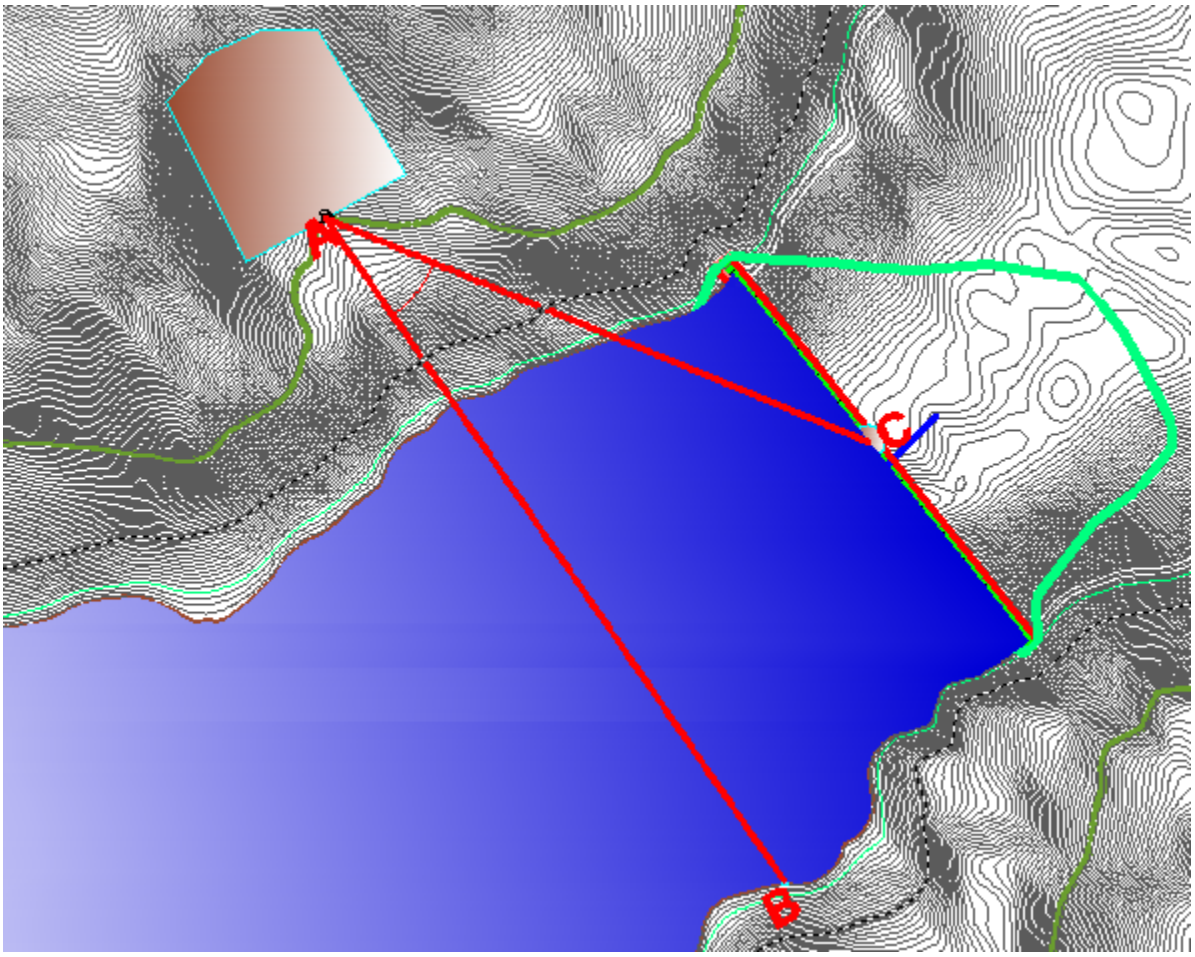

Figure 3. 20 Landslide One (1) with dam layout

The slide impact velocity Vs has been calculated using the required parameter given in Table 2.2 As there is a slope change, it is necessary to use both Eq. (2.2) and Eq. (2.3) for the calculation of Vs. The slide velocity at the point of slope change VsNK is given by

$$V_{sNK} = \sqrt{2 * 9.8 * 50 * (1 - tan20 * cot41)} \quad = 23.9\text{m/s}, \quad from\ \ Eq.(2.2)$$

From this the slide impact velocity Vs can be calculated as

$$V_s = \sqrt{23.9^2 + 2 * 9.81 * 56 * (1 - tan20 * cot30)} = 31.25m/s \quad , from\ Eq.\ (2.3)$$

Table 3. 12 Governing parameters for the slide impact velocity Vs

First slope section				Second slope section			
Term	Symbol	Unit	Value	Term	Symbol	Unit	Value
Drop height of center	ΔZsc	m	50	Drop height of center	ΔZsc	m	56
Dynamic bed friction angle	δ	°	20	Dynamic bed friction angle	δ	°	20
hill slope angle	α	°	41	hill slope angle	α	°	30

(a)

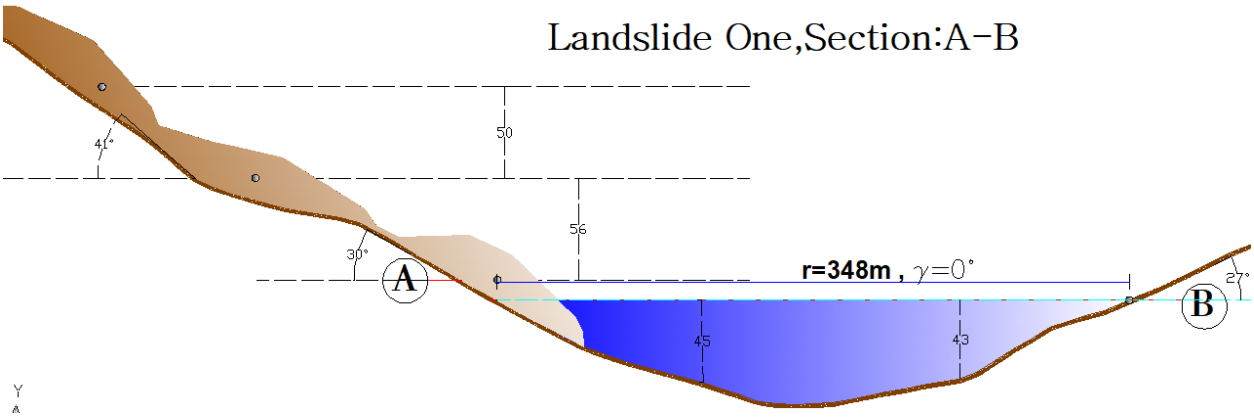

(b)

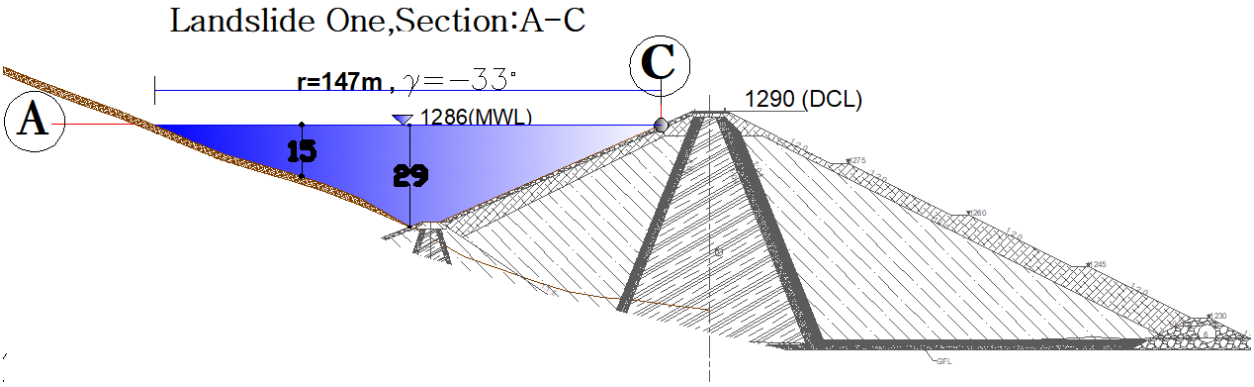

Figure 3. 21 (a) Section A-B with landslide and still water depth h = 45 m on the slide axis, and (b) section A-C with landslide and still water depth h=15m toward the dam

Table 3. 13 Governing parameters for impulse wave generation and the effects on the opposite shore, as well as on the dam

Term	Symbol	Unit	Value	Term	Symbol	Unit	Value
Still water depth (impact zone) for A-B	ha	m	45	Bulk slide density	ρs	kg/m3	1700
Still water depth (impact zone) for A-C	ha	m	15	Bulk slide porosity	n	%	35
Slide thickness	s	m	5	Slide impact angle	a	°	30
Slide width	b	m	60	crest width	bk	m	10
Slide impact velocity	Vs	m/s	31.24621	freeboard	f	m	4
Bulk slide volume	*Vs*-	m3	24000				
Section A-B				Section A-C			
Radial distance	r	m	348	Radial distance	r	m	147
Wave propagation angle	γ	°	0	Wave propagation angle	γ	°	-33
Still water depth (run-up zone)	h	m	43	Still water depth (run-up zone)	h	m	43
Run-up angle	β	°	27	Run-up angle	β	°	23.5

3.4.2.1.2. First Step Computation

The 1st step has been carried out, in respect to Figure 2-9. radially and entirely freely, the impulse wave spreads. Hence, the wave parameters can be calculated using the 3D equations for the reservoir of rectangular form (Subsection 2.7.2.2).

a) Dimensionless parameters and limitations control on the wave generation and propagation computation.

The dimensionless parameters must be within the range of restrictions for usage of the calculation equations in order to make the best forecast possible using this computation process. The following Table 3-14 lists the pertinent dimensionless parameters and restrictions.

Table 3. 14 Dimensionless parameters and limitations control for the calculation of the wave generation and propagation (based on table 2.2.)

Term (Dimensionless parameters)	Symbol	Range	Value	Satisfied?
Slide Froude number A-B	F	0.86-6.83	1.49	yes
Slide Froude number A-C	F	0.86-6.83	2.58	yes
Relative slide thickness A-B	S	0.09-1.64	0.11	yes
Relative slide thickness A-C	S	0.09-1.64	0.33	yes
Relative slide mass A-B	M	0.11-10.02	0.34	yes
Relative slide mass A-C	M	0.11-10.02	3.02	yes
Relative slide density	D	0.59-1.72	1.70	yes
Relative granulate density	pg/pw	0.96-2.75	2.70	yes
Relative slide volume A-B	V	0.05-5.94	0.20	yes
Relative slide volume A-C	V	0.05-5.94	1.78	yes
Bulk slide porosity (%)	n	30.7-43.3	35.00	yes
Slide impact angle (°)	a	30-90	30.00	yes
Relative slide width	B	0.74-3.33	1.33	yes
Relative radial distance section A-B	r/h	(5)-(30)	7.73	yes
Relative radial distance section A-C	r/h	(5)-(30)	9.80	yes
Wave propagation angle A-B (°)	γ	(-90) - (+90)	0.00	yes
Wave propagation angle A-C (°)	γ	(-90) - (+90)	-33.00	yes
Impulse product parameter A-B	P	0.17-8.13	0.36	yes
Impulse product parameter A-C	P	0.17-8.13	1.86	yes

All restrictions are met throughout the wave generation phase, as shown in the above table.

b) Calculation of Wave Generation and Propagation

The wave height H, wave amplitude a, wave period T, and wave length L have all been considered key variables in the analysis of wave generation utilizing the 3D technique as stated in Subsection 2.7.2.3. Using Eqs. (2.7), (2.9), and (2.10), the maximum wave parameter values in the slide impact zone have been calculated independent of the 2D or 3D geometry. However, the calculation equations for the 2D and 3D situations are different when the distance to the point for which the wave parameters are required is $x > x_M$ (2D) or $r > x_M$ (3D) (Subsections 2.7.2.2 and 2.7.2.3). With the use of Eq. (2.8), the maximum wave height H_M's streamwise distance x_M can be computed as

$$X_M(A-B) = (11/2) * 0.36^{1/2} * 45 = 148.1m \qquad from\ Eq \qquad (2.8)$$

$$X_M(A-C) = \left(\frac{11}{2}\right) * 1.86^{1/2} * 15 = 112.55m \qquad from\ Eq \qquad (2.8)$$

We can see from the values that the radial distance r to the reservoir bed in front of point B and to point C on the dam are greater than 148.1m & 112.55m respectively (Table 3.13), therefore, the wave parameters have determined using Eqs. (2.14), (.15) and (2.16).

Section A-B

$$H(r,\gamma) = (3/2) * 0.36^{4/5} cos^2\left(\frac{2*0}{3}\right) * (348/45)^{-2/3} * 45 = 7.6m \quad from\ Eq.(2.14)$$

$$T(r,\gamma) = 15 * \left(\frac{7.6}{43}\right)^{1/4} * (43/9.81)^{1/2} \quad = 20.35s \quad from\ Eq.(2.15)$$

$$a = (4\ /\ 5) * 7.6 = \ 6.1m \qquad from\ Eq. \quad (2.5)$$

$$L(r,\gamma) = 20.35 * 9.81 * (43 + 6.1) = \ 446.65m \qquad from\ Eq. \ (2.16)$$

Section A-C

$$H(r,\gamma) = (3/2)1.86^{4/5} cos^2\left(\frac{2*-33}{3}\right)(147/45)^{-2/3} * 15 = 6.94m \quad from\ Eq.(2.14)$$

$$T(r,\gamma) = 15\left(\frac{6.94}{29}\right)^{1/4} (29/9.81)^{1/2} \quad = 18s \quad from\ Eq.(2.15)$$

$$a = (4\ /\ 5) * 6.94 = \ 5.55m \qquad from\ Eq. \quad (2.5)$$

$$L(r,\gamma) = 18 * 9.81 * (29 + 5.55) = \ 332.1m \qquad from\ Eq. \ (2.16)$$

c) Wave run-up including limitations control

The dimensionless parameters for the dam and the run-up height R have been derived with the aid

of the wave parameters determined in b). Equation (2.17) is valid only for the run-up calculation on dams.

Table 3. 15 Dimensionless parameters and limitations control for the calculation of wave run-up at point B.

Section A-B

Term (Dimensionless parameters)	Symbol	Range	Value	Satisfied?
Relative wave height	H/h	0.011-0.521	0.18	yes
Wave steepness	H/L	0.001-0.013	0.02	not
Run-up angle at B (opposite shore)	β		27.00	
Relative angle	90°/β	1-4.9	3.33	yes

$$R = 1.25 * (0.18)^{5/4} * (0.02)^{-3/20} * (3.33)^{1/5} * 43 = 14.4\,, from\ Eq.\ \ (2.17)$$

Table 3. 16 Dimensionless parameters and limitations control for the calculation of wave run-up at point C

Section A-C

Term (Dimensionless parameters)	Symbol	Range	Value	Satisfied?
Relative wave height	H/h	0.011-0.521	0.24	yes
Wave steepness	H/L	0.001-0.013	0.02	not
Run-up angle at C (Dam)	β		23.50	
Relative angle	90°/β	1-4.9	3.83	yes

$$R = 1.25 * 0.24^{5/4} * (0.02)^{-3/20} * (3.83)^{1/5} * 15 = 7.34\,, from\ Eq.\ \ (2.17)$$

d) Wave Overtopping

As the aforementioned calculation shows the freeboard of f = 4 m is smaller than the run-up height of R = 7.34 m at point C (Dam), this show that a part of the impulse wave will overtop the dam. New limitations govern the determination of the overtopping volume (Subsection 2.8.3):

Point C

Table 3. 17 Dimensionless parameters and limitations control for the calculation of wave overtopping at point C.

Term (Dimensionless parameters)	Symbol	Range	Value	Satisfied?
Relative wave height	H/h	0.019-0.488	0.24	yes
Non linearity	a/H	0.59-0.95	0.80	yes
Wave steepness	H/L	0.02-0.023	0.02	yes
Relative period	T(g/h)^0.5	(9-21)	10.49	yes
Relative wave celerity	c^2/(gh)	0.83-1.4	1.19	yes
Relative wave length	L/h	(6-24)	11.45	yes
Relative wave angle	90°/β	1-4.9	3.83	yes

The appropriate volume $\forall_0$ per unit length of the dam crest for f = 0 has first been calculated as follows in order to determine the overtopping volumes V:

Kq, = 0.41 (β = 90°), κq = 0.47 (β = 45°) and κq = 0.51 (β = 18.4°). since our β is 23.5° by interpolation we got kb is equal to 0.5.

Kb has determined from Figure 2.14 (a) as a function of the relative maximum overtopping depth aMax,T/bK =6.9/10=0.69 and Kb becomes 0.75 and kw = 1.3 for the whole range 18.4° ≤ β ≤ 90°.

$$\kappa = \kappa q \kappa b \kappa w^{3/2} \quad , \qquad \kappa = 0.5*0.75*(1.3)^{3/2}=0.56$$

$$\forall_0 = 1.45 * 0.56 * \left(\frac{6.94}{29}\right)^{4/3} \left(\frac{18}{\sqrt{29/9.81}}\right)^{4/9} 29^2 \ = 286.42 \frac{m3}{m}, from\ Eq\ .\ (2.18)$$

Overtopping Volume V per unit length dam crest for f>0 (m^3/m) becomes

$$\forall = \left(1 - \frac{4}{7.34}\right)^{11/5} * 286.42 = 50.61, \qquad fromEq.(2.19)$$

The duration of overtopping t_0 for the overtopping volume V_0 = 286.42 m3 /m for f = 0 has been

estimated as follow:

$$t_0 = 4\left(18 * \sqrt{9.81/29}\right)^{4/9} (29/9.81)^{1/2} = 19.55s \qquad From\ Eq.\ (2.20)$$

Average discharge q_{0m} per unit length dam crest for f=0 (m^2/s) becomes

$$q_{0m} = 286.42/19.55 = 14.65 \qquad fromEq.(2.21)$$

And Maximum discharge q_{0M} per unit length dam crest f=0 (m^2/s) becomes

q_{0M}=2*q_{0m}=2*14.65=29.3 $m^3/s/m$

Table 3. 18 Limitations for the calculation of the duration of overtopping t0.

Term (Dimensionless parameters)	Symbol	Range	Value	Satisfied?
Relative period	T(g/h)^0.5	14-22	10.49	No
Relative duration of overtopping	t_o(g/h)^0.5	10.5-13.5	11.37	Yes

e) Required freeboard to prevent overtopping

The desirable freeboard f, which takes into account the operation of the dam throughout project life time, which sufficient to ensure that the earthen dam is not overtopped by an impulse wave has determined.

The run-up height at point C (Dam) found to be R = 7.34 m, however the original design freeboard of the dam is 4 m. therefore emergency drawdown of the reservoir by the difference R − f = 3.34 m may be adequate to prevent overtopping, however it is difficult to decide before a new calculation is made in the following approaches. This is because, Certain controlling factors, like the slide impact velocity Vs, may alter as the reservoir level is decreased. In this landslide, lowering the reservoir level by 7m is assumed first and the new freeboard of f = 11 m, and all the above calculations and the above section has been repeated as follow.

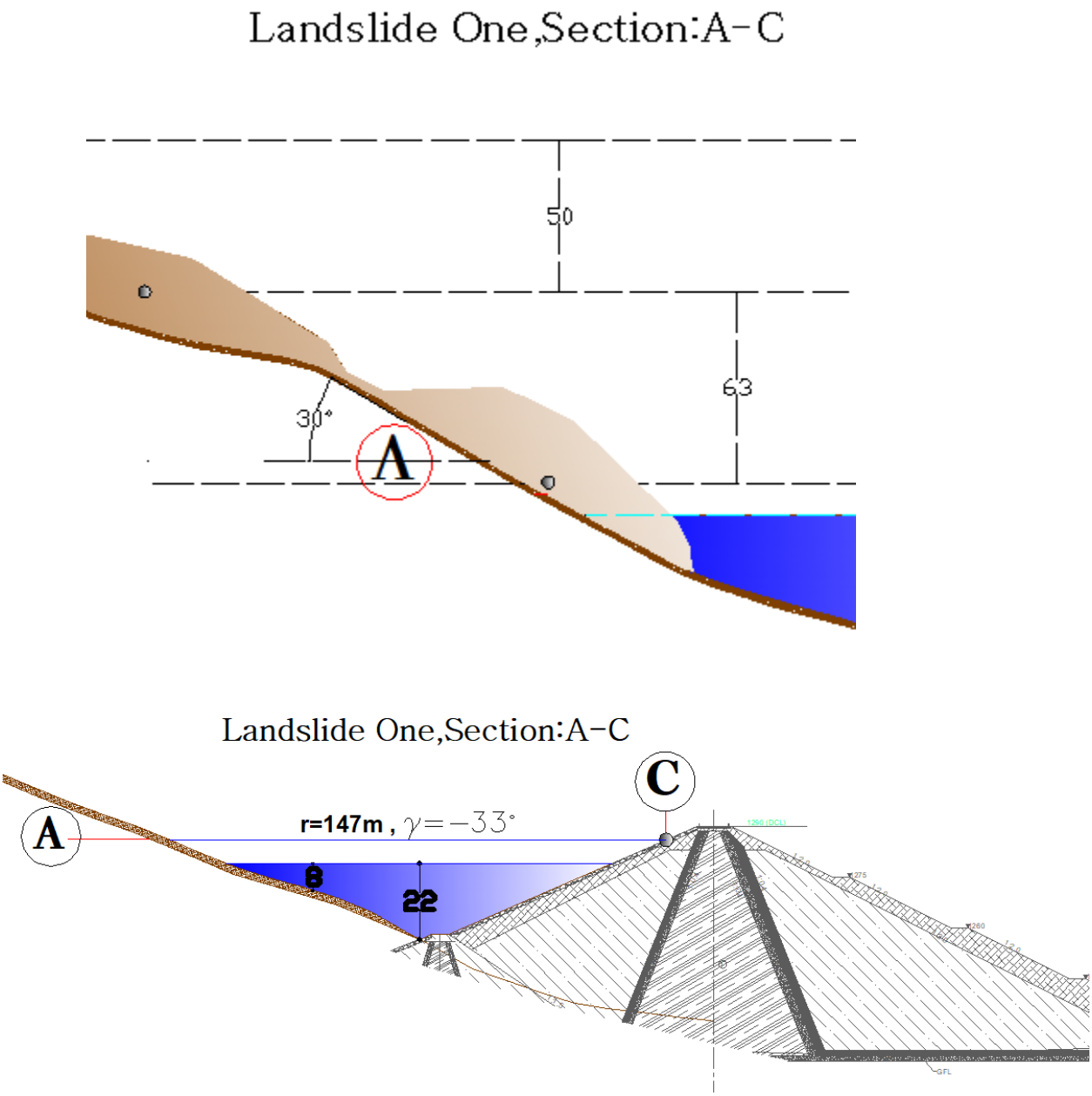

Figure 3. 22 7m lowered section along section A-C

Table 3. 19 New impact zone design parameter after lowering of 7m

Term (Dimensionless parameters)	Symbol	Unit	Value
Emergency drawdown height		m	7
New Still water depth (impact zone)	h_a	m	8
New Still water depth (at dam)	h_c	m	22
New Drop height of the center of gravity of the slide	ΔZsc	m	63

The new slide impact velocity is

$$V_s = \sqrt{23.9^2 + 2 * 9.81 * 63 * (1 - tan20 * cot30)} = 32.05 m/s \quad , from\ Eq.\ (2.3)$$

Table 3. 20 Dimensionless parameters and limitations control on the calculation of the wave generation and propagation in section A-C

Term (Dimensionless parameters)	Symbol	Range	Value	Satisfied?
Slide Froude number	F	0.86-6.83	3.62	yes
Relative slide thickness	S	0.09-1.64	0.63	yes
Relative slide mass	M	0.11-10.02	10.63	not
Relative slide density	D	0.59-1.72	1.70	yes
Relative granulate density	pg/pw	0.96-2.75	2.70	yes
Relative slide volume	V	0.05-5.94	6.25	not
Bulk slide porosity (%)	n	30.7-43.3	35.00	yes
Slide impact angle (°)	a	30-90	30.00	yes
Relative radial distance section at A-C	r/h	(5)-(30)	0.52 18.38	yes
Wave propagation angle at A-C (°)	γ	(-90) - (+90)	-33.00 -0.58	yes
Relative streamwise distance	X	2.7-59.2	35.00	yes
Impulse product parameter	P	0.17-8.13	4.90	yes

$$H(r,\gamma) = (3/2)4.9^{4/5} cos^2\left(\frac{2 * -33}{3}\right)(147/8)^{-2/3} * 8 = 5.28m \quad from\ Eq.(2.14)$$

$$T(r,\gamma) = 15\left(\frac{5.28}{22}\right)^{1/4}(22/9.81)^{1/2} = 15.73s \quad from\ Eq.(2.15)$$

$$a = (4\ /\ 5) * 5.28 = 4.23m \quad from\ Eq.\ (2.5)$$

$$L(r,\gamma) = 15.73 * 9.81 * (22 + 4.23) = 252.23m \quad from\ Eq.\ (2.16)$$

Table 3. 21 New Dimensionless parameters and limitations control for the calculation of wave run-up at point C

Term (Dimensionless parameters)	Symbol	Range	Value	Satisfied?
Relative wave height	H/h	0.011-0.521	0.24	yes
Wave steepness	H/L	0.001-0.013	0.02	not
Run-up angle at C (Dam)	β		23.50	
Relative angle	90°/β	1-4.9	3.83	yes

New wave run-up height R becomes:

$$R = 1.25 * 0.24^{5/4} * (0.02)^{-3/20} * (3.83)^{1/5} * 22 = 10.8m\,, from\ Eq. \quad (2.17)$$

Due to the fact that the new freeboard f = 11m is greater than the new wave run-up R, which is 10.8m, impulse wave overtopping is no longer possible.

3.4.2.1.3. Second Step Computation

Mostly, using the aforementioned generally applicable equations, the characteristics of an impulse wave can be accurately predicted from the reservoir geometry. Nevertheless, due to the following primary causes the computed wave run-up may deviates

i. Volumetric displacement by the bulk slide mass

Reservoir surface area at maximum water level from the actual topographic map is 834,000m^2 And Bulk slide volume (V) become 24,000m^3. From existing historical landslide image geometry 60m wide and 90 m length with assumed 5m slide thickness has been taken for computations

V=s*b*l_s = 5m*60m*80m=24000 m^3.

Then volumetric displacement in depth =$\frac{24000\ \mathrm{m3}}{834{,}000\mathrm{m2}}$= 0.029m.

ii. If the slide mass is Solid body instead of granular

In the new computation the new slide Froude number (F) from table 3.20 has become 3.62 which is greater than 3. For small Froude numbers, the maximum wave amplitude aMb is up to seven times greater for solid bodies than for granular slides. Zweifel (2004).

However, the difference for F > 3.0 is small. This is because, Water is unable to enter the pore volume of the slide with high Froude numbers and slide impact velocities Vs. (figure 2.18). Due to the foregoing logical premises, there won't be any change in wave run-up height.

iii. Due to shoaling (Reservoir shape)

The water wave in terms of depth ca be known by, L/h==$\frac{252.23}{22}$= 11.46, which is intermediate-water wave, ($2 \leq L/h \leq 20$).

The Wave height at impact (H1) is 5. 28m.The new relative still depth (h1/h2) is 0.36.

And the new wave height H_2 at dam= H_1*($\frac{h1}{h2}$)$^{1/4}$, 5.28*($\frac{8}{22}$)$^{1/4}$= 4.1m.

The ratio of H_1/H_2=$\frac{5.28}{4.1}$=1.29, which means Wave Run up due to effect of the increase of the still water depth decrease by 29%.

The second runup depth (R_2) =10.8*-0.29=-3.13m

iv. Due to Constriction

We can take 30% increment of the actual wave run-up R for most reservoir geometry (Müller 1995).

R2= 0.3*10.8= 3.24 m

In conclusion due to all those effects an additional wave run up height becomes,

Total wave run-up height (R_T) =R1+ Volumetric displacement+ Shoaling + Constriction

R_T =10.8+0.029m+-3.13m+3.24m=10.94m

3.4.2.1.4. Overtopping volume and depth with other literature

The overtopping volume of land slide one by Kobel et al. (2017) across the total width is

$\varepsilon = \frac{5.6}{29} = 0.19$ and a_w=29+5.6-33=1.55

$$\frac{\mathrm{V}}{60 * 29^2} = 1.42 * \left[0.19 * \left(\frac{29}{33}\right)^{2.5} * \left(\frac{1.55}{10}\right)^{0.105}\right]^{0.8} = 1.42{W_1}^{0.8}; \qquad from\ (2.22)$$

V= 12,614.47 m^3 with limitation value of $W_1^{0.8}$= 0.176 B_k/w= 0.303

where; $0.35 < {W_1}^{0.8} < 0.95,\ 0.07 < b_k/w\ < 0.53.$

$$\frac{\mathrm{V}}{60 * 29^2} = 1.35 * \left[0.19 * \left(\frac{29}{33}\right)^{(2/0.19)\left(23.5/90^{\circ}\right)^{0.25}} \left(\frac{1.55}{10}\right)^{0.105}\right]^{0.7} = 1.35{W_2}^{0.7}..from\ (\ 2.23\ )$$

V= 9,510.22m^3 with limitation value of $W_2^{0.7}$= 0.14 B_k/w= 0.303

where; $0.15 < {W_2}^{0.7} < 0.95$, $0.07 < b_k/w < 0.53$.

The maximum overtopping depth also has computed by, Kobel et al. (2017) as follow with R^2= 0.95 and R^2 = 0.99 respectively:

$$\frac{d_o}{33} = 1.34 * \left[0.19 * \left(\frac{29}{33}\right)^{1.7} \left(\frac{23.5}{90^{\circ}}\right)^{0.25}\right] = 1.34E_1; 0.40 < E_1 < 0.70 \qquad from\ (\ 2.24\ )$$

d_o= 4.86m and E_1= 0.11

and

$$\frac{d_o}{33} = 1.32\left[0.19 * \left(\frac{29}{33}\right)^{4\left[\left(23.5/90^{\circ}\right)^{-0.21}-0.19\right]} \left(\frac{23.5}{90^{\circ}}\right)^{0.16}\right] = 1.34E_2; 0.10 < E_2 < 0.75..from(\ 2.25\ )$$

d_o= 3.48m and E_2= 0.08

3.4.2.2.Landslide two.

It is located in latitude 323628.8m and longitude 650490.2m on the right side of the reservoir, close to the dam. Similar to landslide one the landslide zonation map also verified that the area is categorized under moderate to high susceptible class (Figure 4.3). there is also visible landslide around this specific location. In addition to that, a geological structure runs through the point from North West to South East like landslide one (Figure 3.16).

3.4.2.2.1. Governing Parameters

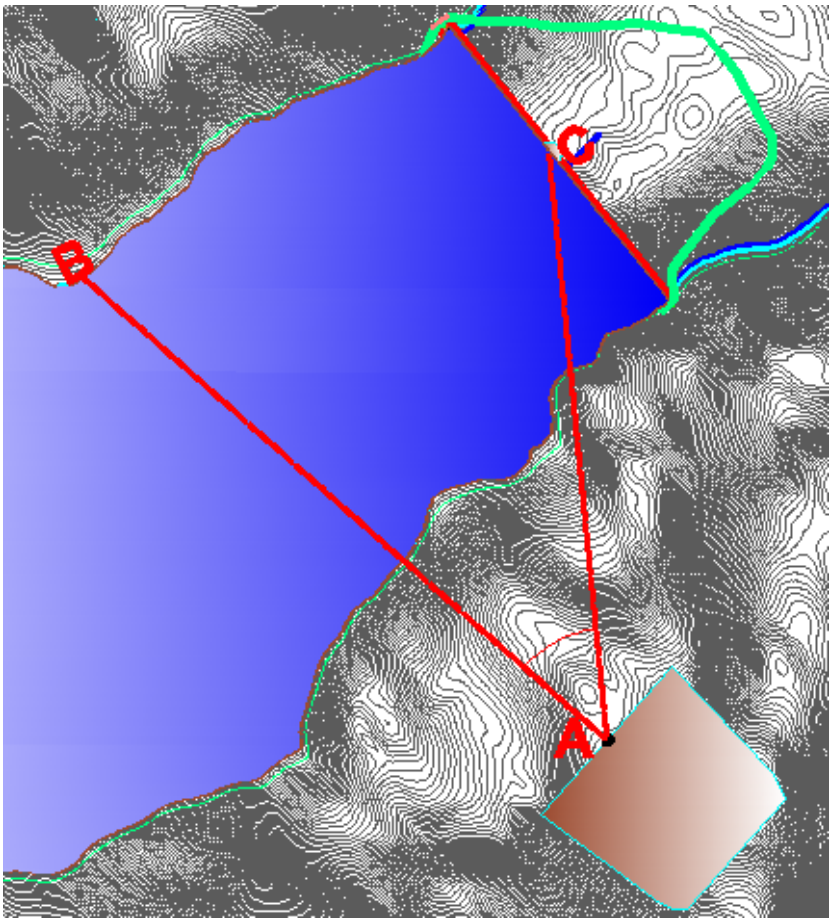

Figure 3. 23. Landslide Two (2) with dam layout

The slide impact velocity Vs has been calculated using the required parameter given in table 2.2 As there is a slope change, it is necessary to use both Eq. (2.2) and Eq. (2.3) for the calculation of Vs. The slide velocity at the point of slope change VsNK is given by

$$V_{sNK} = \sqrt{2 * 9.8 * 35 * (1 - tan20 * cot33)} \quad = 17.4 \text{ m/s}, \quad from\ Eq.(2.2)$$

From this the slide impact velocity Vs can be calculated as

$$V_s = \sqrt{17.4^2 + 2 * 9.81 * 60 * (1 - tan20 * cot35)} = 29.45\, m/s \quad , from\ Eq.\ (2.3)$$

Table 3. 22 Governing parameters for the slide impact velocity Vs

First slope section				Second slope section			
Term	Symbol	Unit	Value	Term	Symbol	Unit	Value
Drop height of center	ΔZsc	m	35	Drop height of center	ΔZsc	m	60
Dynamic bed friction angle	δ	°	20	Dynamic bed friction angle	δ	°	20
Hill slope angle	α	°	33	Hill slope angle	α	°	35

(a)

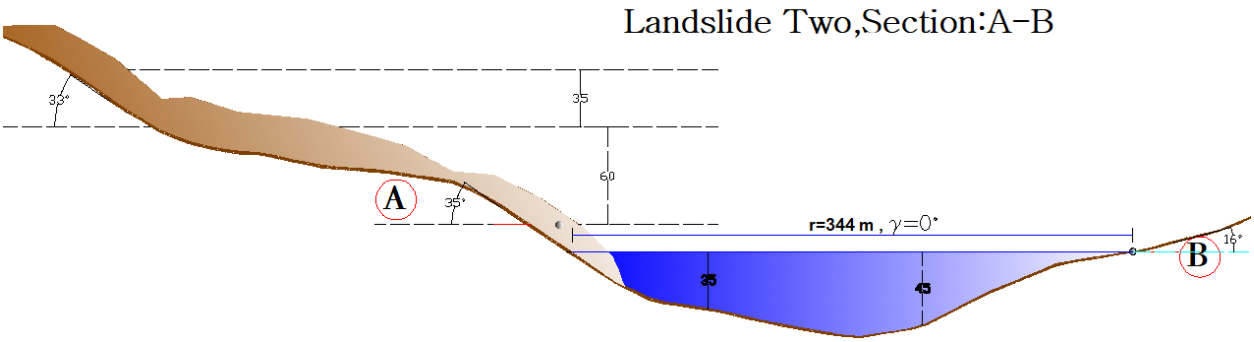

(b)

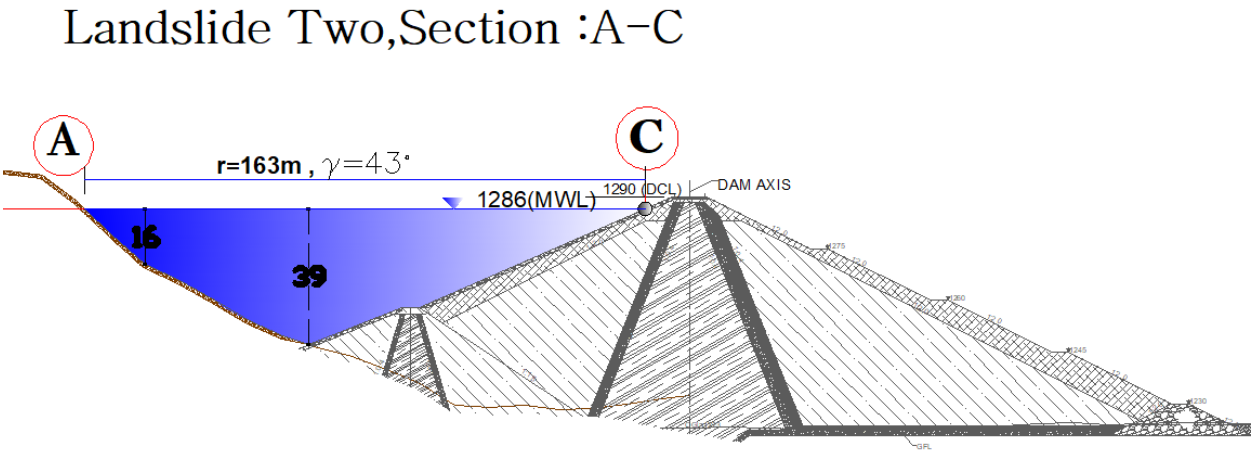

Figure 3. 24 (a) Section A-B with landslide and still water depth h = 45 m on the slide axis, and (b) section A-C with landslide and still water depth h=15m toward the dam

Table 3. 23 Governing parameters for impulse wave generation and the effects on the opposite shore, as well as on the dam

Term	Symbol	Unit	Value	Term	Symbol	Unit	Value
Still water depth (impact zone) for A-B	ha	m	35	Bulk slide density	ρs	kg/m3	1700
Still water depth (impact zone) for A-C	ha	m	16	Bulk slide porosity	n	%	35
Slide thickness	s	m	5	Slide impact angle	a	°	35
Slide width	b	m	60	Crest width	bk	m	10
Slide impact velocity	Vs	m/s	29.45	Freeboard	f	m	4
Bulk slide volume	*Vs*-	m3	27000				
Section A-B				Section A-C			
Radial distance	r	m	344	Radial distance	r	m	163
Wave propagation angle	γ	°	0	Wave propagation angle	γ	°	43
Still water depth (run-up zone)	h	m	45	Still water depth (run-up zone)	h	m	43
Run-up angle	β	°	27	Run-up angle	β	°	23.5

3.4.2.2.2. First Step Computation

According to Figure 2-9, the first stage has been completed. Radially and entirely freely, the impulse wave spreads. As a result, the wave parameters for the rectangular reservoir can be determined using the 3D equations (Subsection 2.7.2.2).

a) Dimensionless parameters and limitations control on the wave generation and propagation computation.

The dimensionless parameters must be within the range of restrictions for application of the calculation equations in order for this computation technique to produce the best predictions. Table 3-14 below provides the pertinent dimensionless parameters and restrictions.

Table 3. 24 Dimensionless parameters and limitations control for the calculation of the wave generation and propagation (based on table 2.2.)

Term	Symbol	Range	Value	Unit	Satisfied?
Slide Froude number A-B	F	0.86-6.83	1.589		yes
Slide Froude number A-B	F	0.86-6.83	2.350		yes
Relative slide thickness A-B	S	0.09-1.64	0.14		yes
Relative slide thickness A-C	S	0.09-1.64	0.31		yes
Relative slide mass A-B	M	0.11-10.02	0.62		yes
Relative slide mass A-B	M	0.11-10.02	2.99		yes
Relative slide density	D	0.59-1.72	1.7		yes
Relative granulate density	pg/pw	0.96-2.75	2.7		yes
Relative slide volume AB	V	0.05-5.94	0.37		yes
Relative slide volume AC	V	0.05-5.94	1.76		yes
Bulk slide porosity	n	30.7-43.3	35		yes
Slide impact angle	a	30-90	35		yes
			0.61		
Relative slide width	B	0.74-3.33	1.71		yes
Relative radial distance section A-B	r/h	(5)-(30)	9.83		yes
Relative radial distance section A-C	r/h	(5)-(30)	10.19		yes
Wave propagation angle A-B	γ	(-90) -(+90)	0.00		yes
			0.00		
Wave propagation angle A-C	γ	(-90) -(+90)	43.00		yes
			0.75		
Relative streamwise distance	X	2.7-59.2	0.00		yes
Impulse product parameter A-B	P	0.17-8.13	0.50		yes
Impulse product parameter A-C	P	0.17-8.13	1.61		yes

All restrictions are met throughout the wave generation phase, as shown in the above table.

b) Calculation of Wave Generation and Propagation

The wave height H, wave amplitude a, wave period T, and wave length L have all been considered key variables in the analysis of wave generation utilizing the 3D approach as mentioned in Subsection 2.7.2.3. Using Eqs. (2.7), (2.9), and (2.10), the maximum wave parameter values in the slide impact zone have been calculated independent of the 2D or 3D geometry. However, the calculation equations for the 2D and 3D situations are different when the distance to the point for which the wave parameters are required is $x > x_M$ (2D) or $r > x_M$ (3D) (Subsections 2.7.2.2 and 2.7.2.3). With the use of Eq. (2.8), the maximum wave height H_M's streamwise distance x_M can be

calculated as

$$X_M(A-B) = (11/2) * 0.5^{1/2} * 35 = 135.7m \qquad from\ Eq \qquad (2.8)$$

$$X_M(A-C) = \left(\frac{11}{2}\right) * 1.61^{1/2} * 16 = 111.6m \qquad from\ Eq \qquad (2.8)$$

The radial distances r to the reservoir beds in front of points B and C on the dam are more than 135.7 m and 111.6 m, respectively, as can be seen from the data in Table 3.13. As a result, the wave parameters have been calculated using Eqs. (2.14), (.15), and (2.16).

Section A-B

$$H(r,\gamma) = (3/2) * 0.50^{4/5} cos^2\left(\frac{2*0}{3}\right) * (344/35)^{-2/3} * 35 = 6.54m \quad from\ Eq.(2.14)$$

$$T(r,\gamma) = 15 * \left(\frac{6.54}{45}\right)^{1/4} * (45/9.81)^{1/2} \quad = 19.84s \quad from\ Eq.(2.15)$$

$$a = (4\ /\ 5) * 6.54 = \ 5.23m \qquad from\ Eq. \quad (2.5)$$

$$L(r,\gamma) = 19.84 * 9.81 * (45 + 5.23) = \ 440.3m \qquad from\ Eq. \ (2.16)$$

Section A-C

$$H(r,\gamma) = (3/2) * 1.61^{4/5} cos^2\left(\frac{2*43}{3}\right) * (163/16)^{-2/3} * 16 = 5.75m \quad from\ Eq.(2.14)$$

$$T(r,\gamma) = 15 * \left(\frac{5.75}{39}\right)^{1/4} * (39/9.81)^{1/2} \quad = 18.53s \quad from\ Eq.(2.15)$$

$$a = (4\ /\ 5) * 5.75 = \ 4.59m \qquad from\ Eq. \quad (2.5)$$

$$L(r,\gamma) = 18.53 * 9.81 * (39 + 4.59) = \ 383.25m \qquad from\ Eq. \ (2.16)$$

c) Wave run-up including limitations control

The run-up height R and the dimensionless parameters for the dam have been derived using the wave parameters determined in b). Equation (2.17) is applicable only for the run-up calculation on dams.

Table 3. 25 Dimensionless parameters and limitations control for the calculation of wave run-up at point B.

Section A-B

Term (Dimensionless parameters)	Symbol	Range	Value	Satisfied?
Relative wave height	H/h	0.011-0.521	0.15	Yes
Wave steepness	H/L	0.001-0.013	0.01	Not
Run-up angle at B (opposite shore)	β		16.00	
Relative angle	90°/β	1-4.9	5.63	Not

$$R = 1.25 * (0.15)^{5/4} * (0.01)^{-3/20} * (5.63)^{1/5} * 45 = 13.4, from\ Eq. \quad (2.17)$$

Table 3. 26 Dimensionless parameters and limitations control for the calculation of wave run-up at point C

Section A-C

Term (Dimensionless parameters)	Symbol	Range	Value	Satisfied?
Relative wave height	H/h	0.011-0.521	0.15	Yes
Wave steepness	H/L	0.001-0.013	0.01	Not
Run-up angle at C (Dam)	β		23.50	
Relative angle	90°/β	1-4.9	3.83	Yes

$$R = 1.25 * (0.15)^{5/4} * (0.01)^{-3/20} * (3.83)^{1/5} * 16 = 4.49\ , from\ Eq. \quad (2.17)$$

d) Wave overtopping

As we can see from the computation above, at point C (the dam), the freeboard of f = 4 m is lower than the run-up height of R = 4.49 m, indicating that a portion of the impulse wave will topple the dam. The calculation of the overtopping volume is subject to new restrictions (Subsection 2.8.3):

Point C

Table 3. 27 Dimensionless parameters and limitations control for the calculation of wave overtopping at point C.

Term (Dimensionless parameters)	Symbol	Range	Value	Satisfied?
Relative wave height	H/h	0.019-0.488	0.15	Not
Non linearity	a/H	0.59-0.95	0.80	Yes
Wave steepness	H/L	0.02-0.023	0.01	Not
Relative period	T(g/h)^0.5	(9-21)	9.29	Yes
Relative wave celerity	c^2/(gh)	0.83-1.4	1.12	Yes
Relative wave length	L/h	(6-24)	9.83	Yes
Relative wave angle	90°/β	1-4.9	3.83	Yes

Following the steps below, the corresponding volume $\forall_0$ per unit length of the dam crest for f = 0 has been calculated in order to obtain the overtopping volumes V:

Kq = 0.41 (β = 90°), κq = 0.47 (β = 45°) and κq = 0.51 (β = 18.4°). since our β is 23.5° by interpolation we got kb is equal to 0.5.

K_b has been calculated as a function of the relative maximum overtopping depth from Figure 2.14 (a).aMax,T/bK =5.75/10=0.575 and Kb becomes 0.7. and kw = 1.3 for the whole range 18.4° ≤ β ≤ 90°.

$$\kappa = \kappa_q \kappa_b \kappa_w^{3/2} \qquad \kappa = 0.5*0.7*(1.3)^{3/2}=0.52$$

$$\forall_0 = 1.45 * 0.52 * \left(\frac{5.75}{39}\right)^{4/3} \left(\frac{18}{\sqrt{39/9.81}}\right)^{4/9} 39^2 = 239.94 \frac{m3}{m}, from\ Eq.\ (2.18)$$

For >0 (m^3/m), Overtopping volume V per unit length dam crest becomes

$$\forall = \left(1 - \frac{4}{4.49}\right)^{11/5} * 239.94 = 1.80, \qquad from\ Eq. (2.19)$$

Following is an estimate of the overtopping duration t_0 for the overtopping volume V_0 = 239.94 m^3

/m for f = 0.

$$t_0 = 4 * \left(18.53 * \sqrt{9.81/39}\right)^{4/9} * (39/9.81)^{1/2} = 21.48s \qquad From\ Eq.\ (2.20)$$

For f=0 (m^2/s) Average discharge q_{0m} per unit length dam crest becomes

$$q_{0m} = 239.94/21.48 = 11.17 \qquad from\ Eq.(2.21)$$

And Maximum discharge q_{0M} per unit length dam crest f=0 (m^2/s) becomes

q_{0M}=2*q_{0m}=2*11.17 =22.34$m^3/s/m$

Table 3. 28 Limitations for the calculation of the duration of overtopping t_0.

Term (Dimensionless parameters)	Symbol	Range	Value	Satisfied?
Relative period		14-22	9.29	No
Relative duration of overtopping		10.5-13.5	10.77	Yes

e) Required freeboard to prevent overtopping

In order to prevent the earthen dam from being overtopped by an impulse wave, the desired freeboard has been calculated while taking into account how the dam would operate during project execution.

The run-up height at point C (Dam) found to be R = 4.49 m, however the original design freeboard of the dam is 4 m. therefore emergency drawdown of the reservoir by the difference R − f = 0.49 m may be adequate to prevent overtopping, however it is hard to decide before a new computation is made in the following methods. This is because, Certain controlling factors, like the slide impact velocity Vs, may alter as the reservoir level is decreased. In this landslide, lowering the reservoir level by 6m is assumed first and the new freeboard of f = 10 m, and all the above computations and the above section has been repeated as follow.

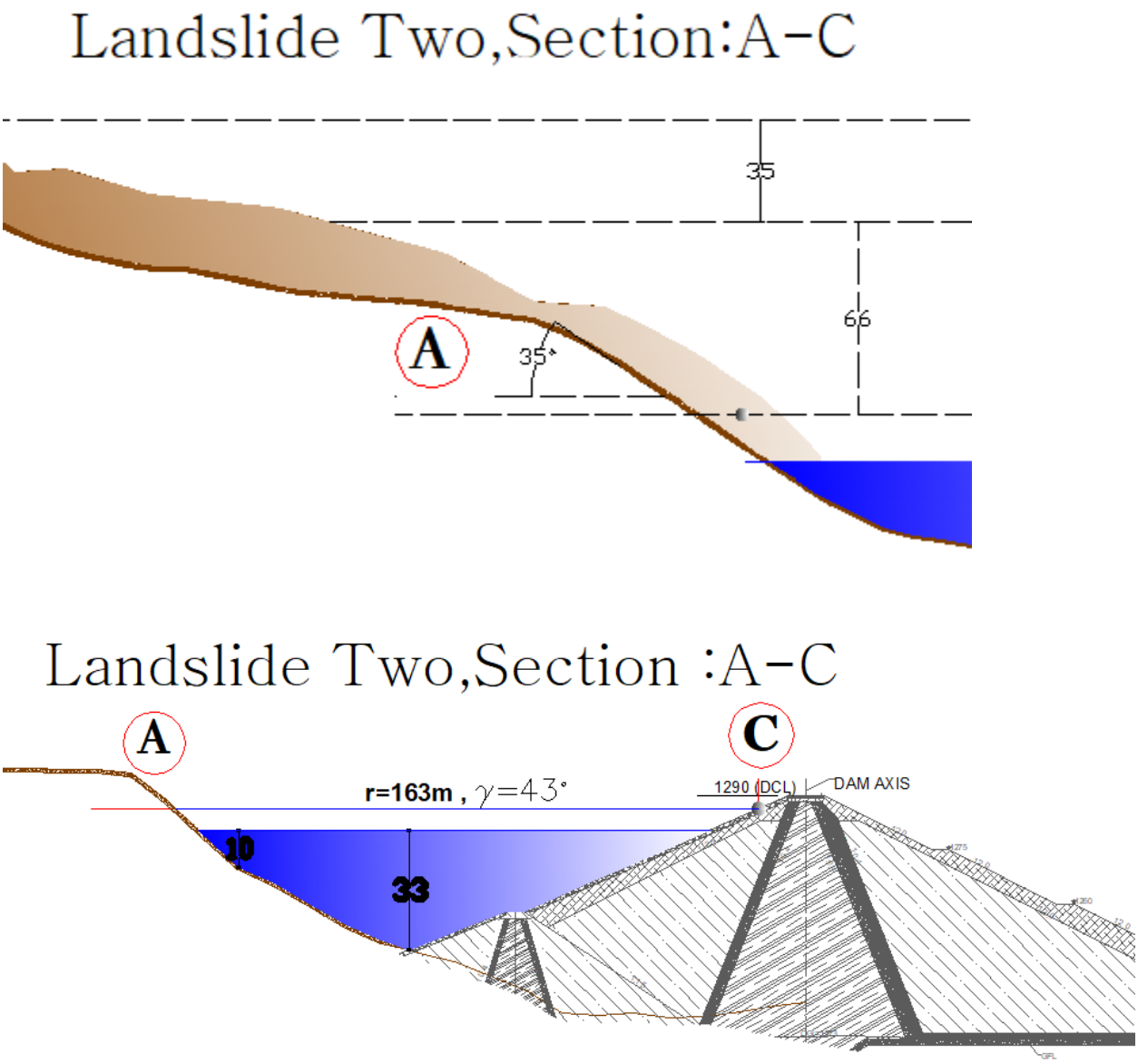

Figure 3. 25. 6m lowered section along section A-C

Table 3. 29. New impact zone design parameter after lowering of 6m

Term (Dimensionless parameters)	Symbol	Unit	Value
Emergency drawdown height			6
New Still water depth (impact zone)	h_a	m	10
New Still water depth (at dam)	h_c	m	33
New Drop height of the center of gravity of the slide	ΔZsc	m	66

The new slide impact velocity is become:

$$V_s = \sqrt{29.45^2 + 2 * 9.81 * 66 * (1 - tan20 * cot35)} = 30.4\, m/s \quad , from\ Eq.\ (2.3)$$

Table 3. 30 Dimensionless parameters and limitations control on the calculation of the wave generation and propagation in section A-C

Term (Dimensionless parameters)	Symbol	Range	Value	Satisfied?
Slide Froude number	F	0.86-6.83	3.07	Yes
Relative slide thickness	S	0.09-1.64	0.5	Yes
Relative slide mass	M	0.11-10.02	7.65	Yes
Relative slide density	D	0.59-1.72	1.7	Yes
Relative granulate density	pg/pw	0.96-2.75	2.7	Yes
Relative slide volume	V	0.05-5.94	4.5	Yes
Bulk slide porosity (%)	n	30.7-43.3	35	Yes
Slide impact angle (°)	a	30-90	35	Yes
			0.61	
Relative slide width	B	0.74-3.33	6	Not
Relative radial distance section A-C	r/h	(5)-(30)	16.3	Yes
Wave propagation angle A-C (°)	γ	(-90)-(+90)	43	Yes
			0.750	
Relative streamwise distance	X	2.7-59.2	0	
Impulse product parameter	P	0.17-8.13	3.36	Yes

$$H(r,\gamma) = (3/2) * 3.36^{4/5} cos^2\left(\frac{2 * 43}{3}\right) * (163/10)^{-2/3} * 10 = 4.73m \quad from\ Eq.(2.14)$$

$$T(r,\gamma) = 15 * \left(\frac{4.73}{33}\right)^{1/4} * (33/9.81)^{1/2} = 16.93s \quad from\ Eq.(2.15)$$

$$a = (4\ /\ 5) * 4.73 = 3.79m \quad from\ Eq.\ (2.5)$$

$$L(r,\gamma) = 16.93 * 9.81 * (33 + 3.79) = 321.65m \quad from\ Eq.\ (2.16)$$

Table 3. 31 New Dimensionless parameters and limitations control for the calculation of wave run-up at point C

Term (Dimensionless parameters)	Symbol	Range	Value	Satisfied?
Relative wave height	H/h	0.011-0.521	0.14	Yes
Wave steepness	H/L	0.001-0.013	0.01	Not
Run-up angle at C (Dam)	β		23.50	
Relative angle	90°/β	1-4.9	3.83	Yes

New wave run-up height R becomes:

$$R = 1.25 * 0.14^{5/4} * (0.01)^{-3/20} * (3.83)^{1/5} * 33 = 8.97m\,, from\ Eq. \quad (2.17)$$

Since the new freeboard f = 10m is greater than the new wave run-up R, which is 8.97m, impulse wave overtopping is no longer probable, as can be seen from the result before the second step computation.

3.4.2.2.3. Second Step Computation

In general, using the aforementioned generally applicable equations, the characteristics of an impulse wave may be rather accurately predicted from the reservoir geometry. However, the calculated wave run-up may vary due to the following key factors and causes:

i. Volumetric displacement by the bulk slide mass

Reservoir surface area at maximum water level from the actual topographic map is found to be 834,000m^2. From existing historical landslide image geometry 60m wide and 90 m length with assumed 5m slide thickness has been taken for computations. Bulk slide volume becomes:

V=s*b*l_s = 5m*60m*90m=27000 m^3

Then volumetric displacement in depth =$\frac{27000\ \mathrm{m3}}{834{,}000\mathrm{m2}}$= 0.032m

ii. If the slide mass is solid body instead of granular

The new slide Froude number (F) from table 3.20 has been calculated again and has now become

3.1, which is higher than 3. The maximum wave amplitude aMb for solid bodies is up to seven times bigger than for granular slides for small Froude numbers. Zweifel (2004)

For F > 3.0, the difference is negligible. This is due to the fact that water cannot enter the pore volume of the slide at high Froude numbers and slide impact velocities Vs (figure 2.18). As a result of the aforementioned logical presumptions, there won't be any change in wave run-up height.

iii. Due to shoaling (Reservoir shape)

The water wave category can be known through, L/h==$\frac{321.65}{33}$= 9.75= it is intermediate-water wave, ($2 \leq L/h \leq 20$).

The Wave height at impact (H_1) is 4.73m, the new relative still depth (h_1/h_2) is 0.30

The new wave height H_2 at dam= $H_1*(\frac{h1}{h2})^{1/4}$, $4.73*(\frac{10}{33})^{1/4}$= 3.51m and,

The ratio of H_1/H_2 =$\frac{4.73}{3.51}$=1.35, which means wave run up obtained in the above will decrease by 35% due to effect of the increase of the still water depth.

R_2= 8.97*-0.35=-3.14m

iv. Due to Constriction

For most reservoir geometries, we can use a 30% raise of the actual wave run-up R. (Müller 1995).

R_2= 0.3*8.97= 2.69 m

In conclusion, due to all those effects an additional wave run up height becomes,

Total wave run-up height (R_T) =R_1+ Volumetric displacement+ Shoaling + Constriction

R_T =8.97+0.032m+-3.14m+2.69m=8.55m

3.4.2.2.4. Overtopping volume and depth with other literature

The overtopping volume of land slide two by Kobel et al. (2017) across the total overtopping width is

$$\varepsilon = \frac{4.6}{39} = 0.12 \text{ and } a_w = 39+4.6-43=0.6$$

$$\frac{V}{60 * 39^2} = 1.42 * \left[0.12 * \left(\frac{39}{43}\right)^{2.5} * \left(\frac{0.6}{10}\right)^{0.105}\right]^{0.8} = 1.42{W_1}^{0.8}; \qquad from\ (2.22)$$

V= 15,215.75 m^3 with limitation value of $W_1^{0.8}$= 0.117, and B_k/w= 0.303

with limitations; $0.35 < {W_1}^{0.8} < 0.95,\ 0.07 < b_k/w\ < 0.53.$

$$\frac{V}{60 * 39^2} = 1.35 * \left[0.19 * \left(\frac{39}{43}\right)^{(2/0.19)\left(23.5/90^{\circ}\right)^{0.25}} \left(\frac{0.6}{10}\right)^{0.105}\right]^{0.7} = 1.35{W_2}^{0.7} .. from\ (2.23)$$

V= 9,793.43 m^3 with limitation value of $W_2^{0.7}$= 0.079, and B_k/w= 0.303

with limitations; $0.15 < {W_2}^{0.7} < 0.95$, $0.07 < b_k/w < 0.53$.

The maximum overtopping depth also has computed by, Kobel et al. (2017) as follow with R^2= 0.95 and R^2 = 0.99 respectively:

$$\frac{d_o}{43} = 1.34 * \left[0.12 * \left(\frac{39}{43}\right)^{1.7} \left(\frac{23.5}{90^{\circ}}\right)^{0.25}\right] = 1.34E_1; 0.40 < E_1 < 0.70 \qquad from\ (2.24)$$

d_o= 4.11m and E_1= 0.071

and

$$\frac{d_o}{43} = 1.32\left[0.12 * \left(\frac{39}{43}\right)^{4\left[(23.5/90^{\circ})^{-0.21}-0.12\right]}\left(\frac{23.5}{90^{\circ}}\right)^{0.16}\right] = 1.34E_2; 0.10 < E_2 < 0.75..from(\ 2.25\ )$$

d_o= 3.25 and E_2= 0.057

3.4.2.3.Landslide three.

This is located at 321522.3 m latitude and 650201.7 m longitude, on the right side of the dam, at the end of the reservoir dam. As shown by the generated landslide zonation map (Figure 4.3), Similar to landslide one and two the area is categorized under high susceptible class. there is also actual landslide at this specific location. In addition to that, a geological structure runs through the point from North East to South West (Figure 3.16).

3.4.2.3.1. Governing parameters

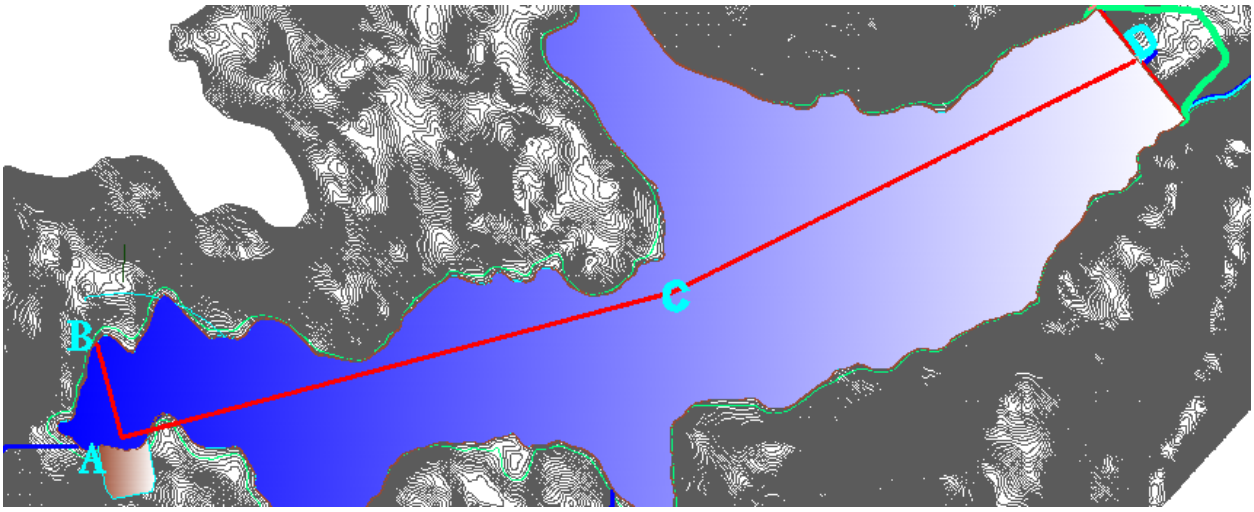

Figure 3. 26 Landslide Three (3) with dam layout

Using Eq. (2.2), the slide impact velocity Vs has been determined using the necessary parameter shown in table 2.2.

$$V_s = \sqrt{2 * 9.8 * 25 * (1 - tan20 * cot21)} \quad = 5.04 \text{ m/s}, \quad from \ Eq.(2.2)$$

Table 3. 32 Governing parameters for the slide impact velocity Vs

Slope section			
Term	Symbol	Unit	Value
Drop height of center	ΔZsc	m	25
Dynamic bed friction angle	δ	°	20
Hill slope angle	α	°	21

(a)

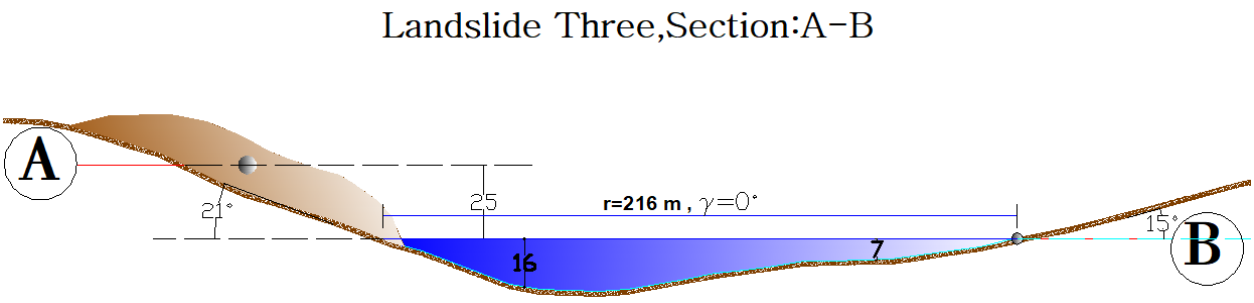

(b)

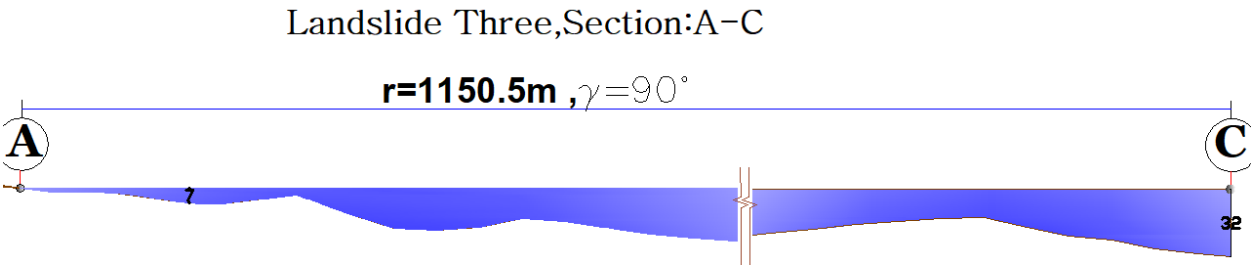

(c)

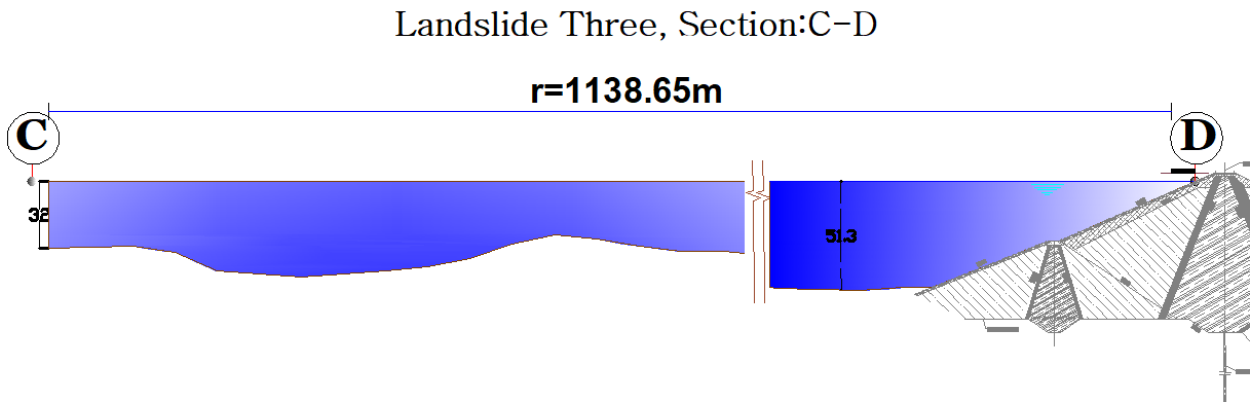

Figure 3. 27 (a) Section A-B with landslide and still water depth h = 45 m on the slide axis, and (b) section A-C with landslide and still water depth h=15m toward the dam

Table 3. 33. Governing parameters for impulse wave generation and the effects on the opposite shore, as well as on the dam

Term	Symbol	Unit	Value	Term	Symbol	Unit	Value
Still water depth (impact zone) for A-B	h_a	m	16	Bulk slide density	ρs	kg/m^3	1700
Still water depth (impact zone) for A-C	h_a	m	7	Bulk slide porosity	n	%	35
Slide thickness	s	m	5	Slide impact angle	a	°	21
Slide width	b	m	60	crest width	b_k	m	10
Slide impact velocity	Vs	m/s	5.04	freeboard	f	m	4
Bulk slide volume	*Vs*-	m^3	24000				
Section A-B				Section A-C			
Radial distance	r	m	216	Radial distance	r	m	1150.5
Wave propagation angle	γ	°	0	Wave propagation angle	γ	°	90
Still water depth (run-up zone)	h	m	7	Still water depth (run-up zone)	h	m	43
Run-up angle	β	°	15	Run-up angle	β	°	23.5

3.4.2.3.2. First step computation

The first phase has been completed, as shown in Figure 2-9. Radially and entirely freely, the impulse wave propagates. As a result, the wave parameters for the rectangular reservoir can be determined using the 3D equations (Subsection 2.7.2.2).

f) Dimensionless parameters and limitations control on the wave generation and propagation computation.

The dimensionless parameters should be within the range of restrictions for usage of the calculation equations in order to make the best forecast possible using this computation procedure. The following Table 3-14 lists the appropriate dimensionless parameters and restrictions.

Table 3. 34 Dimensionless parameters and limitations control for the calculation of the wave generation and propagation (based on table 2.2.)

Term (Dimensionless parameters)	Symbol	Range	Value	Satisfied?
Slide Froude number	F	0.86-6.83	0.40	No
Slide Froude number	F	0.86-6.83	0.61	No
Relative slide thickness A-B	S	0.09-1.64	0.31	Yes
Relative slide thickness A-C	S	0.09-1.64	0.71	Yes
Relative slide mass	M	0.11-10.02	2.66	Yes
Relative slide mass	M	0.11-10.02	13.88	No
Relative slide density	D	0.59-1.72	1.70	Yes
Relative granulate density	pg/pw	0.96-2.75	2.70	Yes
Relative slide volume A-B	V	0.05-5.94	1.56	Yes
Relative slide volume A-C	V	0.05-5.94	8.16	No
Bulk slide porosity	n	30.7-43.3	35.00	Yes
Slide impact angle	a	30-90	21.00	No
			0.37	
Relative slide width	B	0.74-3.33	3.75	Yes
Relative radial distance section A-B	r/h	(5)-(30)	13.50	Yes
Relative radial distance section A-C	r/h	(5)-(30)	164.36	No
Wave propagation angle A-B	γ	(-90)-(+90)	0.00	Yes
			0.00	
Wave propagation angle A-C	γ	(-90)-(+90)	90.00	Yes
			1.57	
Relative streamwise distance	X	2.7-59.2	0.00	Yes
Impulse product parameter A-B	P	0.17-8.13	0.28	Yes
Impulse product parameter A-C	P	0.17-8.13	0.97	Yes

As we can see in the above table, some restrictions are not met throughout the wave generation phase, indicating that there may be some variance from the calculated outcome.

g) Calculation of Wave Generation and Propagation

The wave height H, wave amplitude a, wave period T, and wave length L have all been considered key variables in the analysis of wave generation utilizing the 3D approach as mentioned in Subsection 2.7.2.3. Using Eqs. (2.7), (2.9), and (2.10), the maximum wave parameter values in the slide impact zone have been calculated independent of the 2D or 3D geometry. However, the calculation equations for the 2D and 3D situations are different when the distance to the point for which the wave parameters are required is $x > x_M$ (2D) or $r > x_M$ (3D) (Subsections 2.7.2.2 and 2.7.2.3). With the use of Eq. (2.8), the maximum wave height H_M's streamwise distance x_M can be computed as

$$X_M(A-B) = (11/2) * 0.28^{1/2} * 16 = 46.6m \qquad from\ Eq \qquad (2.8)$$

$$X_M(A-C) = \left(\frac{11}{2}\right) * 0.97^{1/2} * 7 = 37.9m \qquad from\ Eq \qquad (2.8)$$

In order to determine the wave parameters, Eqs (2.14), (.15), and (2.16) were used. As we can see from the values, the radial distances r to the reservoir bed in front of points B and C on the dam are more than 46.6 m and 37.9 m, respectively (Table 3.13).

Section A-B

$$H(r,\gamma) = (3/2) * 0.28^{4/5} cos^2\left(\frac{2*0}{3}\right) * (216/16)^{-2/3} * 16 = 1.5m \quad from\ Eq.(2.14)$$

$$T(r,\gamma) = 15 * \left(\frac{1.5}{7}\right)^{1/4} * (7/9.81)^{1/2} \quad = 8.7s \quad from\ Eq.(2.15)$$

$$a = (4\ /\ 5) * 1.5 = \ 1.2m \qquad from\ Eq. \quad (2.5)$$

$$L(r,\gamma) = 8.7 * 9.81 * (7 + 1.2) = \ 77.8m \qquad from\ Eq. \ (2.16)$$

Section A-C

$$H(r,\gamma) = (3/2) * 0.97^{4/5} cos^2\left(\frac{2*90}{3}\right) * (1150.5/7)^{-2/3} * 7 = 0.1m \quad from\ Eq.(2.14)$$

$$T(r,\gamma) = 15 * \left(\frac{0.1}{51.3}\right)^{1/4} * (51.3/9.81)^{1/2} \quad = 6.9s \quad from\ Eq.(2.15)$$

$$a = (4\ /\ 5) * 0.1 = \ 0.07m \qquad from\ Eq. \quad (2.5)$$

$$L(r,\gamma) = 6.9 * 9.81 * (51.3 + 0.07) = \ 155.5m \qquad from\ Eq. \ (2.16)$$

h) Wave run-up including limitations control

The run-up height R and the dimensionless parameters for the dam have been derived using the wave parameters determined in b). Equation (2.17) only applies to run-up calculations for dams.

Table 3. 35 Dimensionless parameters and limitations control for the calculation of wave run-up at point B.

Section A-B

Term (Dimensionless parameters)	Symbol	Range	Value	Satisfied?
Relative wave height	H/h	0.011-0.521	0.22	Yes
Wave steepness	H/L	0.001-0.013	0.02	Not
Run-up angle at B (opposite shore)	β		15.00	
Relative angle	90°/β	1-4.9	6.00	Not

$$R \ = 1.25 * (0.22)^{5/4} * (0.02)^{-3/20} * (6)^{1/5} * 7 \ = 3.37, from\ Eq. \quad (2.17)$$

Table 3. 36 Dimensionless parameters and limitations control for the calculation of wave run-up at point C

Section A-C

Term (Dimensionless parameters)	Symbol	Range	Value	Satisfied?
Relative wave height	H/h	0.011-0.521	0.0017	Not
Wave steepness	H/L	0.001-0.013	0.0005	Yes
Run-up angle at C (Dam)	β		23.50	
Relative angle	90°/β	1-4.9	3.83	Yes

$$R = 1.25 * (0.0017)^{5/4} * (0.0005)^{-3/20} * (3.83)^{1/5} * 7 = 0.012m\,, from\ Eq.\ (2.17)$$

i) Wave overtopping

Since there won't be any overtopping in the first step competition due to the Run up depth being significantly smaller than the freeboard, it is best to check the second step computation as follows.

3.4.2.3.3. Second Step Computation

Using the aforementioned generally applicable equations, the characteristics of an impulse wave may be rather accurately predicted from the reservoir geometry. The computed wave run-up, however, may vary as a result of the following primary causes.

i. Volumetric displacement by the bulk slide mass

Reservoir surface area at maximum water level from the actual topographic map found to be 834,000m^2. From existing historical landslide image geometry 60m wide and 80 m length with assumed 5m slide thickness has been taken for computations. Bulk slide volume becomes:

$$V=s*b*l_s = 5m*60m*80m=24{,}000\ m^3$$

Then volumetric displacement in depth $=\frac{24000\ m3}{834{,}000m2}= 0.029m$

ii. If the slide mass is solid body instead of granular

For small Froude numbers, the maximum wave amplitude aMb is up to seven times greater for solid bodies than for granular slides. Zweifel (2004)

$\frac{\alpha_{Mb}/7-0.07/7}{\alpha_{Mb}/7} = 1 - 0.26 * 0.61$ for $0.5 \leq F \leq 3.0$ from Eq. (2.23)

α_{Mb} =0.431029

Then the ratio of the two becomes,

$$\frac{\alpha_{Mb}}{\alpha_M} = 6.32$$

Which is an increase of about 632% compared with the calculation in the 1st step.so that

Wave Run up due to influence of the solid body=6.32*R_1, 6.32*0.01=0.07m.

iii. Due to shoaling (Reservoir shape)

Water wave depth can be known by L/h==$\frac{155.5}{51.3}$= 3.03m= it is intermediate water wave, ($2 \leq L/h \leq 20$).

The Wave height at impact (H_1) is 0.085m, the new relative still depth (h_1/h_2) is 0.14.

The new wave height H_2 at dam= $H_1*(\frac{h1}{h2})^{1/4}$, $0.1*(\frac{7}{51.3})^{1/4}$= 0.05m.

The ratio of H_1/H_2 =$\frac{0.085}{0.05}$=1.65, which means wave run up decrease by 65% due to effect of the increase of the still water depth.

R_2= 0.01*-0.65=--0.008m

iv. Due to Constriction

For most reservoir geometries, we can use a 30% increment of the actual wave run-up R. (Müller 1995).

R_2= 0.3*0.01= 0.004 m

Generally due to all those effects an additional wave run up height becomes

Total wave run-up height (R_T) =R_1+ Volumetric displacement+ Solid body +Shoaling + Constriction

R_T =0.01+0.07m +0.029m+-0.008m+0.004m=0.11m

This demonstrates that the new run-up total is lower than the freeboard. Therefore, assuming the dam's freeboard is designed and fixed appropriately, we may conclude that there won't be any overtopping of discharge caused by this specific landslide impulse wave.

3.4.2.4. Bulk Slide Volume Estimation

One of the very challenges of this study was estimating the exact bulk volume of the slide mass in each identified impact zone.it needs detail subsurface investigation through geophysical and core drilling. To model the slide area, shear parameter of the subsurface soil and rock material should be found at a significant depth. However, in this study it is very difficult terms of cost and time to find these data. In this study to compute the slide bulk volume, the researcher just was taken the width and length of the slide mass from the observed existing landslide and different thickness was taken for sensitivity analysis of the three-landslide impact zone.

4. RESULTS AND DISCUSSION

4.1. Land slide zonation map

Figure 4.1 A and B displays the outcomes of weighting in pair-wise comparison for each influential component and the criteria tree in ILWIS. Slope received the most weight (0.282), then geology (0.213), soil (0.139), and land use (0.101). Aspect, curvature, distance to road, and river had the lowest weights, with values of 0.039, 0.056, 0.079, and 0.090, respectively. The inconsistency value is 0.0466. this indicates that the selected process was consistency according to the SMCE validation.

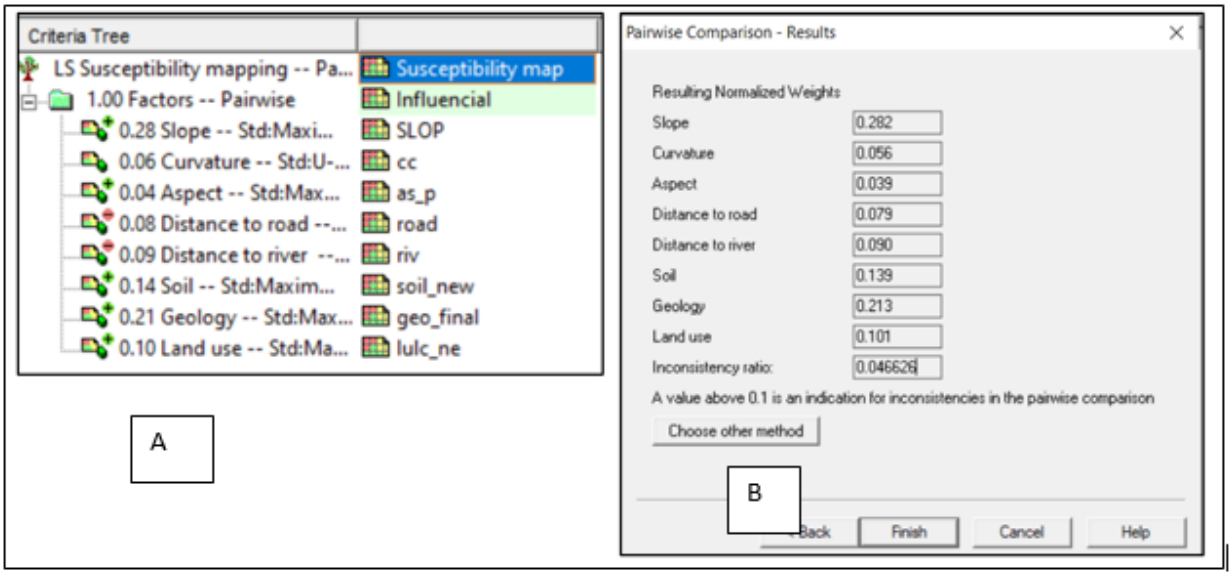

Figure 4. 1 A-Criteria tree, B- Final weight of pairwise comparison

Figure 4.2 displays the landslide susceptibility index map results for Sego project. The degree of vulnerability was determined for every location. The majority of the area was more than 0.6, with the greatest value for the result being 0.97 and the lowest being 0.52. In order to create the final map of landslide susceptibility classes, a cross validation technique was employed to compare the mapped landslide location data with the map of landslide susceptibility classes. The histogram suggests a distribution that is close to being normal.

GIS base classification (natural breaks) shows good accuracy of the implemented model. Because by using the natural breaks classification more than 57.75% of the landslide in the inventory are in

the class of high and very high landslide susceptibility class. Different study used this method to classify the landslide susceptibility indexes for example (Milevski & Dragicevic, 2018).

The landslide as very and highly susceptible zone which was mostly the steep slope and places near the river, road, built and leptosols area. The highly susceptible zone was almost 57.75 % of the study area and the range value for the final weight 0.69-0.97. This class represents most of the landslides with very high frequency and very high density of landslides. Medium susceptibility class it consists of 35.20% of the landslides and has the range of susceptibility value between 0.62-0.69. For very low and low classes all the values below 0.62 were classified as low susceptibility and it consists of only 7.1% of the mapped landslides. Table 4.1 shows the classes with corresponding area and percentage and Figure 4.3 shows spatial distribution of Landslide susceptibility classes.

Table 4. 1 Landslide susceptibility classes with their area and percentage

No	Classes	Hectares	km^2	%
1	Very low	195.0	1.77	2.77
2	Low	305.4	2.78	4.33
3	Medium	2477.2	22.55	35.15
4	High	1325.9	12.07	18.82
5	Very high	2743.6	24.98	38.93

The result of classified landslide susceptibility map shows that most of the planned reservoir and dam sites locations were in the classes of medium to very high susceptible zones (Figure 4.4).

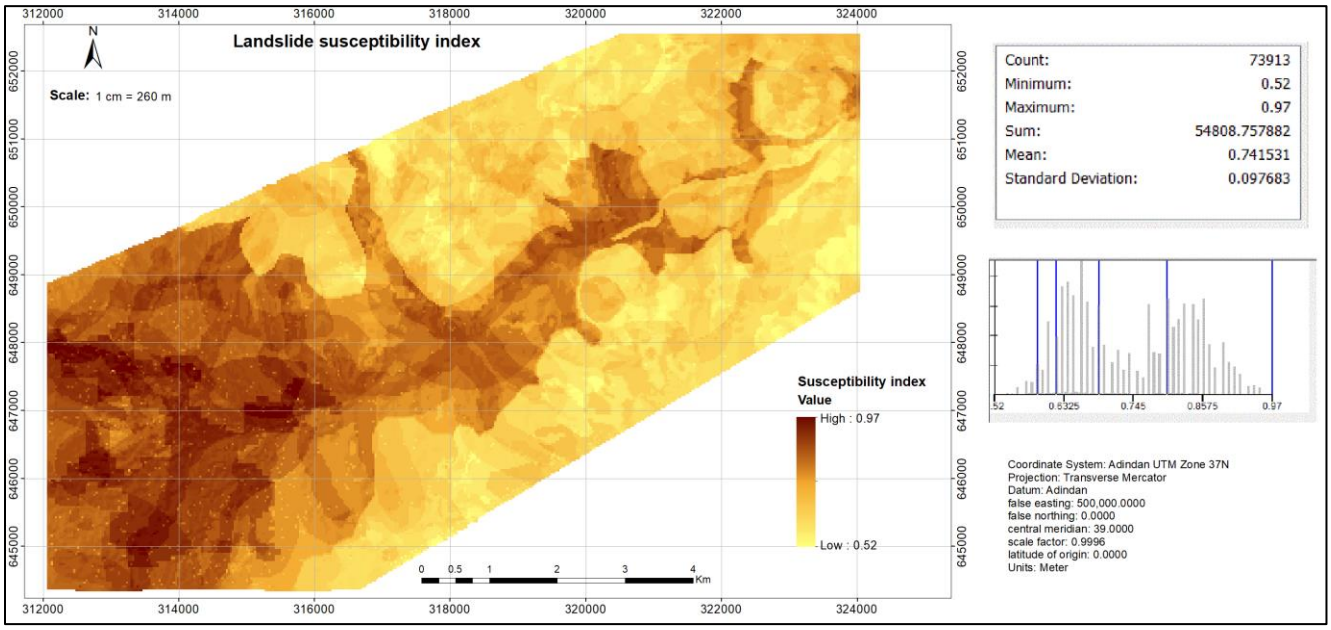

Figure 4. 2 landslide susceptibility index

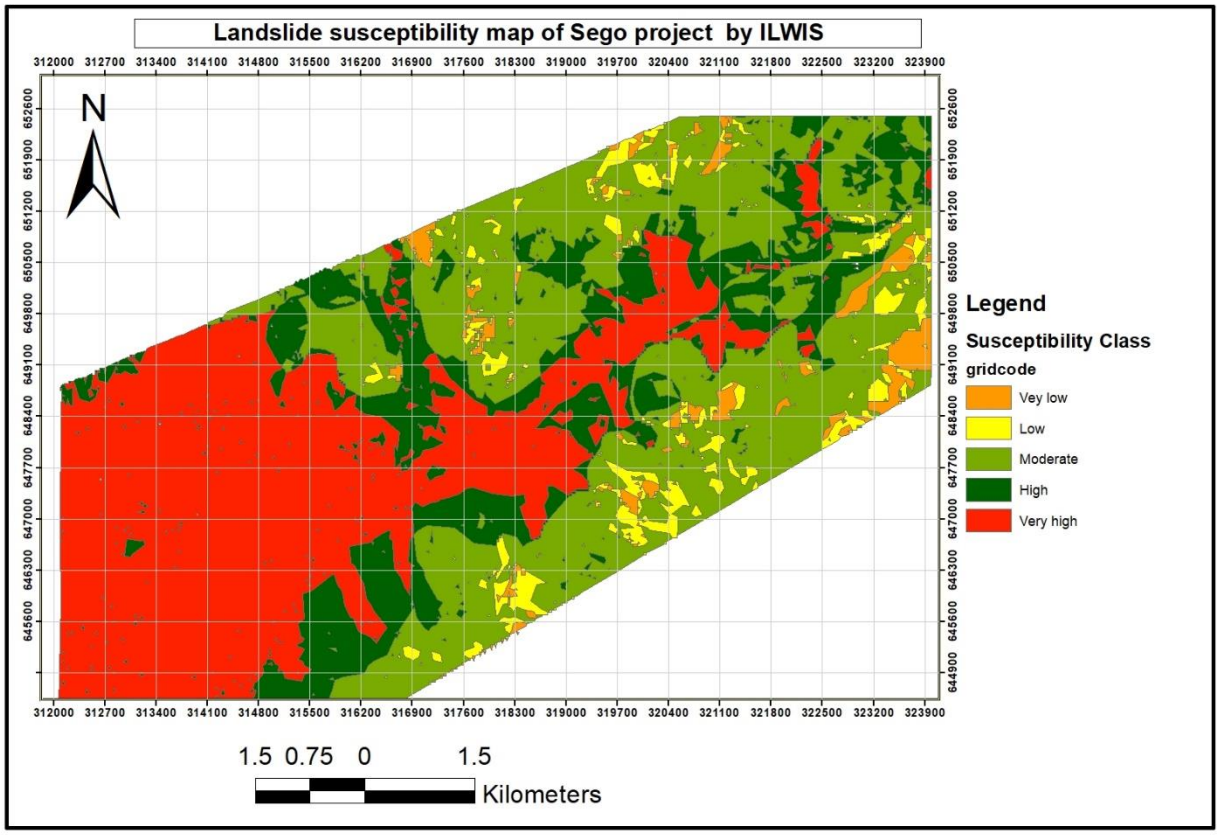

Figure 4. 3 Landslide susceptibility classes

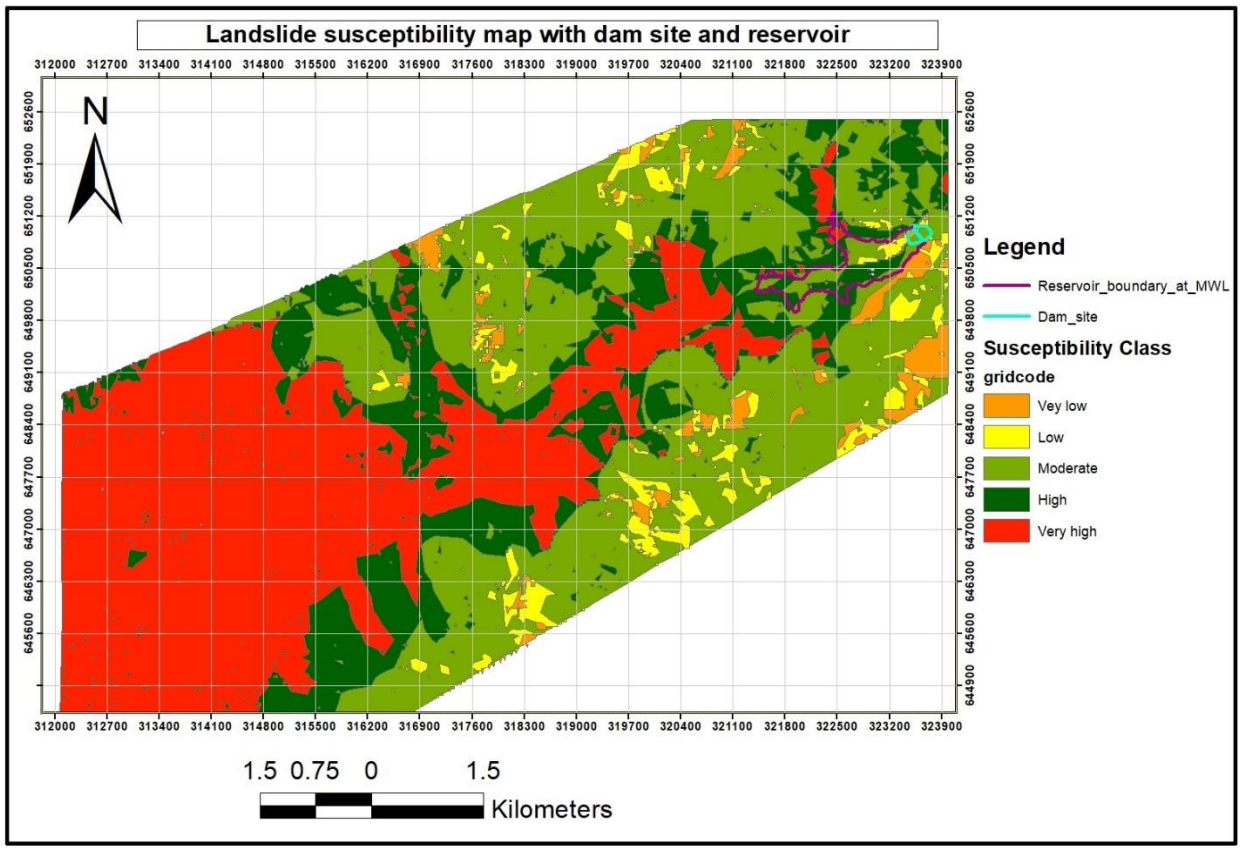

Figure 4. 4 Landslide susceptibility classes with dam site and reservoir

4.2. Impulse wave generation and propagation

4.5.1. Landslide One

The first landslide's impulse wave generation and propagation were examined in detail using a 3D model by Heller (2007) and the conversion method of Huber and Hager (1997), and the results were as follows: before and after an emergency lowering of the reservoir.

The wave height, which is the vertical distance between the crest and the trough, of this particular landslide mass was determined to be 6.94m using the radial distance, wave propagation angle, and impulse product parameter. and the wave periods which is the length of time it takes for one complete wave to pass a specific point were found to be 18.04 seconds using value of the wave height and the still water depth at the dam. and based on wave height, an amplitude of 5.55m, or 80% of the wave height, was discovered. Finally based on the wave period and amplitude, the wave length was discovered to be 332.14 meter which is the horizontal distance between succeeding crests and troughs (Table 4.2).

Table 4. 2 Wave parameters result for landslide one before and after emergency drawdown

Parameter	Unit	With original design	After 7m emergency drawdown
Wave height (H)	m	6.94	5.28
Wave period (T)	s	18.04	15.73
Wave amplitude (a)	m	5.55	4.23
Wave length (L)	m	332.14	252.23

As we can see from the results, all wave parameters' values drop following an emergency drawdown with a new impact velocity. The findings demonstrated that the safety of the dam can be ensured by lowering the reservoir level in the event of a landslide or if geodetic technologies indicate the possibility of a mass movement. To accomplish this, the evacuation mechanism should be adequately planned and designed during design phase of the project.

Since determining the exact thickness of the slide mass is challenging, a sensitivity analysis was conducted using the following ranges of landslide thickness to determine how wave parameters affected the outcome (Table 4.3).

Table 4. 3 Sensitivity analysis and wave parameter result for landslide one

			Slide thickness (m)					
Term	**Symbol**	**Unit**	**5m**	**6m**	**7m**	**8m**	**9m**	**10m**
Slide impact velocity	Vs	m/s	32.05	32.05	32.05	32.05	32.05	32.05
Slide Froude number	F		3.62	3.62	3.62	3.62	3.62	3.62
Impulse product parameter	P		4.90	5.62	6.31	6.97	7.62	8.24
Wave Height	H	m	5.28	5.89	6.47	7.00	7.52	8.01
Wave amplitude	a	m	4.23	4.72	5.17	5.60	6.01	6.41
Wave Period	T	s	15.73	16.16	16.54	16.87	17.17	17.45
Wave Length	L	m	252.23	261.63	270.03	277.67	284.72	291.3

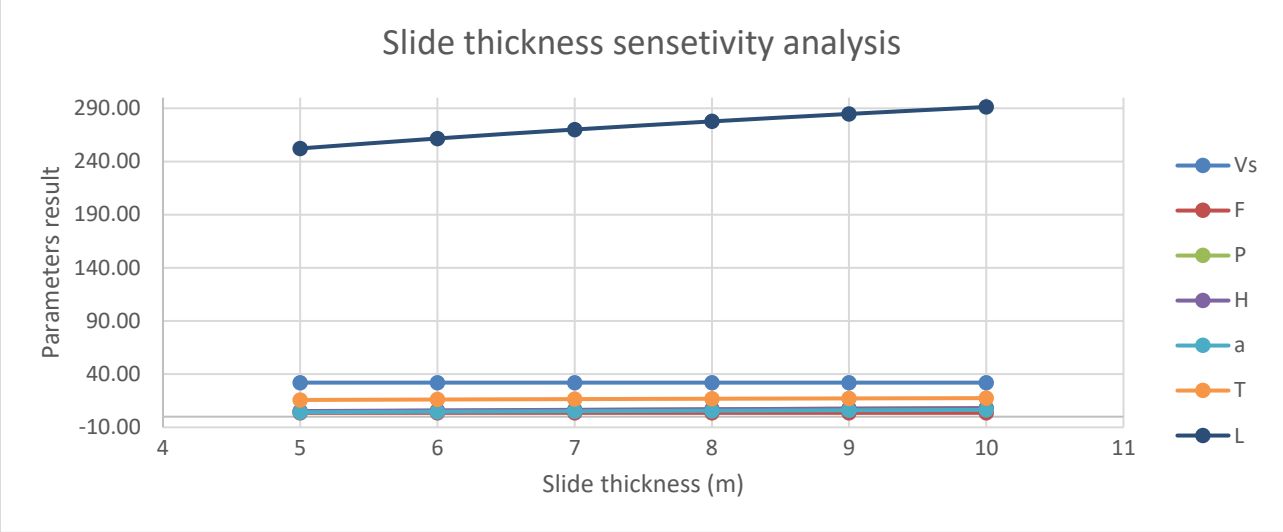

Figure 4. 5 Sensitivity analysis and wave parameter result for landslide one

The slide impact velocity and slide froude number, as shown in the table and figure, are constant across all thicknesses and are unaffected by the volume of the slide mass. because only the drop height and still water depth have an impact on both. However, when the volume of the landslide mass increases, so do the remaining wave parameters, including impulse product parameter, wave height, amplitude, period, and length (Figure 4.5).

4.5.2. Landslide two

Similar to the first landslide, the second's impulse wave generation and propagation were closely analyzed using a 3D model by Heller (2007) and the conversion method of Huber and Hager (1997). The results were as follows both before and after an emergency reservoir dropping.

The radial distance, wave propagation angle, and impulse product parameter were used to calculate the wave height of this specific landslide mass, which was found to be 5.75m. When utilizing the value of the wave height and the still water depth at the dam, it was discovered that the wave periods were 18.53 seconds. and an amplitude of 4.6m was found. The wave length was finally determined to be 383.25 meters based on the wave period and amplitude (Table 4.4).

Table 4. 4 Wave parameters result for landslide two before and after emergency drawdown

Parameter	Unit	With original design	After 6m emergency drawdown
Wave height (H)	m	5.75	4.73
Wave period (T)	s	18.53	16.93
Wave amplitude (a)	m	4.60	3.79
Wave length (L)	m	383.25	321.65

Similar to landslide one, as we can see from the findings, all wave parameters' values decrease after an emergency drawdown with a new impact velocity. The results showed that in the event of a landslide or if geodetic technologies suggest the potential of a mass movement, the safety of the dam may be guaranteed by lowering the reservoir level. This can be achieved by carefully planning and designing of reservoir withdrawal mechanism.

Since it can be difficult to establish the precise thickness of the slide mass, a sensitivity study was carried out using the following ranges of landslide thickness to see how wave factors affected the result (Table 4.5).

Table 4. 5 Sensitivity analysis and wave parameter result for landslide one

			Slide thickness (m)					
Term	**Symbol**	**Unit**	**5m**	**6m**	**7m**	**8m**	**9m**	**10m**
Slide impact velocity	Vs	m/s	30.39	30.39	30.39	30.39	30.39	30.39
Slide froude number	F		3.07	3.07	3.07	3.07	3.07	3.07
Impulse product parameter	P		3.36	3.85	4.32	4.78	5.22	5.65
Wave Height	H	m	4.73	5.28	5.79	6.28	6.74	7.18
Wave amplitude	a	m	3.79	4.23	4.63	5.02	5.39	5.74
Wave Period	T	s	16.93	17.40	17.81	18.17	18.49	18.79
Wave Length	L	m	321.65	332.53	342.17	350.88	358.86	366.24

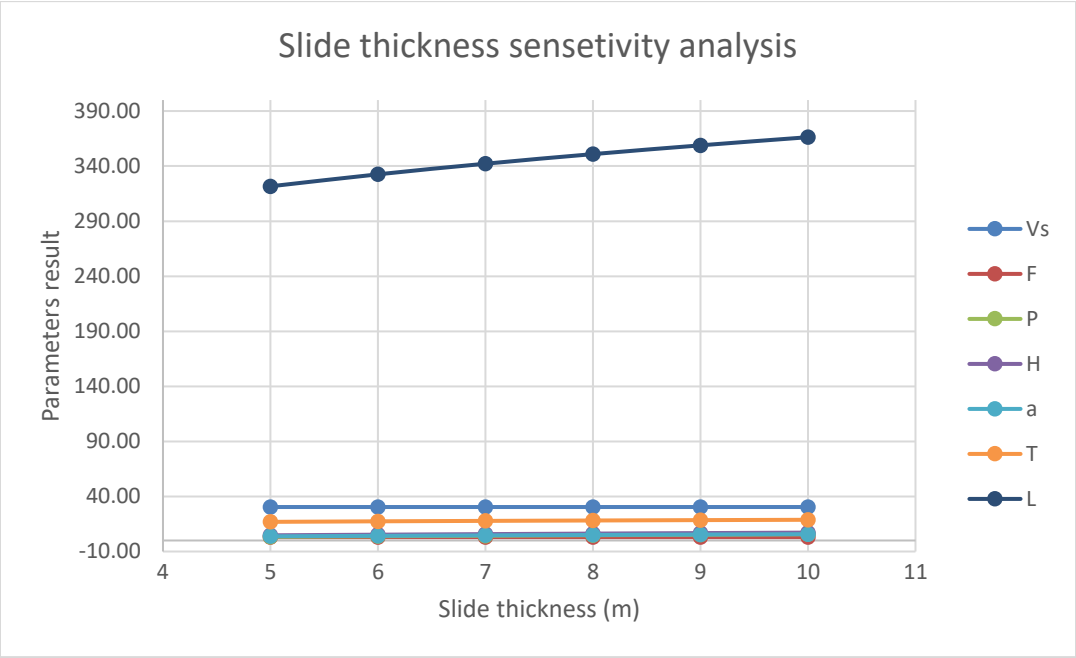

Figure 4. 6 Sensitivity analysis and wave parameter result for landslide one

The sensitivity analysis showed that the volume of the slide mass has no impact on the slide impact velocity or slide Froude number, which are displayed in the table 4.5 and figure 4.6 respectively. because the still water depth and drop height are the only factors which affect both. However, the remaining wave parameters, such as the impulse product parameter, wave height, amplitude, period, and length, rise along with the landslide mass volume figure (4.6).

4.5.3. Landslide three

Landslide three's impulse wave generation and propagation were thoroughly examined using a 3D model by Heller (2007) and the conversion method of Huber and Hager (1997), with the same analysis of landslide one and two and the results were as follows before and after an emergency lowering of the reservoir.

The wave height of this particular landslide mass, which was determined to be 0.1m, was calculated using the radial distance, wave propagation angle, and impulse product parameter. Using the computed wave height and the dam's still water depth, it was determined that the waves had periods of 6.93 seconds and an amplitude of 0.07 m. based on the wave period and amplitude, the final calculated wave length was 155.5 meters (Table 4.6).

Table 4. 6 Wave parameters result for landslide three

Parameter	Unit	Value
Wave height (H)	m	0.1
Wave period (T)	s	6.93
Wave amplitude (a)	m	0.07
Wave length (L)	m	155.5

The outcome demonstrated that this landslide point's values for all wave parameters are much lower than those of landslides one and two. This is due to the impact location's distance from the dam.

Since determining the exact thickness of the slide mass is very difficult, a sensitivity analysis was also conducted using the following ranges of landslide thickness for land slide three to determine how wave parameters affected by landslide mass volume (Table 4.7).

Table 4. 7 Sensitivity analysis and wave parameter result for landslide three

			Slide thickness (m)					
Term	**Symbol**	**Unit**	**5m**	**6m**	**7m**	**8m**	**9m**	**10m**
Slide impact velocity	Vs	m/s	5.04	5.04	5.04	5.04	5.04	5.04
Slide froude number	F		0.61	0.61	0.61	0.61	0.61	0.61
Impulse product parameter	P		0.97	1.11	1.25	1.38	1.50	1.63
Wave Height	H	m	0.09	0.10	0.10	0.11	0.12	0.13
Wave amplitude	a	m	0.07	0.08	0.08	0.09	0.10	0.10
Wave Period	T	s	6.93	7.12	7.28	7.43	7.56	7.68
Wave Length	L	m	155.46	159.78	163.53	166.85	169.84	172.55

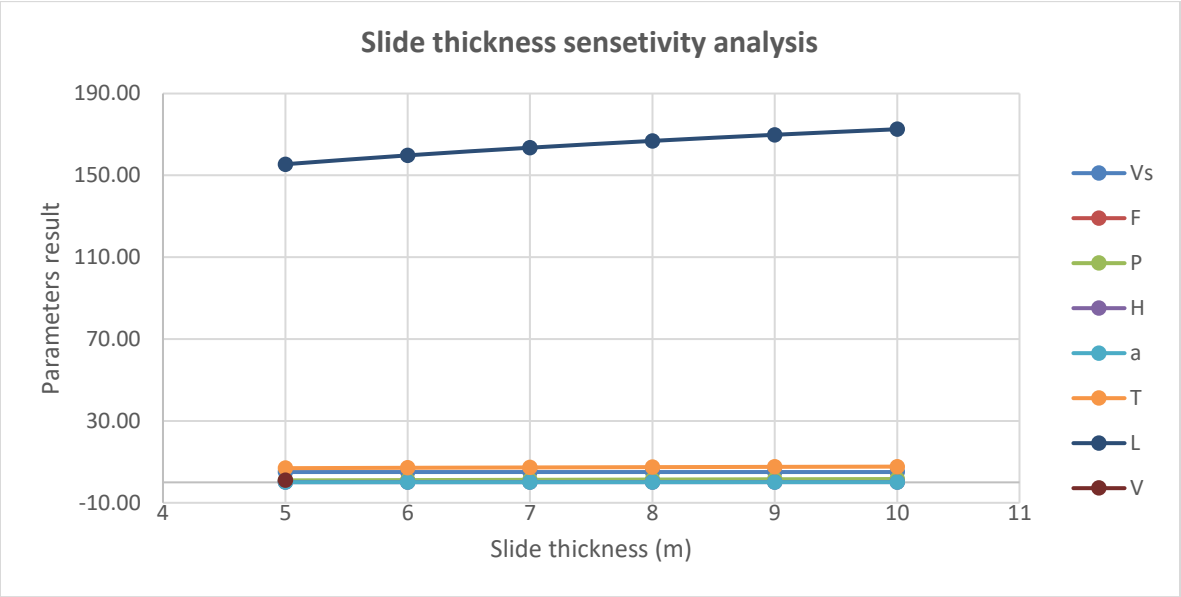

Figure 4. 7 Sensitivity analysis and wave parameter result for landslide three

The slide mass volume has no bearing on the slide impact velocity or slide froude number, which are displayed in the table 4.7 and figure 4.7 respectively. Only the drop height and still water depth have an effect on both, therefore. The remaining wave parameters, such as the impulse product parameter, wave height, amplitude, period, and length, however, also grow along with the landslide mass volume. However, the increment is insignificant compared with the slide mass volume.

4.3. Impulse wave run-up and flood overtopping

4.6.1. Land slide one

The depth and volume of the flood overtopping have been calculated using the results of the wave generating parameter of the landslide one (Table 4.8).

Table 4. 8.Wave run-up and flood overtopping result of landslide one

Parameter	Unit	Value
Wave run-up for original design (R)	m	7.34
Wave run-up after emergency drawdown (R)	m	10.94
Overtopping Volume per unit length dam crest for f=0 ($\forall_0$)	m^3/m	286.42
Overtopping Volume per unit length dam crest for f>0 ($\forall$)	m^3/m	50.61
Duration of overtopping to for f=0(t_0)	s	19.55
Average discharge per unit length dam crest for f=0 (q_{0m})	m^2/s	14.65
Maximum discharge per unit length dam crest f=0 (q_{0M})	m^2/s	29.30

The calculated wave runup, as shown in the result, is 7.34 meters, which is higher than the freeboard specified in the design (figure 4.8). For the safety of the dam, there must be enough freeboard to avoid overtopping.

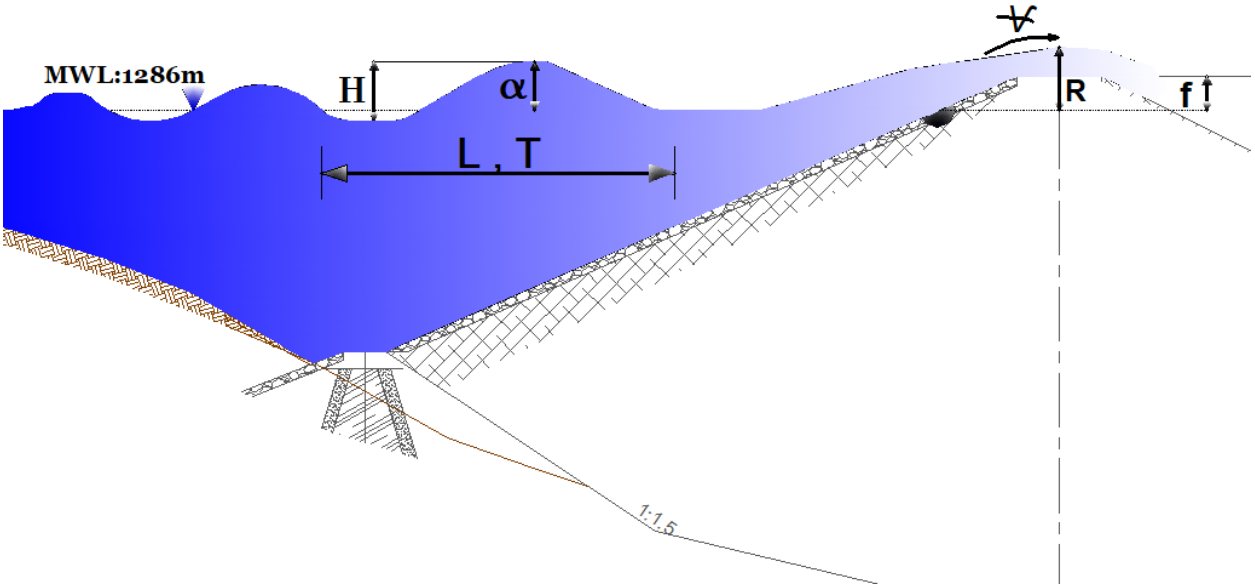

Figure 4. 8 Impulse wave sketch with Run-up and other parameter of landslide one in A-C section at MWL of 1286m

The overtopping volume and discharge have been calculated (Table 4.8) for f=0 and f>0 because the overtopping flood is certain with the original design of freeboard. It was discovered that the overtopping volumes, $\forall_0$ and V per unit length dam crest for f=0 and f>0 were 286.42 m^3/m and 50.61 m^3/m, respectively. And 19.55 seconds have been calculated as the overtopping duration t_0 for the overtopping volume V_0 for f = 0. But for the whole dam axis the overtopping volume were multiplied by the dam axis length. Since the dam axis length is 268m, the total overtopping volume found to be 13,564.3 m^3 for f>0.

The maximum discharge q_{0M} per unit length dam crest for f =0 (m^2/s) was determined to be 29.3 m^3/s/m, while the average discharge q_{0m} per unit length was found to be 14.65 m^3/s/m, but for f > 0, there is no empirical equation available for the discharge. As V less than V_0, the values of q_{0m} and q_{0M} are higher for f = 0 and serve as upper limiting values for the unknown values with f > 0. therefore, the average discharge q_{0m} and maximum discharge q_{0M} per unit length dam crest for f>0 (m^2/s) would be 14.65 m^3/s/m and 29.3 m^3/s/m respectively.

The new run-up height after 7 m of reservoir drawdown was found to be 10.8, and the total run-up depth after the second step of computation was found to be 10.94 m. As we can see from the results, it is not possible for an impulse wave to overtop in either scenario since the new freeboard, which is 11 meters, is greater than the new wave run-up.

Therefore, we may assume that if the dam freeboard is designed appropriately and if the dam owner provides for this type of reservoir drawdown during the project operation, there won't be any overtopping of discharge caused by this specific landslide impulse wave (Figure 4.9).

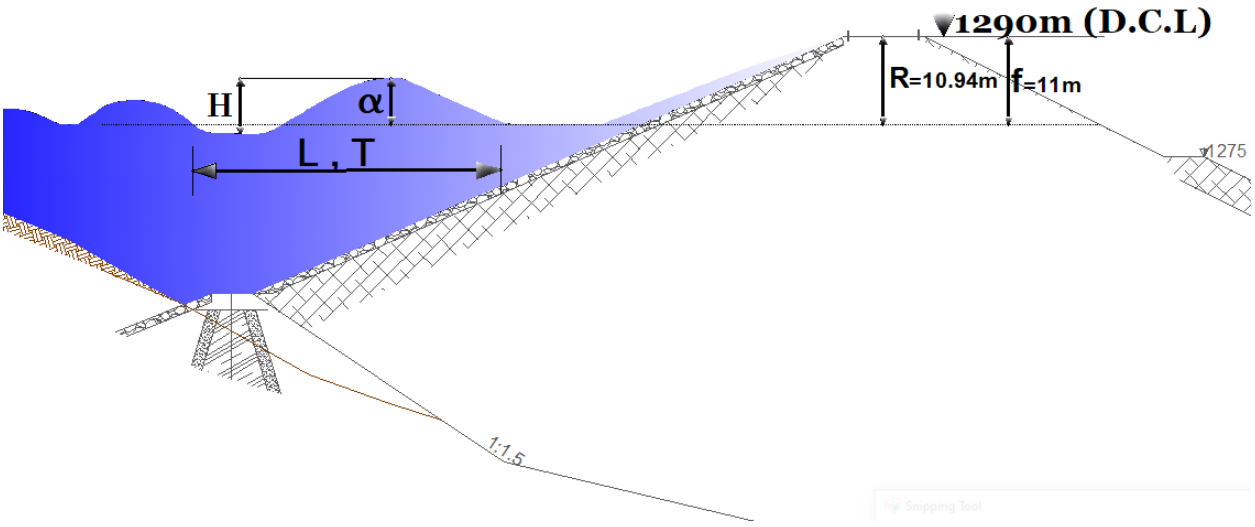

Figure 4. 9 Impulse wave sketch with Run-up and other parameter of landslide one in A-C section at MWL of 1279m

Sensitivity analysis has been performed with the following different landslide thicknesses to observe the impact of the mass volume of the landslide on wave run up height (Table 4.9).

Table 4. 9 Sensitivity analysis of slide thickness against run up height for landslide one

			Slide thickness (m)					
Term	**Symbol**	**Unit**	**5m**	**6m**	**7m**	**8m**	**9m**	**10m**
Overtopping Volume V per unit length dam crest for f>0	V	m^3/m	50.61	79.34	110.39	142.97	176.61	211
Run-up height	R	m	10.94	12.41	13.80	15.14	16.42	17.67

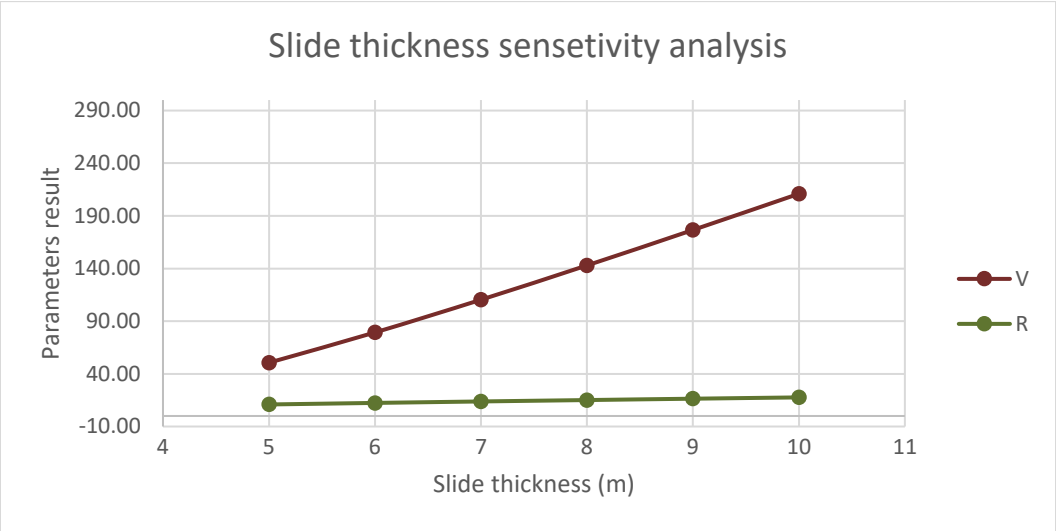

Figure 4. 10 Sensitivity analysis of slide thickness against run up height for landslide one

As we can notice from the table and the figure 4.10, the wave run height and landslide volume are directly correlated significantly, and as the volume increases, so does the run up depth.

4.3.1. Landslide two

The depth and volume of the flood overtopping have been calculated using the results of the wave generating parameter of the landslide two too (table 4.10).

Table 4. 10 Wave run-up and flood overtopping result of landslide two

Parameter	Unit	Value
Wave run-up for original design (R)	m	4.49
Wave run-up after emergency drawdown (R)	m	8.55
Overtopping Volume per unit length dam crest for f=0 (Vo)	m3/m	239.94
Overtopping Volume per unit length dam crest for f>0 (V)	m3/m	1.80
Duration of overtopping to for f=0(t_0)	s	21.48
Average discharge per unit length dam crest for f=0 (q_{0m})	m2/s	11.17
Maximum discharge per unit length dam crest f=0 (q_{0M})	m2/s	22.34

The calculated wave runup is 4.49 meters, which is higher than the freeboard stated in the design (Figure 4.11), as seen in the result. There must be enough freeboard to prevent overtopping for the dam's security similar to landslide one.

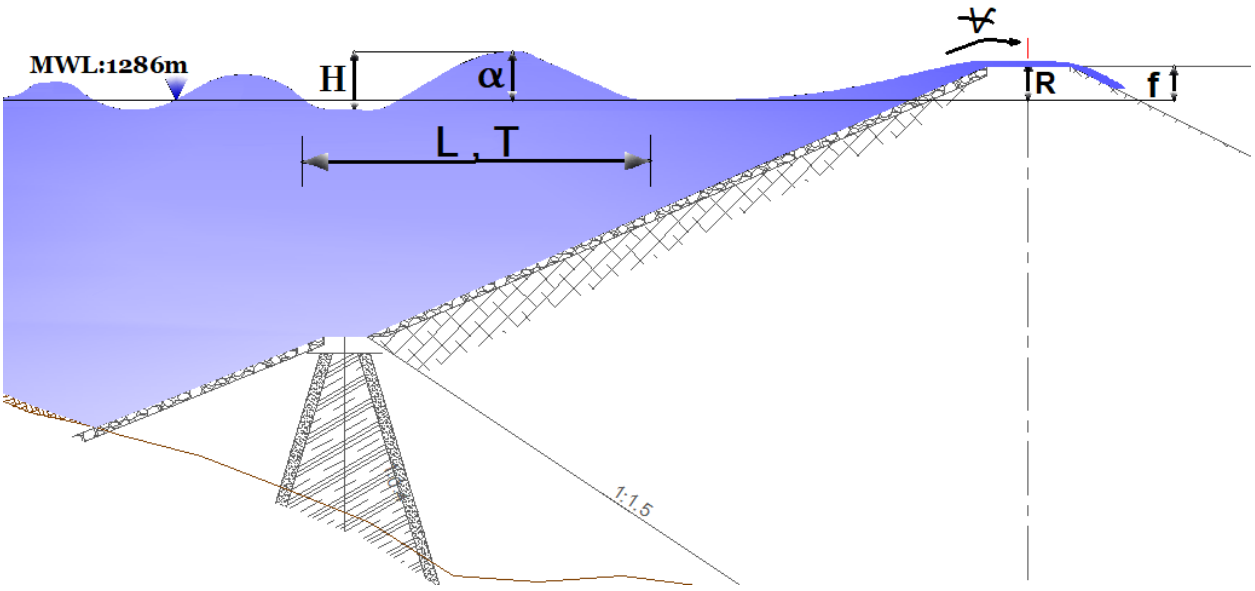

Figure 4. 11. Impulse wave sketch with Run-up and other parameter of landslide two in A-C section at MWL of 1286m

Due to the certainty of the overtopping flood in the original freeboard design, the overtopping volume and discharge have been computed (Table 4.10) for f=0 and f>0. The overtopping volumes, $\forall_0$ and $\forall$ per unit length dam crest were found to be 239.94 m^3/m and 1.8 m^3/m, respectively, for f=0 and >0. Furthermore, when f = 0, the overtopping period t_0 for the overtopping volume $\forall_0$ has been computed to be 21.48 seconds. the total overtopping volume across the dam axis found to be 482.4m^3 for f>0.

The maximum discharge q_{0M} per unit length dam crest for f=0 (m^2/s) was determined to be 22.34 $m^3/s/m$, while the average discharge q_{0m} per unit length was found to be 11.17 $m^3/s/m$. even if for f > 0, there is no empirical equation available for the discharge, As $\forall$ less than $\forall_0$, the values of q_{0m} and q_{0M} are higher for f = 0 and serve as upper limiting values for the unknown values with f > 0. therefore, the average discharge q_{0m} and maximum discharge q_{0M} per unit length dam crest for f=0 (m^2/s) would be 11.17 $m^3/s/m$ and 22.34 $m^3/s/m$ respectively.

The total run-up depth after the second stage of computation was found to be 8.55 m, and the new run-up height after 6 m of reservoir drawdown was found to be 8.97. Given that the new freeboard is 10 meters and the new wave run-up is 8.55 meters, it is evident from the results that an impulse wave cannot overtop in any situation for the given landslide volume.

We can therefore draw the conclusion that this particular landslide impulse wave won't result in any discharge overtopping, provided that the dam owner plans and implements the suggested reservoir drawdown strategy throughout the project's operational life (Figure 4.12).

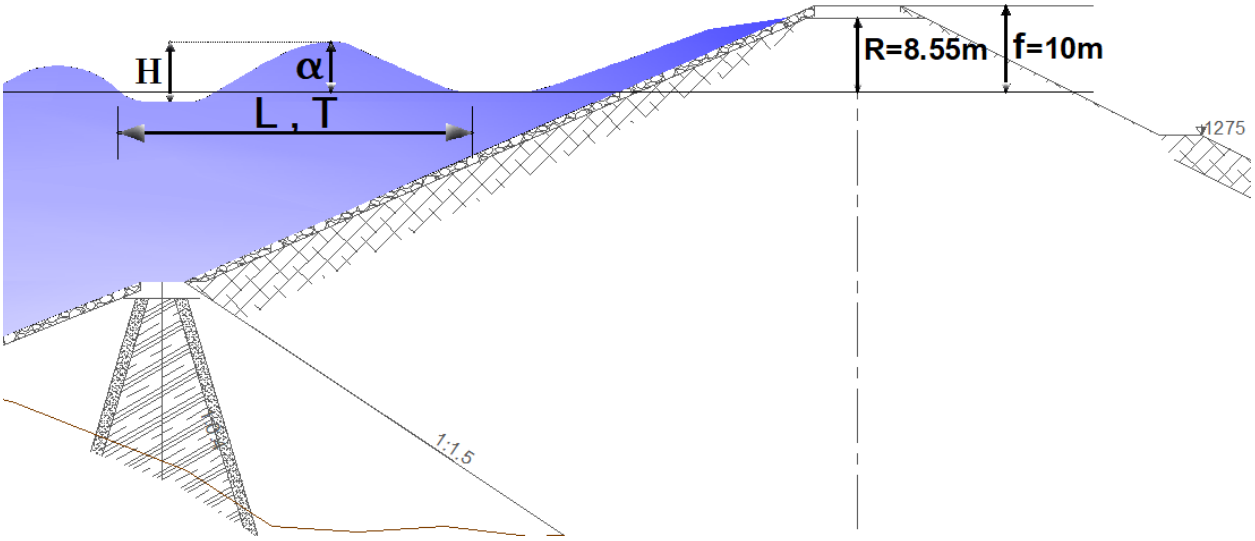

Figure 4. 12 Impulse wave sketch with Run-up and other parameter of landslide two in A-C section at MWL of 1279m

For landslide two, sensitivity analysis was also done on the following various landslide thicknesses to determine the effect of the landslide's mass volume on wave run up height (Table 4.11).

Table 4. 11 Sensitivity analysis of slide thickness against run up height for landslide two

			Slide thickness (m)					
Term	**Symbol**	**Unit**	**5m**	**6m**	**7m**	**8m**	**9m**	**10m**
Overtopping Volume V per unit length dam crest for *f*>0	V	m^3/m	1.80	9.39	21.49	36.86	54.65	74.27169
Run-up height	R	m	8.55	9.70	10.79	11.83	12.83	13.79456

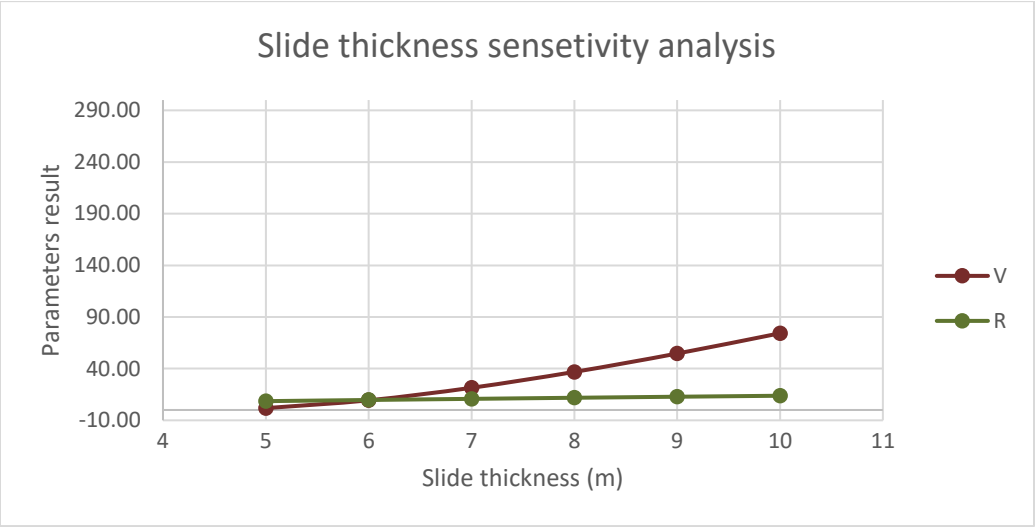

Figure 4. 13 Sensitivity analysis of slide thickness against run up height for landslide two

As we can see from the table and the figure 4.13, the wave run depth and landslide volume are directly correlated significantly, and as the volume increases, so does the run up depth.so that the worst scenario should be considered and expect to be conservative and safer.

4.3.2. Landslide three

The calculated wave runup is found to be 0.012 meters. The total run-up depth with the second step of computation was found to be 0. 11meter.The freeboard which is 4 meters, is much greater than wave run-up. Therefore, assuming the dam's freeboard is designed and fixed appropriately, we may conclude that there won't be any overtopping of discharge caused by this specific landslide impulse wave even for large slide mass volume (figure 4.14).

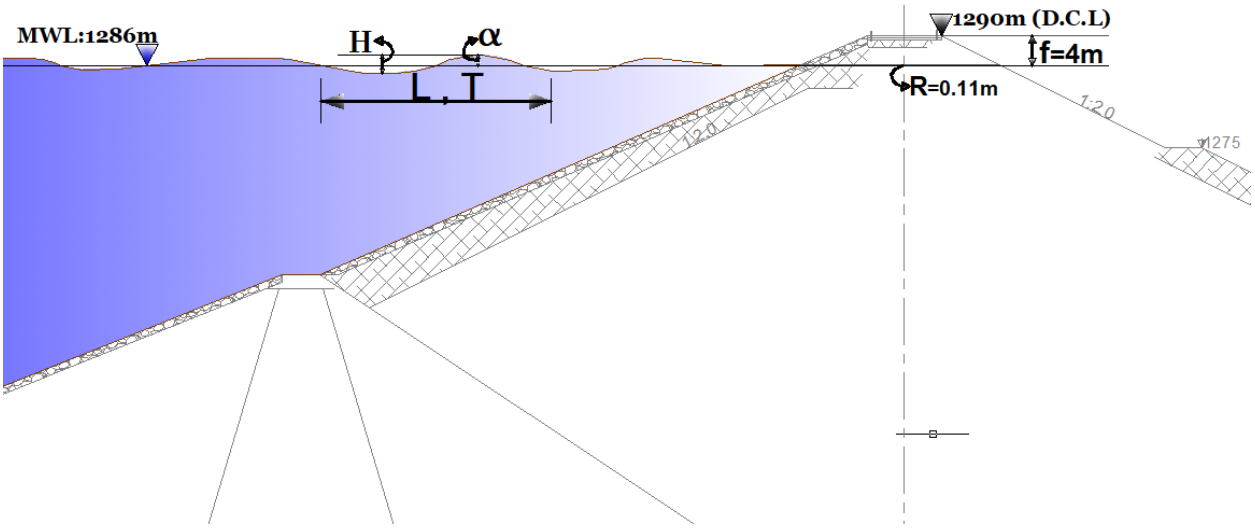

Figure 4. 14 Impulse wave sketch with Run-up and other parameter of landslide three in A-C section at MWL of 1286m

Sensitivity analysis of the following different landslide thicknesses was also performed for this specific impact location to assess the effects of the landslide's mass volume on wave run up (Table 4.12).

Table 4. 12 Sensitivity analysis of slide thickness against run up height for landslide three

			Slide thickness (m)					
Term	**Symbol**	**Unit**	**5m**	**6m**	**7m**	**8m**	**9m**	**10m**
Run-up height	R	m	0.11	0.13	0.14	0.16	0.18	0.19

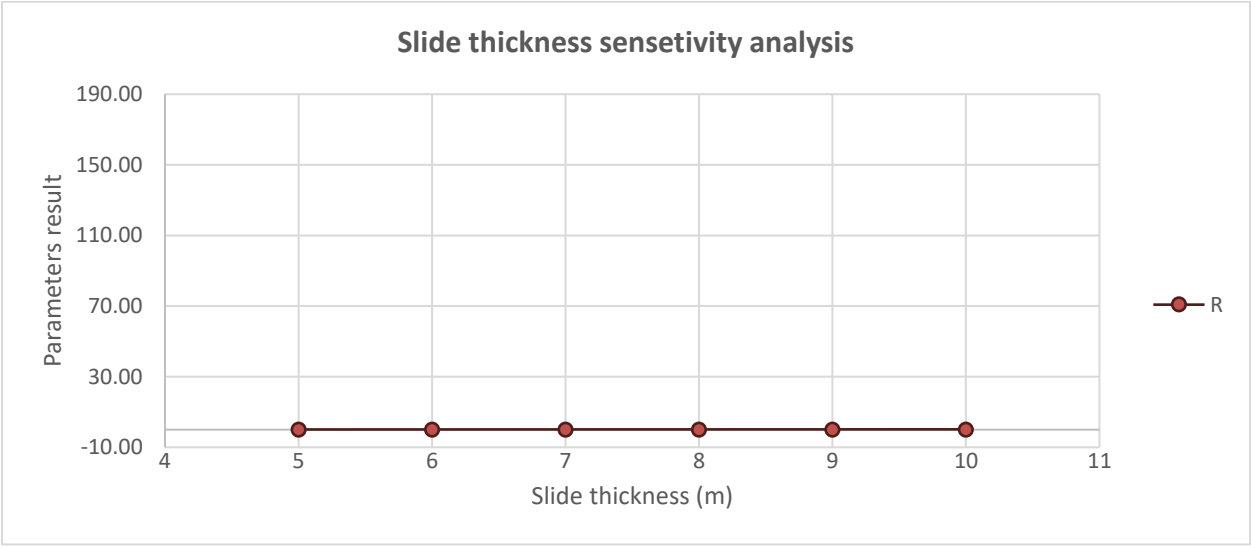

Figure 4. 15.Sensitivity analysis of slide thickness against run up height for landslide three

The sensitivity results reveal that (table 4.12.and figure 4.15), for this specific landslide site, the wave runup increases insignificantly with an increase in landslide mass volume. This is due to the impact area being much farther away from the dam.

So far, the analysis was done only for each landslide sites separately, however what if the three potential landslides occur at the same time due to different causes specially during earthquake. Even if the probability is low, we were checking this Scenario to see the effect on the adopted freeboard.

Computing the wave height, wave length, wave period and wave run up depth combinedly for all the three-landslide site is much difficult and the model used in this study is not yet allowed for such kind of condition. However, the run-up height due to volumetric displacement by the combined bulk slide mass were can be checked.
The total expected volume of bulk slide mass is 75000 m^3 and the reservoir surface area at maximum water level is 834,000m^2 Volumetric displacement becomes 0.1 meter. Even if the run up depth due to Volumetric displacement of the three potential site is small, unexpected additional landslide in the reservoir rim may be happen. Taking in to account these reasons the freeboard adopted for landslide should be taken the largest one from the three sites.

One of the challenges of this study was estimating the bulk slide mass of the land slide. Because it needs a detail study of subsurface investigation of reservoir rim such as geological mapping, geophysics and core drilling investigations in all potential landslide sites. But in sego dam the only data got from consultancy office is geological mapping. The bulk mass is result of slide length, slide width and slide thickness. in this study, the length and the width of the slide were approximately taken from Google Earth historical imagery but the slide thickness was assumed to be 5m for the first computation and sensitivity analysis was done from 5m up to 10m slide thickness independently.

The other challenge may encounter is how can suddenly lowering the reservoir level at maximum level during emergency time, how 6m or 7m possibly lower suddenly. This can solve by two methods: the first thing is providing adequate size of evacuation outlet considering the stability of

upstream of the dam and the second one is providing monitoring mechanism like geodetic technologies from identified potential landslide site and getting information so that if we have early information we can prepare accordingly and we can start lowering of the water before the slide takes place. Like dam instrumentation there should be reservoir instrumentation at identified site.

4.4. Comparison to other literature

In section 2.4.3 of this thesis, the techniques for predicting the overtopping volume and depth in the literature are discussed. It has been compared between the overtopping volumes calculated from Heller, et al. (2009) and Kobel, at al. (2017). the overtopping volume across the dam axis was found to be 13,564.3m^3 and 482.4 m^3 According to Heller (2009), and 12,614.5m^3 and 9,793.43 m^3 with wave overtopping volume parameter ($W_1^{0.8}$) of 0.2, and B_k/w= 0.303 According to Kobel (2017), for landslides one and two, respectively (figure 4.16).

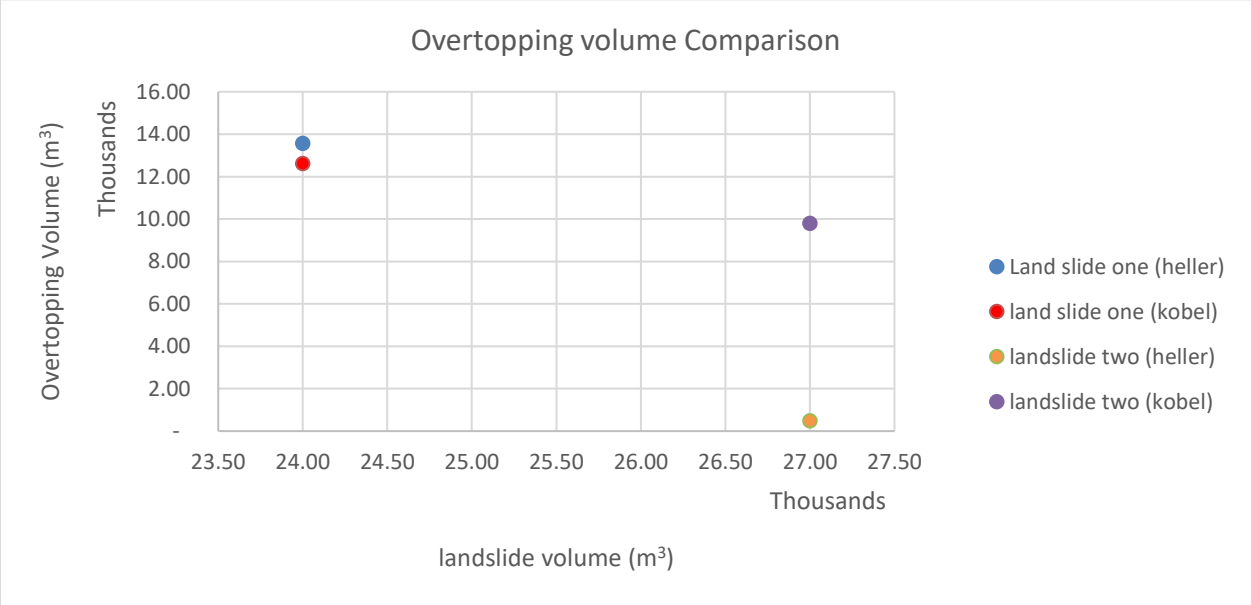

Figure 4. 16 Comparison of overtopping volume by heller (2009) and kobel (2017)

Generally Comparing the two scholars the results of overtopping volume of Kobel's et al. (2017) was found to be relatively similar result with Heller (2009) for landslide one, but for landslide two

the result of kobel is much higher than heller and it is over estimated. This is due to the research made by Kobel was on rigid dam and solid slide body material and other limitation criteria.

Another parameter estimation which compared to other literature is the overtopping depth, it has been compared between the overtopping depth calculated from Heller, et al. (2009) and Kobel, at al. (2017). According to Heller (2009), the overtopping depth over the dam crest was 3.34 m and 0.49m. According to Kobel (2017), the overtopping depth of landslides one and two was found to be 3.48m and 3.25m with overtopping volume parameter ($E_{2)}$ of 0.057 and Coefficient of determination (R^2) = 0.99, respectively. the result of overtopping depth over the dam crest computed by equation of the two researchers relatively almost the same specially for land slide one.

5. Conclusion and Recommendation

5.1. Conclusion

Landslide susceptibility assessment for planned Sego dam and reservoir areas was conducted. And wave generation, propagation and overtopping of three landslide sites has assessed. From the result of this thesis conclude could be made in following major.

- From the landslide impulse wave analysis result we can conclude that wave run up is high for landslide near to the dam, with the same landslide volume, wave run up height of landslide one was 98.5 % higher than landslide three.
- From the result we can conclude that landslides which takes place near to the dam generate large volume of flood and large wave height and run up depth.
- We can conclude also in addition to estimating appropriate slide volume, planning of emergency reservoir evacuation and implementing during operation of the project is very crucial.
- Since the dam is embankment dam overtopping of flood even in centimeters result dam breach which is very dangerous for downstream inhabitant and investments.
- From the analysis we can conclude that some parameters are very sensitive for determination of the wave run up for instance the still water depth, drop height, bulk slide volume and impulse product parameter. But the remaining parameter have insignificant contribution for wave run. Like the slide front angle and dynamic bed friction angle
- Overtopping volume and wave run up has linear relationship with bulk slide volume.

5.2. Recommendation

The study analyzed and create the landslide susceptibility map with different type of influential factor maps. Based on the findings of the landslide susceptibility assessment map and impulse wave parameters the following recommendations are provided:

- The study assessed the potential of landslide in the proposed dam and reservoir site so, the result shows that the dam and reservoir areas fall in medium to very high susceptible classes. Therefore, it is very important and crucial to assess the risk of landslide in the area before the construction.

- During the design stage the water level in the reservoir must be studied carefully because the variation of water level can reactivate old landslides and induced new landslides.
- Most of the time landslide prevention and protections are very expensive but less expensive or economical methods should be provided for the identified landslide impact zone like: slope stabilization using native vegetation and drainage improvement, vegetation placement and management.
- Detail geotechnical investigation should be carried out specially around the reservoir rim.
- Proper and latest model for slide volume estimation should be used to provide adequate freeboard of the dam and carful reservoir lowering technics before commencement of project construction should be assessed.
- We may not identify all landslide points in the project by investigation so that the inhabitant which settle downstream of the dam should have aware and emergency action plan should be prepared.
- The science of impulse wave generation and propagation is somehow not much addressed yet the model we used for this research is just with a lot of limitation, so that detail research is required in this field of study to produce good models.
- As standard or guidelines the design procedure for the design of freeboard against landslide generated waves along with wind wave should be prepared in Ethiopia.
- In sego dam the bottom outlet is planned to use for reservoir evacuation. therefore, the size of the bottom outlet should be considered the sudden drawdown of the reservoir during emergency of landslide taking in to account the stability of the dam.
- Reservoir instrumentation or monitoring system should be planned in the reservoir rim to control any earth movement during life period of the dam.

Reference

- Ahlqvist O. 2009. Overlay (in GIS). In Kitchin R, Thrift N (eds) International Encyclopedia of Human Geography, Volume 8, pp. 48–55.
- Aleotti P, Chowdhury R (1999) Landslide hazard assessment: summary review and new perspectives. Bull Eng Geol Environ 58(1):21–44.
- Aman, A., Mammo, T., and Wieland, M. (2019). Seismic safety evaluation of Tekeze arch dam. pp. 2635–2648
- Ardizzone, F., Cardinali, M., Carrara, A., Guzzetti, F., and Reichenbach, P.: Impact of mapping errors on the reliability of landslide hazard maps, Nat. Hazards Earth Syst. Sci., 2, 3–14, https://doi.org/10.5194/nhess-2-3-2002, 2002.
- Ataie-Ashtiani B, Najafi-Jilani A (2006) Prediction of submerged landslide generated waves in dam reservoirs: an applied approach. Dam Eng XVII 3:135–155.
- Ataie-Ashtiani B, Nik-khah A (2008) Impulsive waves caused by subaerial landslides.Environ Fluid Mech 8(3):263–280.
- Ayenew, T., & Barbieri, G. (2005). Inventory of landslides and susceptibility mapping in the Dessie area, northern Ethiopia. Engineering Geology, 77(1-2), 1-15. https://doi.org/10.1016/j.enggeo.2004.07.002.
- Cao, Z., Yue, Z., and Pender, G. (2011b). Landslide dam failure and flood hydraulics. Part I: experimental investigation. Nat. Hazards 59, 1003–1019.doi: 10.1007/s11069-011-9814-8.
- Cao, Z., Yue, Z., and Pender, G. (2011c). Landslide dam failure and flood hydraulics. Part II: coupled mathematical modelling. Nat. Hazards 59, 1021– 1045. doi: 10.1007/s11069-011-9815-7.
- Carvalho RF, Carmo JS (2007) Landslides into reservoirs and their impacts on banks.Environ Fluid Mech 7(6):481–493
- Chen, R., Shao, S., and Liu, X. (2015). Water–sediment flow modeling for field case studies in Southwest China. Nat. Hazards 78, 1197–1224. doi: 10.1007/s11069- 015-1765-z.
- Chen, S. C., Lin, T. W., and Chen, C. Y. (2015). Modeling of natural dam failure modes and downstream riverbed morphological changes with different dam materials in a flume test. Eng. Geol. 188, 148–158. doi: 10.1016/j.enggeo.2015.01.016.
- Chung C.J.F., Fabbri A.G., 2003. Validation of spatial prediction models for landslide hazard mapping. Natural Hazards, 30: 451-472.
- Dai FC, Lee CF, Li J, Xu ZW (2008) Assessment of landslide susceptibility on the natural terrain of Lantau Island, Hong Kong. Environ Geol 40:381–91.

- Dazzi, S., Vacondio, R., and Mignosa, P. (2019). Integration of a levee breach erosion model in a GPU-accelerated 2D shallow water equations code. Water Resour. Res. 55, 682–702. doi: 10.1029/2018wr023826
- ECDSWC. (2022). Sego Dam Final Design Report. Addis Ababa: Ethiopian construction design and supervision works corporation.
- Enet F, Grilli S (2005) Tsunami landslide generation: modelling and experiments. Ocean Wave Measurement and Analysis, Fifth Intl Symposium WAVES, Madrid, Spain.
- Fread, D. L. (1988). BREACH, an Erosion Model for Earthen Dam Failures. Washington, DC: NOAA.
- Fuchu, D., and Chack F.L., 2002. Landslides on natural terrain –physical characteristics and susceptibility mapping in Hong Kong. Mountain Research and Development, Vol. 22(1), pp. 40-47
- Fujisawa, K., Kobayashi, A., and Aoyama, S. (2009). Theoretical description of embankment erosion owing to overflow. Géotechnique 59, 661–671. doi: 10.1680/geot.7.00035.
- G.F. Wieczorek, Landslide triggering mechanisms, in: Landslides Investigation and Mitigation, edited by: Turner, A. K. and Schuster, R. L., special report 247. National Academy Press, Washington D.C, 1996.
- G.G.D. Zhou, P. Cui, H.Y. Chen, X.H. Zhu, J.B. Tang, Q.C. Sun, Experimental study on cascading landslide dam failures by up stream flows, Landslides, Vol. 10, No. 5, 2013, pp. 633-643.
- Grilli ST, Watts F (2005) Tsunami generation by Submarine mass failure; I: modelling, experimental validation, and sensitivity analyses. J of Waterway Port Costal and Ocean Eng, ASCE, pp 283–297.
- Hailemariam Gugsa, T., and Schneider, J.F. (2010). Rock Mass Classification of Karstic Terrain in the Reservoir Slopes of Tekeze Hydropower Project. p. 831.
- Hanson, G. J., Cook, K. R., and Temple, D. M. (2002). "Research results of largescale embankment overtopping breach tests, in: dam safety 2002," in Proceedings of the Association of State Dam Safety Officials, Tampa, and FL. doi: 10.21608/erjm. 2013.67430.
- Heller, V. (2007). Landslide generated impulse waves - Prediction of near field characteristics. ETH/VAW 177.
- Heller, V.; Hager, W.H.; Minor, H.-E. Landslide Generated Impulse Waves in Reservoirs: Basics and Computation; VAW-Mitteilung 211; ETH: Zürich, Switzerland, 2009.

  -He, K., Li, X., Yan, X. & Guo, D., 2008. The landslides in the Three Gorges Reservoir Region, China and the effects of water storage and rain on their stability, Environment. Geol., 55, 55–63.
- Hong Y, Hiura H, Shino K, Sassa K, Suemine A, Fukuoka H, Wang GH (2005) The influence of intense rainfall on the activity of large-scale crystalline schist landslides in Shikoku Island, Japan. Landslides 2:97–105.

- Hongchao Zheng, Zhenming Shi, Danyi Shen, Ming Peng, Kevin J. Hanley, Chenyi Ma and Limin Zhang (2021). Recent advances in stability and failure mechanisms of landslide dams.
- Huang, W., Cao, Z., Carling, P., and Pender, G. (2014). Coupled 2D hydrodynamic and sediment transport modeling of megaflood due to glacier dam-break in Altai Mountains. Southern Siberia. J Mt. Sci. 11, 1442–1453. doi: 10.1007/ s11629-014-3032-2.
- J.E. Costa, Floods from dam failures, U.S. Geological Survey, Open-File Rep. No. 85-560, 1985.
- J.E. Costa, R.L. Shuster, The formation and failure of natural dams, Geol. Soc. Am. Bull. 100, 1988, pp. 1054-1068.
- Javadi, N., and Mahdi, T. F. (2014). Experimental investigation into rockfill dam failure initiation by overtopping. Nat. Hazards 74, 623–637. doi: 10.1007/s11069-014-1201-9
- Jones FO, Embody DR, Peterson WL, Hazlewood RM (1961) Landslides along the Columbia River Valley, Northeastern Washington: descriptions of landslides and statistical analyses of data on some 200 landslides in pleistocene sediments. US Government Printing Office.
- Kakinuma, T., and Shimizu, Y. (2014). Large-scale experiment and numerical modeling of a riverine levee breach. J. Hydraul. Eng. 140:04014039. doi: 10.1061/(asce)hy.1943-7900.0000902.
- Kessarkar, P.M., Srinivas, K. Suprit, K., and Chaubey, A.K., 2011. Proposed landslide mapping method for Canacona region. National institute of Oceanography, (Council of Scientific and Industrial Research, Dona Paula, Goa,) pp. 5.
- Kimio INOUE, Toshio MORI and Takahisa MIZUYAMA, Three Large Historical Landslide Dams and Outburst Disasters in the North Fossa Magna Area, Central Japan, 2012.
- Li, J., Cao, Z., Pender, G., and Liu, Q. Q. (2013). A double layer-averaged model for dam-break flows over mobile bed. J. Hydraul. Res. 51, 518–534. doi: 10.1080/ 00221686.2013.812047.
- Liu PLF, Wu TR, Raichlen F, Synolakis CE, Borrero JC (2005) Runup and rundown generated by three-dimentional sliding masses. J Fluid Mech 536:107–144.
- Loukola, E., and Huokuna, M. (1998). "A numerical erosion model for embankment dams failure and its use for risk assessment," in Proceedings of "CADAM (Concerted Action on Dam Break Modelling)", Munich: Munich Meeting, 8–9.
- Mohamed, A. A. A., Samuels, P. G., Morris, M. W., and Ghataora, G. S. (2002). "Improving the accuracy of prediction of breach formation through embankment dams and flood embankments," in Proceedings of the International Conference on Fluvial Hydraulics, Louvain-la-Neuve, Belgium.
- Morris, M. W., Hassan, M., and Vaskinn, K. A. (2007). Breach formation: field test and laboratory experiments. J. Hydraul. Res. 45, 9–17. doi: 10.1080/00221686.2007.9521828.

- Morris, M. W., Kortenhaus, A., and Visser, P. J. (2009). Modelling Breach Initiation and Growth. FLOODsite Report T06-08-02. Wallingford: FLOODsite. FLOODsite Project, HR.
- Najafi-Jilani A, Ataie-Ashtiani B (2007) Estimation of near-field characteristics of tsunami generation by submarine landslide. Ocean Eng 35:545–557.
- Nakamura K (1990) on reservoir landslide. Bull Soil Water Conserv 10(1):53–64 (In Chinese).
- Netsanet N., Fjóla G. Sigtryggsdóttir, Leif L. and Asie k.(2019). Case Study of Dam Overtopping from Waves Generated by Landslides Impinging Perpendicular to a Reservoir's Longitudinal Axis
- Ouyang, C., He, S., and Xu, Q. (2014). MacCormack-TVD finite difference solution for dam break hydraulics over erodible sediment beds. J. Hydraul. Eng.141:06014026. doi: 10.1061/(asce)hy.1943-7900.0000986.
- Panizzo A, Girolamo PD, Di Risio M, Maistri A, Petaccia A (2005) Great landslide events in Italian artificial reservoirs. Nat Hazards Earth Syst Sci 5:733–740.
- Paronuzzi P, Rigo E, Bolla A (2013) Influence of filling–drawdown cycles of the Vajont reservoir on Mt. Toc slope stability. Geomorphology 191:75–93
- Peng, M., and Zhang, L. M. (2017). Breaching parameters of landslide dams. Landslides 9, 13–31. doi: 10.1007/s10346-011-0271-y
- Petley, D,2000 http://sci.port.ac.uk/geology/staff/dpetley/imgs/enggeolprac/vaiont1.html
- Pickert, G., Weitbrecht, V., and Bieberstein, A. (2011). Breaching of overtopped river embankments controlled by apparent cohesion. J. Hydraul. Res. 49, 143–156. doi: 10.1080/00221686.2011.552468.
- R. Awal, N. Nakagawa, K. Kawaike, Y. Baba, H. Zhang, Prediction of flood/debris flow hydrograph due to landslide dam failure by overtopping and sliding, Annuals of Disaster Prev. Res. Inst., Kyoto Univ., No. 51B, 2008, pp. 603-611.
- Riemer, W., Pantartzis, P., Krapp, L. and Scourtis, C., 1996. Investigation and monitoring of landslides at the Polyphyton Project in Greece. Paper presented in the 7th Int. Symp. On Landslides, Trondheim,Norway.
- Risio M, Bellotti G, Panizzo A, Girolamo PD (2009) Three-dimensional experiments on landslide generated waves at a sloping coast. Coast Eng 56:659–671.
- Schmocker, L., and Hager, W. H. (2009). Modelling dike breaching due to overtopping. J. Hydraul. Res. 47, 585–597. doi: 10.3826/jhr.2009.3586
- Schmocker, L., Frank, P. J., and Hager, W. H. (2014). Overtopping dike-breach: Effect of grain size distribution. J. Hydraul. Res. 52, 559–564. doi: 10.1080/00221686.2013.878403
- Schuster RL (1979) Reservoir-induced landslides. Bull Int Assoc Eng Geol 20:8–15
- Schuster, R.L., Wieczorek, G.F. (2002). Landslide triggers and types. Proc. 1st European Conf.Landslides, Prague, 59-78. Rybář, J., Stemberk, J., Wagner, P. eds. Balkema, Tokyo.
- Semenza E (2000) La storia del Vajont, raccontata dal geologo che ha scoperto la frana.Tecomproject, Ferrara.

- Shigihara Y, Goto D, Imamura F, Kitamura Y, Matsubara T, Takaoka K, Ban K (2006) Hydraulic and numerical study on the generation of a subaqueous landslide-induced tsunami along the coast. Nat Hazards 39:159–177.
- Singh, V. P., and Scarlatos, P. D. (1988). Analysis of gradual earth-dam failure. J. Hydraul. Eng. 114, 21–42. doi: 10.1061/(asce)0733-9429(1988) 114:1(21)
- Soeters R, Van Westen CJ (1996) Slope instability recognition analysis and zonation. In: Turner KT, Schuster RL (eds) Landslides: investigation and mitigation. Transportation Research Board National Research Council, Special Report No 247, Washington, DC, pp 129–77.
- Steven, N.W.; Simon, D. The 1963 landslide and flood at Vaiont reservoir Italy. A tsunami ball simulation.Ital. J. Geosci. 2011, 130, 16–26.
- T. Takahashi, Debris flow, monographs series of IAHR, Balkema, 1991, pp. 1-165.
- Tsai TL (2008) the influence of rainstorm pattern on shallow landslide. Eng Geol 53(7):1563–1569
- U.S. Army Corps of Engineers, 2002, Coastal Engineering Manual, EM 1110-2-1100. (With 2008 changes). http://140.194.76.129/publications/eng-manuals/EM_1110-2-1100_vol/PartI/PartI.htm
- Van der Meer, et al., "Flow Depths and Velocities at Crest and Inner Slop of a Dike, in Theory, and with the Wave Overtopping Simulator, Coastal Engineering, 2010.
- van Westen CJ, Castellanos E, Kuriakose SL (2008) Spatial data for Landslide Susceptibility, Hazard, and Vulnerability assessment: an overview. Eng Geol 102(3):112–131.
- Varnes D.J., 1978. Slope movement types and processes: Landslide analysis and control. Transportation Research Board, National Academy Sciences, Washington
- Vita PD, Reichenbach P, Bathurst JC, Borga M, Crozier GM, Glade T, Hansen A, Wasowski J (1998) Rainfall-triggered landslides: a reference list. Environ Geol 35(2–3):219–233
- Volz, C., Frank, P. J., Vetsch, D. F., Hager, W. H., and Boes, R. M. (2017). Numerical embankment breach modelling including seepage flow effects. J. Hydraul. Res.55, 480–490.doi:10.1080/00221686.2016.1276104.
- Wu, W., and Li, H. (2017). A simplified physically-based model for coastal dike and barrier breaching by overtopping flow and waves. Coast. Eng. 130, 1–13.doi: 10.1016/j.coastaleng.2017.09.007
- X.K. Do, R.K. Regmi, K.S. Jung, Study on the formation and geometries of rainfall-induced landslide dams, KSCE (revised), 2015.
- Y.Satofuka, T. Mori, T. Mizuyama, K. Ogawa, K. Yoshino, Prediction of floods caused by landslide dam collapse, Journal of disaster research, Vol. 5, No. 3, 2010, pp. 288-295.
- Z. Cao, Z. Yue, G. Pender, Landslide dam failure and flood hydraulics, Part 2: coupled mathematical modelling, Nat. Hazards, Vol. 59, No. 2, 2011, pp. 1021-1045.
- Zagonjolli, M. (2007). Dam break Modelling, Risk Assessment and Uncertainty Analysis for Flood Mitigation. ISBN 9 780415 455947 (Taylor & Francis Group). London, UK: Taylor & Francis.
- Zhao, T. L., Chen, S. S., Fu, C. J., and Zhong, Q. M. (2018). Influence of diversion channel section type on landslide dam draining effect. Environ. Earth Sci. 77,54–62.
- Zhu, Y. H., Visser, P. J., and Vrijling, J. K. (2004). "Review on embankment dam breach modeling," in New Developments in Dam Engineering, (London: Taylor & Francis Group), 1189–1196. doi: 10.1201/9780203020678.ch147
- Zweifel A, Hager WH, Minor HE (2006) Plane impulsive waves in reservoirs. Journal of Waterway, Port, Costal, and Ocean Engineering 132:358–368. doi:10.1061/(ASCE)0733-950X.

Appendices

Table A. 1 Prepared Template for Computation of the landslide impulse wave

Landslide generated impulse waves in reservoirs -basics and Computation Spread sheets			
Project name	Example 1	Operator	Amdemariam S.
Computational point	Point C	Date	2023
Governing parameters			
Wave generation (Subsection 3.2.2.)			
Slide impact velocity, Vs (m/s)	=	Bulk slide density, ρs (kg/m^3)	=
Bulk slide volume, Vs (m^3)	=	Bulk slide porosity, n (%)	=
Slide thickness, s (m)	=	Slide impact angle, α (°)	=
Slide or reservoir width, b (m)	=	Still water depth, h (m)	
Wave propagation (3D or 2D) (Subsection 3.2.2)			
Wave basin (3D)		Wave channel (2D)	
Radial distance, r (m)	=	Streamwise distance x (m)	0
Wave propagation angle γ (°)	=		
Wave run-up and overtopping (Subsection 3.3.2			
Still water depth, h (m)	=	Freeboard, f (m)	
Run-up angle, β (°)	=	Crest width b $_k$ (m)	
Main Results			
Wave height, H, (H_M) (m)			
Wave amplitude, α, (α_M) (m)			
Wave period, T, (T_M) (s)			
Wave Length, L, (L_M)(m)			
Run-up height R (m)			
Overtopping volume V_o per unit length dam crest for f=0 (m^3/m)			
Duration of overtopping t_o for f=0			
Average discharge q $_{0m}$ per unit length dam crest for f=0 (m^2/s)			
Maximum discharge q $_{0M}$ per unit length dam crest f=0 (m^2/s)			
Overtopping volume per unit length dam crest, V (m^3/m)			
Limitations			
Number of not satisfied limitations in (2D) or (3D), respectively			

Table A. 2 Sample Computation of impulse wave analysis of landslide one by the template

Landslide generated impulse waves in reservoirs -basics and Computation Spread sheets			
Project name	Example 1	Operator	Amdemariam S.
Computational point	Point C	Date	2023
Governing parameters			
Wave generation (Subsection 3.2.2.)			
Slide impact velocity, Vs (m/s)	31.25	Bulk slide density, ρs (kg/m^3)	1700
Bulk slide volume, Vs (m^3)	24000	Bulk slide porosity, n (%)	35
Slide thickness, s (m)	5	Slide impact angle, α (°)	41
Slide or reservoir width, b (m)	60	Still water depth (m)	29
Wave propagation (3D or 2D) (Subsection 3.2.2)			
Wave basin (3D)		Wave channel (2D)	
Radial distance, r (m)	147	Streamwise distance x (m)	95.45887644
Wave propagation angle γ(°)	-33		
Wave run-up and overtopping (Subsection 3.3.2			
Still water depth, h (m)	29	Freeboard, f (m)	4
Run-up angle, β (°)	23.5	Crest width b $_k$ (m)	10
Main Results			
Wave height, H, (H_M) (m)			6.94
Wave amplitude, α, (α_M) (m)			5.55
Wave period, T, (T_M) (s)			18.04
Wave Length, (L_M)(m)			332.14
Run-up height R (m)			7.34
Overtopping volume V_o per unit length dam crest for f=0 (m^3/m)			286.424504
Duration of overtopping t_o for f=0			19.55
Average discharge q $_{0m}$ per unit length dam crest for f=0 (m^2/s)			14.65
Maximum discharge q $_{0M}$ per unit length dam crest f=0 (m^2/s)			29.30
Overtopping volume per unit length dam crest, V (m^3/m)			50.61
Limitations			
Number of not satisfied limitations (2D) or (3D)			4